Presynaptic action potential modulation in a neurological channelopathy

Umesh Saravanan Vivekananda

No: 110091548

A thesis submitted to University College London for the degree of Doctor of Philosophy

Department of Clinical and Experimental Epilepsy, UCL Institute of Neurology

April 2017

Declaration

I, Umesh Vivekananda, confirm that the work presented in this thesis is my original research work. Where contributions of others are involved, this has been clearly indicated in the text.

Abstract

Channelopathies are disorders caused by inherited mutations of specific ion channels. Neurological channelopathies in particular offer a window into fundamental physiological functions such as action potential modulation, synaptic function and neurotransmitter release.

One such channelopathy Episodic Ataxia type 1 (EA1), is caused by a mutation to the gene that encodes for the potassium channel subunit Kv1.1. This channel is predominantly found in presynaptic terminals and EA1 mutations have previously been shown to result in increased neuronal excitability and neurotransmitter release. A possible reason is that presynaptic action potential waveforms are affected in EA1. Thus far, direct electrophysiological recording of presynaptic terminals has been limited to large specialised synapses e.g. mossy fibre boutons, or axonal blebs, unnatural endings of transected axons. This is not representative of the vast majority of small synapses found in the forebrain. Using a novel technique termed Hopping Probe Ion Conductance Microscopy (HPICM) I have been able to directly record action potentials from micrometer sized boutons in hippocampal neuronal culture. I have shown that in a knockout model of Kv1.1 and in a knockin model of the V408A EA1 mutation, presynaptic action potentials are broader than in wild type; however action potentials are unaffected in the cell body.

Finally in some central synapses neurotransmitter release has been shown to depend on not only action potentials received in the presynaptic terminal, but also on slow subthreshold membrane potential fluctuations from the soma, termed analogue-digital signalling. Kv1 channels have been implicated in partly mediating this form of signalling. I have shown via dual recordings from the soma and small presynaptic boutons, that analogue-digital signalling occurs in wild type and knockout of Kv1.1, but is abolished in the V408A EA1 mutation. This implies that analogue-digital signalling may not depend on Kv1.1 in particular, rather a change in the stoichiometry of the Kv1 channel.

Acknowledgements

I would like to take this opportunity to thank numerous friends who have helped me on this PhD journey.

I am indebted to my primary supervisor, Professor Dimitri Kullmann. He is an inspiration to me. His endless helpful suggestions and encyclopaedic neuroscience knowledge were invaluable. I am also indebted to my secondary supervisor, Dr Kirill Volynski. His patient advice, especially with matters of microscopy were much appreciated. I also thank both for undertaking the unenviable task of proof reading this thesis (!).

I count my time at the Department of Clinical and Experimental Epilepsy, UCL as one of the happiest in my career. So many amazing scientists provided help during my research but I thank in particular Dr Yarik Ermolyuk, Dr Rahima Begum, Dr Vincent Magloire, Dr Ivan Pavlov, Dr Alistair Jennings (for extracurricular help), Dr Elizabeth Nicholson, Jonathan Cornford and my clinical compatriot Dr Sarah Crisp. I would like to thank Dr Stuart Martin for help with genotyping. My deepest gratitude is extended to Dr Marife Cano and more recently Dr Andres Vicente for their crucial help in culturing neurons and genotyping. Juliet Solomon was encouraging, administration efficiency personified and an inexhaustible source of trivia!

This project would not have progressed without the support of my collaborators, Dr Pavel Novak (now at QMUL) and Prof Yuri Korchev (Imperial). Their patience and continued help were much appreciated when I was learning about SICM.

I am grateful to Dr Chris Turner, Dr Matthew Parton and Prof Matthew Walker for allowing me to join their muscle and epilepsy clinics respectively and sharing their clinical wisdom.

I would like to thank Action Medical Research and especially the Wellcome Trust for awarding me a Clinical Research Fellowship to carry out this work. Without their unfailing commitment and support this project would not have happened.

Finally I would like to thank my family. Words cannot express how grateful I am to my parents for the inexhaustible encouragement (and support financial and otherwise!) they have always provided me. My wife, Elizabeth, has been everything to me through this process – I promise no more writing up! And Noah maybe one day when you are bored you may read this, thank you for always making me smile. Finally I thank God for the opportunity of this PhD, and being there through the highs and lows.

Publications

1. Vivekananda U, Novak P, Bello OD, et al. (2017). Kv1.1 channelopathy abolishes presynaptic spike width modulation by subthreshold somatic depolarisation. PNAS 114; 2395-2400

2. Novak P, Gorelik J, Vivekananda U, et al. (2013). Nanoscale-targeted patch-clamp recordings of functional presynaptic ion channels. Neuron 79; 1067-77

Awards for this project

Mansell Prize for Neuroscience Research, Medical Society of London. June 2017

Gordon Holmes Prize in Neurosciences, Royal Society of Medicine. April 2016

Queen Square Prize in Neurology. October 2015

Wellcome Trust Clinical Research Fellowship. June 2012

Table of contents

Table of figures

Table of tables

Abbreviations

AED	Antiepileptic drugs
AFM	Atomic Force Microscopy
AIS	Axon Initial Segment
AMPA	2-1mino-3-(5-methyl1-3-oxo-1,2-oxazol-4-yl)propanoic acid
AP	Action potential
araC	Cytosine β-D-arabinofuranoside
ATP	Adenosine-5'-triphosphate
AZ	Active zone
BSA	Bovine serum albumin
CM	caesium methanosulphonate
CNS	Central nervous system
DIC	Differential interference contrast microscopy
DIV	Days in vitro
DL-AP5	DL-2-Amino-5-phosphonopentanoic acid
DMEM/F12	Dulbecco's Modified Eagle Medium: Nutrient Mixture F-12
DMSO	Dimethyl sulfoxide
DPBS	Dulbecco's Phosphate Buffered Saline

DTx-K Dendrotoxin-K

EA1 Episodic Ataxia Type 1

EA2 Episodic Ataxia Type 2

EB Extracellular buffer

EDTA Ethylenediaminetetraacetic acid

EGTA Ethylene glycol tetraacetic acid

EM Electron microscopy

EPSC Excitatory post synaptic current

EPSP Excitatory post synaptic potential

FHM Familial Hemiplegic Migraine

GABA Y-aminobutyric acid

GFP Green fluorescent protein

GM Glial medium

GTP Guanosine-5'-triphosphate

HBSS Hanks balanced salt solution

HEPES 4-(2-hydroxyethyl)-1-piperazineethanesulfonic acid

HET Heterozygous

HOM Homozygous

HPICM Hopping Probe Ion Conductance Microscopy

KGluc	Potassium gluconate
KI	Knock-in
KO	Knock-out
LED	Light Emitting Diode
NB	Neurobasal complete
NBQX	2,3-dihydoxy-6-nitro-7-sulfamoyl-benzo(f)quinoxaline-2,3-dione
NMDA	N-methyl-D-aspartic acid
NMJ	Neuromuscular junction
P0	Postnatal day zero
PTX	Picrotoxin
RFP	Red fluorescent protein
RMP	Resting membrane potential
SICM	Scanning Ion Conductance Microscopy
SNARE	Soluble NSF attachment protein receptor
SPM	Scanning Probe Microscopy
SRC1	SynaptoRed C1
t/2	Action potential half width
TEA	Tetraethylammonium chloride
TTX	Tetrodotoxin

VGCC	Voltage gated calcium channel
VGKC	Voltage gated potassium channel
VGSC	Voltage gated sodium channel
ω-aga	ω-agatoxin IVA
WT	Wild type

1. Introduction

Channelopathies are disorders caused by inherited mutations of specific ion channels. At a basic level neurological channelopathies provide unique insights into neuronal circuit development, synaptic function and neurotransmitter release. This information can in part explain the pathophysiology of common related paroxysmal disorders such as idiopathic epilepsy and migraine, affecting 1% and 10% of the population respectively (Kullmann, 2010).

Conventional approaches to study the consequences of ion channel mutations using heterologous expression in *Xenopus Laevis* oocytes, human embryonal kidney cells and other simple systems only provide indirect insights into the consequences of ion channel mutations for action potential generation and neurotransmitter release. In principle, knock-in mouse models overcome this limitation.

Some channelopathies are caused by mutations of genes encoding channels that are normally expressed at presynaptic terminals. Up to now, direct investigation of presynaptic ion channel activity has been limited to large specialised calyceal synapses, which are not representative of the majority of synapses in the brain. This thesis describes the application of a novel technique called Scanning Ion Conductance Microscopy (SICM) that was used to directly assess the ion channel function in these micrometre sized synaptic boutons. One early question posed was whether voltage-gated calcium channels that trigger vesicle release in small synapses are confined to the active zone.

This thesis also concentrates on the channelopathy Episodic Ataxia Type 1 (EA1), a disorder characterized by paroxysmal cerebellar incoordination and interictal myokymia (Rajakulendran et al., 2007). EA1 is caused by dominantly inherited mutations of *KCNA1*, which encodes the presynaptic and axonal potassium channel subunit $K_V1.1$. EA1 mutations increase neuronal excitability and neurotransmitter release in neuronal cultures (Heeroma et al., 2009). Although this could be explained by impaired action potential repolarization, leading to an increase in presynaptic calcium influx, the action potential duration measured at the cell body was unaffected in this study. This leaves open the possibility that only the pre-synaptic action potential waveform is broadened in EA1, a question that now can be addressed using SICM.

Finally in some central synapses neurotransmitter release has been shown to depend not only on action potential invasion of the presynaptic terminal, but also on slow subthreshold membrane potential fluctuations propagating from the soma, a process called analogue-digital signalling. Furthermore, due to their electrophysiological properties and axonal localization, K_V1 channels have been proposed to underlie this form of modulation by affecting the presynaptic action potential shape. Using a Kv1.1 knockout mouse, and a mouse model of EA1, we have attempted to understand the role of $K_V1.1$ in analogue-digital signalling.

Thus the aims of the thesis are to

1. Optimise SICM to gain direct electrophysiological recording from small hippocampal synapses in neuronal cultures
2. Use SICM to predict the location of voltage gated calcium channels in small synapses
3. Compare the presynaptic action potential waveform in neurons from a Kv1.1 knockout mouse, an Episodic Ataxia type 1 knock-in mouse, and wild type controls
4. Understand the role of K_V1 channels in axonal analogue-digital signalling.

In this introduction I will discuss the fundamental mechanisms of action potential generation and synaptic neurotransmitter release, with a brief overview of the voltage-gated ion channels that play an integral part in these phenomena. I will also review the clinical manifestations of a number of the currently known neurological channelopathies, and in particular EA1.

1.1 Nerve excitability

It has long been known that ions play a crucial role in muscle and nerve excitability. In a seminal series of papers from 1881 to 1887 Sidney Ringer demonstrated that to maintain an isolated frog heart beating, the perfusing solution had to contain specific relative concentrations of sodium, potassium and calcium (Ringer and Buxton, 1887). Work by Walter Nernst involving diffusion of electrolytes in solution to create electrical potentials strongly suggested an ionic mediator for bioelectric potentials (Nernst 1888). A negative resting membrane potential (RMP) was partly explained

by Bernstein, who proposed that (i) the cell membrane was selectively permeable to potassium ions (ii) intracellular potassium concentration was high and (iii) extracellular potassium concentration was low (Overbeek, 1956). Further explanation of the RMP was provided by the Donnan equilibrium, which accounts for the relatively high intracellular concentration of large molecular weight anions (e.g. negatively charged proteins) that maintains opposite potassium and chloride gradients across the membrane and sets a resting potential. It took two British physiologists, Alan Hodgkin and Andrew Huxley to show in their now famous squid giant axon experiments, that the internal voltage became markedly positive during an action potential (AP) (Hodgkin, 1939). They postulated that this flux was due to increased membrane permeability to sodium ions. Further analysis by the pair led to the Hodgkin-Huxley model for AP generation that is used today, which quantitatively predicts the relative membrane permeability to sodium and potassium ions to evolving membrane potential over time (Hodgkin and Huxley, 1952).

A typical neuron consists of a cell body or soma, dendrites and an axon. The axon is responsible for the conduction of information from the cell body to the nerve terminal. I will now discuss the functional and molecular properties of the three key segments of the axon; the axon initial segment, the axon proper, and the presynaptic terminal.

1.1.1 The Axon Initial Segment (AIS)

The AIS is located between 20 and 40μm from the soma in unmyelinated axons. The scaffolding protein ankyrinG (ankG) is crucial to assembly of the AIS, with sodium and K_V7 channels targeted to the AIS by ankG (Garrido et al., 2003; Pan et al., 2006). However targeting of Kv1 channels in the AIS is under the control of the postsynaptic density 93 (PSD-93) protein, a member of the membrane-associated guanylate kinase (MAGUK) family (Ogawa et al., 2008).

Variations in membrane potential as a result of somato-dendritic integration of a number of synaptic inputs trigger an action potential at the initial segment of the axon (AIS) if they surpass a voltage threshold (Debanne et al., 2011). This proposed role for the AIS would require the region to be highly excitable. Immunohistochemistry (Lorincz and Nusser, 2008a), sodium imaging (Fleidervish et al., 2010) and outside-out patch clamp recordings of the soma and axon (Hu 2009) have shown that sodium channels are present at a higher density in the AIS compared to the somato—dendritic compartment, in the region of 20 – 1000 fold higher (Boiko et al., 2003; Kole et al., 2008; Wollner and Catterall, 1986). $Na_V1.1$, $Na_V1.2$ and $Na_V1.6$ are the main isoforms responsible for spike initiation in cortical neurons in mammals. $Na_V1.1$ is predominantly found in rodent GABAergic neurons (Ogiwara et al., 2007). $Na_V1.2$ and $Na_V1.6$ are found in myelinated and unmyelinated neurons, with $Na_V1.2$ initially expressed and gradually replaced by $Na_V1.6$ through development (Boiko et al., 2001, 2003; Lorincz and Nusser, 2008a).

Potassium channels in the AIS are key in repolarising action potential and regulating neuronal excitability. As K_V1 subunits have a relatively low activation threshold, and so a significant proportion of the current produced by these channels is activated at voltages close to the resting membrane potential (Dodson and Forsythe, 2004; Shu et al., 2007a). $K_V1.1$ and $K_V1.2$ are predominant in the AIS with immunohistochemistry evidence for these subunits in both excitatory and inhibitory neurons (Inda et al., 2006; Lorincz and Nusser, 2008a). $K_V1.1$ and $K_V1.2$ are found more distal to $Na_v1.6$ in the AIS and are associated contribute to a greater current in this region than at the soma. Both subunits also contribute to determine spike duration in the axon (Geiger and Jonas, 2000). $K_V2.2$ in the medial nucleus of the trapezoid body aids maintenance of high frequency firing by causing interspike hyperpolarisation (Johnston et al., 2008) Members of the K_V7 family ($K_V7.2$ – $K_V7.5$) generate muscarinic agonist-sensitive, subthreshold and non-inactivating potassium current, the so-called M-current. $K_V7.2$ and $K_V7.3$ are also located in the AIS of hippocampal principal cells, where they regulate AP spiking and threshold (Shah et al., 2002, 2008; Yue and Yaari, 2006).

Although sodium and potassium channels are sufficient to generate action potentials and repolarise the membrane, a further role for calcium channels has been identified in axons. T-and R-type voltage-gated calcium channels, are found in the AIS of Purkinje calls and neocortical pyramidal neurons and are involved in spike-timing, burst-firing, and action potential threshold. $Ca_V2.1$ (P/Q **Section 4.3**) and $Ca_V2.1$ (N-type) channels have also been located in the Calyx of Held (Inchauspe et al., 2012),

the AIS of Layer 5 neocortical pyramidal neurons and activate BK potassium channels to affect cell excitability (Yu et al., 2010) (Figure 1.1).

1.1.2 Main axon

In unmyelinated axons $Na_V1.2$ channels are evenly distributed in order to facilitate action potential conduction (Boiko et al., 2003; Westenbroek et al., 1989) A number of potassium channels are also present in order to control excitability, including $K_V1.2$ in Schaffer collaterals (Palani et al., 2010), $K_V1.3$ in parallel fibre axons of cerebellar granule cells (Kues and Wunder, 1992), $K_v3.3$ and $K_V3.4$ in hippocampal mossy fibre axons (Chang et al., 2007), and K_V7 channels in CA1 pyramidal cell axons (Gu et al., 2005).

In myelinated axons, Schwann cells, a type of glial cell, wrap multiple layers of their plasma membrane, myelin, around an axon. In addition, at regular intervals the myelin is interrupted by exposed patches of axon called Nodes of Ranvier, that regularly divide sections of myelination with intermodal distance ranging between 200 μm and 2 mm (Lussier and Rushton, 1951). The molecular organisation of the node of Ranvier and juxtaparanodal region is dependent on interactions between proteins from the axon and myelinating glia. During development of the Node of Ranvier, $Na_V1.2$ channels initially are present and then replaced by $Na_V1.6$ (Boiko et al., 2001). Nodes of Ranvier have a very high density of sodium channels, one study reporting twice the density of $Na_V1.6$ than at the AIS in central neurons (Lorincz and

Nusser, 2008a). An impulse is generated at the node and 'jumps' from node to node, termed saltatory conduction. Saltatory conduction is further enforced by the juxtaparanodal representation of potassium channels, namely $K_V1.1$ and $K_V1.2$, and nodal expression of $K_V3.1b$ and $K_v7.2/K_V7.3$, that all act to decrease reexcitation of the axon (Devaux et al., 2003, 2004; Wang et al., 1993; Zhou et al., 1999).

1.1.3 Axon terminal

Spike propagation down the axon ultimately results in the activation of synapses with the opening of presynaptic calcium channels, namely $Ca_V2.1$ and $Ca_V2.2$ (Holderith et al., 2012; Lenkey et al., 2015). Indeed, the $Ca_V2.2$ subunit possesses a specific binding amino acid motif to the presynaptic protein scaffold (Maximov and Bezprozvanny, 2002) and specific deletions to the synaptic protein interaction site in $Ca_V2.1$ inhibit its localisation to axon terminals (Mochida et al., 2003). K_V channels also exhibit a great diversity in the axon terminal. $K_V1.1$ and $K_v1.2$ are present at synaptic terminals in the middle molecular layer of the hippocampal dentate gyrus and terminals of cerebellar basket cells (Wang et al., 1994). $K_v1.4$ are richly represented in mossy fibre boutons, determining spike duration and neurotransmitter release (Geiger and Jonas, 2000). High voltage activated K_V3 subunits have been found in the axon terminals of both excitatory and inhibitory neurons and act to limit action potential duration, and therefore calcium influx and release probability (Chow et al., 1999; Elezgarai et al., 2003; Goldberg et al., 2005).

Hyperpolarisation-activated cyclic nucleotide-gated cationic (HCN) channels are represented in the axon terminals of basket cells both at the hippocampus and cerebellum (Luján et al., 2005; Notomi and Shigemoto, 2004) with their role thought to involve stabalisation of membrane potential at the terminal. G protein inwardly rectifying potassium (GIRK) channels are also found at presynaptic terminals and in the cortex and cerebellum they are activated by $GABA_A$ receptors and function to control action potential duration (Ladera et al., 2008).

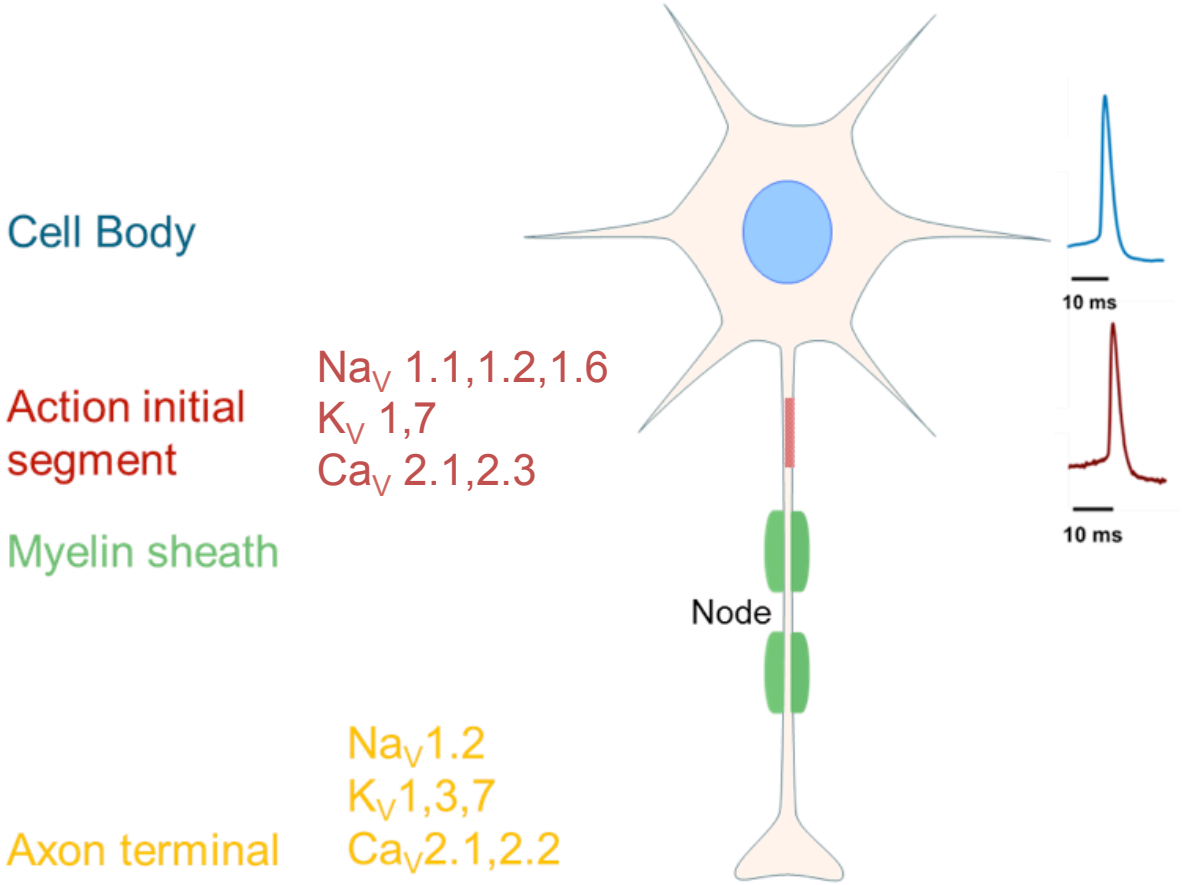

Figure 1.1 **Cartoon of typical neuron**. Channel subunits thought to be associated with particular axonal regions are included. Typical action potential seen at the action initial segment (red) and typical back propagated action potential seen at cell body (blue). Adapted from (Debanne et al., 2011).

1.2 The action potential

The biophysical mechanisms underlying an AP to the best of our current knowledge are as follows. As discussed before the resting membrane potential (RMP) in relation to the external environment is negative (around -70mV) due to the effect of potassium permeability and negatively charged intracellular proteins. As the axon receives a stimulus, membrane sodium channels open in a voltage-dependent manner causing an increased permeability to sodium. During an action potential, the membrane potential moves from near the RMP to close to the sodium reversal potential (around +40mV) as the rapid flux of sodium ions drives an inward current into the cell. To estimate how many sodium ions flow it is helpful to view the membrane as a capacitor. The capacitance of a typical patch of membrane is typically 1μF/cm^2. As charge (Q in Coulomb) = V C, the charge resulting from a 0.11 V shift is 0.11 x 10^{-6} = 1.1 x 10^{-7} Q. As one Coulomb represents the net charge of 6.2 x 10^{18} monovalent ions, this leads to an estimate of the number of ions flowing through the membrane for an action potential as 6.82 x 10^{11} per cm^2 or 6820 per μm^2. This depolarisation is seen as the AP upstroke. In addition this inward current causes depolarisation of adjacent areas of membrane, which opens more channels in these areas causing further inward current and propagation of the nascent signal. The inward sodium current ceases when certain conditions are satisfied, including i) the cell reaches the equilibrium potential for sodium and ii) the already open sodium channels have inactivated, which commences the absolute refractory period (Hodgkin and Huxley, 1952).

The downstroke of the AP results from a contribution of fast inactivation of Na^+ channels and activation of delayed rectifier potassium channels, which are voltage sensitive (Dodson and Forsythe, 2004; Doyle et al., 1998; Isomoto et al., 1997; Neusch et al., 2003). As these channels open upon depolarization, albeit more slowly than sodium channels, potassium ions flow out of the cell restoring the resting membrane potential. Furthermore, potassium channel de-activation is relatively slow compared to sodium channel kinetics, so there is temporary impermeability to sodium but sustained permeability to potassium, causing an after-hyperpolarisation, which takes the membrane to a slightly more negative potential, around -80mV. The refractory period is divided into absolute refractory period followed by relative refractory period. The absolute refractory period is due to the inactivation of sodium channels that remain inactivated until the membrane hyperpolarises. They then de-inactivate and return to a responsive state. During this period no second AP can be generated. The relative refractory period accounts for the time between hyperpolarisation of the membrane and potassium conductance returning to a resting value. During this period the membrane is at a higher threshold, meaning a greater stimulus would be required to generate a second AP.

Action potentials occur in an 'all-or-none' manner, and key to this phenomenon is the threshold for spike initiation. Interestingly it appears that the current threshold for spike initiation is lower in the distal AIS compared to the soma. Conversely the voltage threshold (defined as membrane potential where the rate of change of voltage passes an accepted value, usually 10-50V/s (Anderson et al., 1987)) is higher in the AIS compared to the soma. This is partly due to the abundant Na^+ channels in the AIS causing a depolarising ramp immediately prior to an action

potential. $Na_V1.2$ and $Na_V1.6$ are asymmetrically distributed in the AIS; $Na_V1.2$ is predominantly found in the 25 μm closest to the soma and requires substantial depolarisation for activation. $Na_V1.6$ is found 25 – 50 μm from the soma and is activated by relatively little depolarisation. This configuration is thought to work as thus: depolarisation in the postsynaptic compartment spreads beyond the soma into the AIS. It will not be sufficient to activate the high threshold $Na_V1.2$ channels in the proximal AIS but would activate the low threshold $Na_V1.6$ channels in the distal axon, resulting in a forward propagating AP. The opening of $Na_V1.6$ channels then drives opening of the initially bypassed $Na_V1.2$ channels inducing a secondary wave of inward sodium current and causing a backpropagating AP. As this occurs the $Na_V1.6$ channels now in an inactivated state prevents the possibility of a secondary forward-propagating AP (Dulla and Huguenard, 2009; Hu et al., 2009). Variability in AP spike threshold may be dependent on the stochastic opening of voltage-gated channels, the temporal relationship between spikes, and the frequency of the subthreshold waveform during propagation.

1.2.1 Cable theory

Fast spread of neuronal activity occurs by electric current, dependent on basic properties of the nerve cell termed electrotonic properties. Our understanding of electrotonic properties have derived from unrelated work including heat conduction in solids (H.S. Carslaw and J.C. Jaeger, 1959) and submarine telegraph cables, hence the use of the word ‘cable’ when discussing neurons. The cable can then be subdivided into compartments, with its constituent organelles, for which an

equivalent electrical circuit can be derived including membrane capacitance (C_m), membrane resistance (r_m), resting membrane potential (E_r) and internal resistance (r_i) (W. Rall, 1958).

A key parameter determining electrotonic spread is the length constant (λ) of the cable. Under steady state conditions electrotonic potential obeys the formula:

$V = V_0e^{-x/\lambda}$, where λ is the characteristic length of the cable and defined as square root of r_m/r_i and for an infinite cable and V_0 is the potential at the site of input (i.e. x = 0). Thus when x = λ, and values for internal and membrane resistance are assumed, electrotonic potential would decay by 63% of the value at the site of input. As the equation dictates, a larger membrane resistance is associated with a larger space constant resulting in reduced attenuation of electrotonic potential. Conversely a larger internal resistance is associated with a smaller λ leading to greater attenuation of V. R_i is estimated at 200Ω cm in mammalian neurons. By derivation λ is also related to the square root of diameter difference; thus a larger diameter axon will have a larger λ.

An assumption of classical cable theory is that neuronal processes are infinitely long. To relate characteristic length of neurons (λ) to their 'real' length (L) the following equation is observed: $L = x/\lambda$. From this one can see that for very long axons, electrotonic potential would decay by only a small fraction of the original value for each λ, making it safe to assume it is of infinite length. However this would not be the

case for other neuronal processes such as dendritic branches. As this thesis concerns axonal propagation, we can consider them as infinite cables.

1.2.2 Transient signal spread

In addition to the steady state electrotonic properties, passive spread of transient potentials depends on membrane capacitance. The membrane capacitance (C_m) and membrane resistance (R_m) are responsible for defining the time constant (τ) of the membrane ($\tau = R_mC_m$). τ is the voltage response of the membrane in terms of the electrotonic properties of the patch when a transient potential such as a current step is applied. This is important as the charging and discharging of the membrane in response to a current step are determined by τ.

Signal spread may be explained by a two compartment model (Shepherd and Koch, 1998)(Figure 1.2.3). Localised conductance changes across a membrane, for example during an action potential or current step, propagate via two routes. First, the inward positive charge in a particular compartment opposes the negative charge on the inside of the lipid membrane (the charge responsible for the negative action potential), thus depolarising the membrane capacitance (C_m); and flows as a current through the membrane via the resistance of open ionic membrane channels (R_m). Second, the charge spreads via internal resistance (R_i) to the neighbouring compartment. This is called a local current.

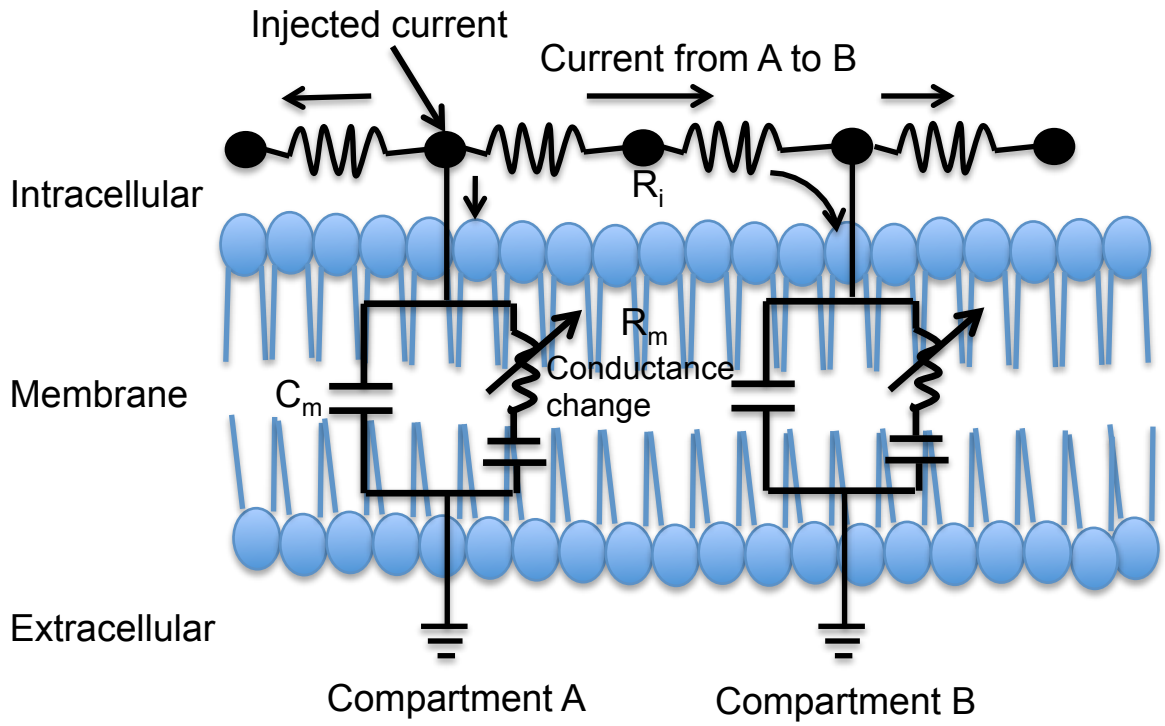

Figure 1.2.3 Diagram of the two compartment model. C_m membrane capacitance; R_m membrane resistance; R_i internal resistance. Adapted from (Squire et al., 2003)

In an unmyelinated axon, which is the focus of this thesis, local current spreading through the internal resistance to the neighbouring compartment permitting the action potential to propagate along the axonal membrane. Speed of propagation is dependent on the electrotonic properties of the axon and the kinetics of the action potential. C_m is important in controlling rate of change of membrane potential in response to brief signals such as APs. R_i increases opposition to electrotonic current, especially in thin axons with shorter characteristic lengths. Increasing R_m promotes current further along the membrane and increases the characteristic length. However it also increases membrane τ, slowing the response of the neighbouring compartment. Finally diameter of the axon reduced R_i thus increasing the characteristic length. Other factors include channel density. The greater the

density of sodium channels, the steeper the AP upstroke, thus creating a larger spatial voltage gradient. This means that the depolarization of the nearby axonal segment is quicker, resulting in an increased conduction velocity. Axonal patch-clamp recordings have measured conduction velocity to be 0.2 m/s in unmyelinated axons such as Schaffer collaterals and mossy fibre axons (Andersen et al., 2000; Kress et al., 2008) and 0.38 m/s in CA3 pyramidal axons (Meeks and Mennerick, 2007).

Briefly, myelinated axons are equipped for fast conduction. Myelination effectively introduces more series resistances and capacitances in the circuit, and therefore increasing R_m and decreasing C_m. The Hursh factor states that rate of propagation of an impulse in a myelinated axon is six times the diameter of the axon in micrometres (Hursh, 1939). as mentioned above, Node of Ranvier. Therefore a myelinated axon is a passive cable with active booster sites.

1.2.3 AP waveform

The presynaptic AP shape has an important role in controlling neurotransmitter release and synaptic strength. The waveform itself determines the calcium signal produced in order to promote synaptic vesicle fusion. In hippocampal mossy fibre boutons (MFBs), large specialised presynaptic terminals that made by axons of dentate granule cells on CA3 pyramidal neurons, it has been estimated that the calcium influx scales roughly linearly with AP width (Geiger and Jonas, 2000). At

these presynaptic boutons AP width is roughly half of that recorded at the soma. However during repetitive stimulation, AP width at the terminal increases but at the soma remains fixed. Using pre- and postsynaptic recordings at granule cell/CA3 neurons, it was demonstrated that AP broadening caused increased presynaptic calcium influx and doubled EPSC amplitude (Geiger and Jonas, 2000). It has been suggested that presynaptic AP broadening is due to inactivation of potassium channels. Potential candidates include $K_V1.1$ and $K_V1.4$ as both subunits have been identified at MFBs; however both demonstrate relatively small single-channel conductances (Wei et al., 2005). K_V3 channels have been reported to show around a 10-fold greater repolarisation efficacy compared to K_V1 with a suggested role of promoting brevity of presynaptic AP (Alle et al., 2011). Large-conductance calcium and voltage-activated potassium channels (BKCa) have also been found at MFBs, and are thought to mediate fast activating/fast inactivating and sustained potassium current during long depolarisations (Knaus et al., 1996; Kues and Wunder, 1992).

Cumulative sodium channel inactivation from repetitive stimulation also causes a decrement in AP amplitude (Williams and Stuart, 1999). Depolarisation of the presynaptic terminal results in synaptic depression in hippocampal cells (He et al., 2002) and Shaffer collateral-CA1 synapses (Meeks and Mennerick, 2007). Interestingly this phenomenon is not seen in GABAergic synapses (Meeks and Mennerick, 2007).

1.2.4 'Analogue' and 'Digital' axonal signalling

Neuronal circuitry operations have conventionally been viewed as occurring through the “analogue” interaction of synaptic potentials in the dendrite and soma, followed by the initiation of an action potential in the axon, in an all-or-none or “digital” manner. More recently it has been shown that voltage fluctuations associated with dendrosomatic synaptic activity propagate significant distances along the axon, and that modest changes in the somatic membrane potential of the presynaptic neuron modulate the amplitude and duration of axonal action potentials. This hybrid analogue-digital modulation of synaptic transmission has been described in invertebrates (Nicholls and Wallace, 1978; Shimahara and Peretz, 1980), cortical CNS synapses (Kole et al., 2007a; Shu et al., 2006), cerebellar (Bouhours et al., 2011; Christie et al., 2011) and, of relevance to this project, hippocampal synapses (Bialowas et al., 2015; Debanne et al., 1997; Sasaki et al., 2011; Scott et al., 2008) (Figure 1.2.4).

Analogue-digital facilitation by subthreshold somatic depolarization leads to increases in glutamate (Kole et al., 2007) or GABA release (Christie et al., 2011). Two independent mechanisms have been reported to account for the analogue–digital enhancement of transmission in central synapses: increase in basal Ca^{2+} concentration and inactivation of presynaptic K^+ channels**.** Propagated depolarization can facilitate synaptic transmission by the opening of voltage-gated calcium (Ca_V) channels, which results in an increase in basal Ca^{2+} concentration in presynaptic terminals. It appears that $Ca_V2.1$ and to a lesser extent $Ca_V2.2$ channels are responsible for this facilitation, whether in the axon terminal (Bouhours et al., 2011)

or in the axon itself (Yu et al., 2010), The increase in basal Ca^{2+} concentration triggered by subthreshold depolarization may directly promote neurotransmitter release or accelerate the recruitment of vesicles to the active zone (Neher and Sakaba, 2008).

Axons contain a high density of voltage-gated K^+ (K_V) channels. Initially it was shown that activation of an I_A like potassium conductance could locally abort propagation of presynaptic action potentials in CNS axons (Debanne et al., 1997). It was then thought that depolarization of the somatic region of the presynaptic neuron could facilitate synaptic transmission as a consequence of voltage-inactivation of a specific type of K^+ channel. In neocortical and hippocampal pyramidal neurons, for example, the K_V1 channels generate a fast-activating but slowly-inactivating D-type current (I_D) that reduces spike duration and thus controls neurotransmitter release (Boudkkazi et al., 2011; Shu et al., 2007a). Pharmacological inactivation of I_D with 4-aminopyridine or dendrotoxin enhances synaptic strength at hippocampal and neocortical synapses possibly by broadening the presynaptic spike in the terminal, resulting in higher release of neurotransmitter (Saviane et al., 2003). Also, the kinetics of the analogue–digital enhancement fit well with the inactivation kinetics of I_D (Kole et al., 2007a; Shu et al., 2006). Finally, voltage inactivation of K_V1 channels causes a significant enhancement of the calcium transient in the presynaptic terminal evoked by the propagating spike in the presynaptic terminal (Yu et al., 2010). Enhanced neurotransmitter release by the inactivation of K_V1 channels is not restricted to just depolarization of the presynaptic neuron. Extrinsic signals, such as glutamate released from astrocytes, that are present abundantly adjacent to hippocampal

axons and their terminals can also modulate the width of action potentials in axons and enhance synaptic transmission in an analogue manner (Debanne et al., 2013; Sasaki et al., 2011).

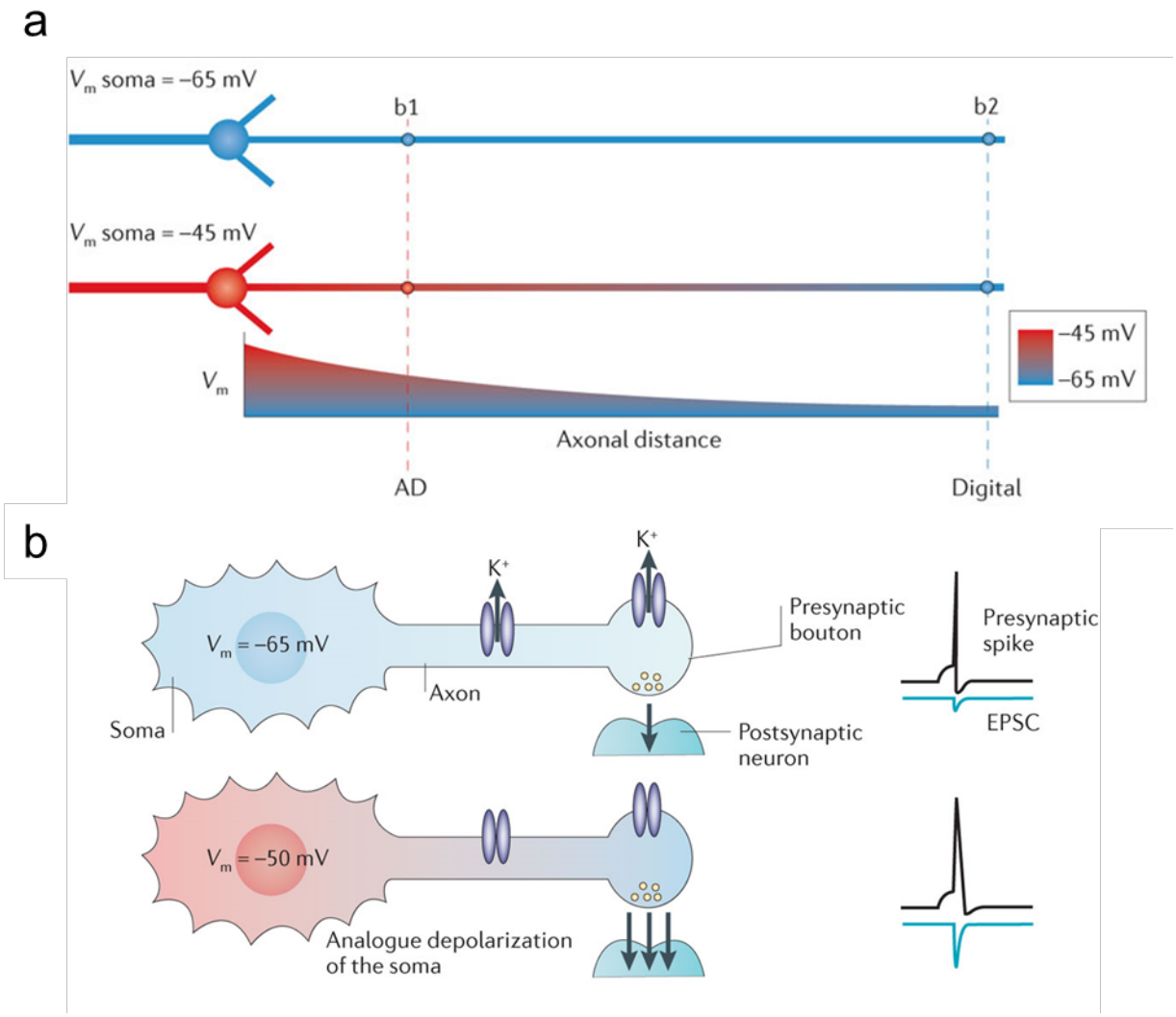

Figure 1.2.4 Schematic of analogue-digital facilitation (a) Spatial gradient of hybrid and digital (top) and analogue-digital (bottom) transmission. Due to cable properties, analogue-digital transmission is restricted to proximal presynaptic boutons (b1), whereas pure digital transmission occurs at distal boutons (b2); V_m, membrane voltage (b) Facilitation resulting from voltage-inactivation of voltage-gated K_V1 channels. With digital-only signalling (top neuron), the neuronal membrane voltage

(V_m) rests at −65 mV and K_V1 channels remain open, resulting in a rapid termination of the spike response. Analogue subthreshold depolarization (bottom neuron; −50 mV at the soma) propagates from the somatic compartment and along the axon to the terminal (the gradual decay in depolarization is indicated by red-to-blue shading), resulting in closure of K_V1 channels and attenuated K^+ efflux. This produces a broader action potential and results in enhanced spike-evoked Ca^{2+} entry and incremented neurotransmitter release (single black arrow). Adapted from (Debanne et al., 2013).

1.3 The synapse

Electrical and Chemical Synapses

To our knowledge, chemical synapses number trillions in the adult human brain and have a crucial role in information processing between neurons. Synapses are broadly divided into electrical and chemical synapses. Electrical synapses are composed of direct intercellular connections or gap junctions that allow the direct passive flow of univalent ions between cells. The main function of electrical synapses is to synchronize electrical activity among populations of neurons (Bennett and Zukin, 2004).

However most synapses are chemical. Chemical neurotransmission involves the release of neurotransmitters or neuropeptides from the pre-synaptic cell, and their diffusion across a space or synaptic cleft, which typically measures between 15 and 25 nm, to act on postsynaptic receptors (Südhof, 1995). The chemical neurotransmitters that are released from the presynaptic cell are packaged into synaptic vesicles in the presynaptic membrane. These vesicles fuse with the presynaptic membrane, releasing the neurotransmitter into the synaptic cleft. Various different types of chemical neurotransmitter exist and can be classified either by structure into amino acids (such as glutamate, γ-aminobutyric acid (GABA and glycine), monoamines (including dopamine, noradrenaline and serotonin), peptides (including somatostatin, substance P and opioids) and others such as acetylcholine; or by their action i.e. whether they are excitatory or inhibitory. Glutamate is the predominant excitatory neurotransmitter in the central nervous system (CNS),

binding to multiple different excitatory receptors including NMDA receptors, AMPA receptors and kainate receptors, which allow influx of positively charged ions and subsequent depolarization of the postsynaptic neuron.

1.3.1 Mechanism of chemical synaptic transmission

Initially neurotransmitters are synthesised in the cell body or at the presynaptic terminal. Neurotransmitters are then loaded into synaptic vesicles via active transport, a process involving an electrochemical gradient created by a proton pump which transports H^+ ions (Ahnert-Hilger et al., 2003). Neurotransmitter uptake into vesicles occurs via specific vesicular transporters that use either the proton or the electrical gradient. The synaptic vesicles containing neurotransmitter then dock near the synaptic terminal adjacent to presynaptic Ca^{2+} channels due to the action of a protein complex containing RIM proteins (Südhof, 2013). The area where the synaptic vesicles cluster is known as the “active zone”, an electron dense region directly opposite the postsynaptic density. At small central glutamatergic synapses typically 8-10 vesicles are docked and thought to be immediately ready for release (Schikorski and Stevens, 2001; Xu-Friedman et al., 2001).

Resting intracellular calcium concentration is around 0.1 μM, with a reversal potential of +50 mV. The action potential at the presynaptic nerve terminal membrane triggers a conformational change in VGCCs, which allows entry of Ca^{2+} from the extracellular space (Katz and Miledi, 1967; Schneggenburger and Neher, 2005). The subsequent

increase in intracellular Ca^{2+}, which, at the release site, reaches a concentration in the order of tens of micromoles per litre. There are two phases to calcium evoked neurotransmitter release; a synchronous fast phase that occurs up to 0.5ms. after calcium influx, and a slower asynchronous release. Members of the synaptotagmin family (Syt1, Syt2, and Syt9) function as calcium sensors for synchronous release and Syt7 for asynchronous release (Südhof, 2013). Most is known about Syt1, a synaptic vesicle protein with two cytoplasmic C_2 domains (C_2A and C_2B) that bind Ca^{2+}. It has been proposed that upon Ca^{2+} influx, Ca^{2+} binding to the C_2B domain especially of Syt1 promotes bringing vesicle and plasma membranes together and in tandem with C−terminal zippering of the SNARE complex (as discussed later), causes membrane fusion.

It is thought that for vesicle and presynaptic nerve terminal membrane fusion to occur, the respective bilayers bend to cause destabilisation and create a stalk where the proximal leaflets have fused and the distal leaflets create a fusion pore that then expands (Chernomordik and Kozlov, 2008). SNARE proteins are key to exocytosis and include the synaptic vesicle protein Synaptobrevin/VAMP (vesicle-associated membrane protein) and the plasma membrane proteins SNAP−25 and Syntaxin−1 (Rizo and Xu, 2015). One model involves the three SNAREs forming into a tight complex that draws the membranes close to each other. Another model suggests that the starting point of exocytosis may be with Syntaxin−1 in a self-inhibited conformation, that then binds to Munc18-1 (a member of the Sec1/Munc18 protein family) to form a complex on the plasma membrane, which orchestrates a partially assembled SNARE complex, thus priming the membrane for fusion (Südhof and Rothman, 2009). Indeed intermediates where only the N−terminal half of the SNARE

complex has assembled either in zig−zag or half zippered array, have been viewed in vitro (Kümmel et al., 2011; Li et al., 2014). Another small soluble protein associated with the SNARE complex named Complexin has an intriguing role in both promoting and inhibiting exocytosis, with evidence of its interaction with Syt1 and SNAREs (Dai et al., 2007; Tang et al., 2006). It is thought the central helix of Complexin stabalises the SNARE complex whereas the accessory helix has an inhibitory role. A model would be that before calcium influx into the presynaptic terminal, the negatively charged accessory helix of Complexin prevents membrane fusion through electrostatic repulsion. However Syt1 interacts with Complexin resulting in dissolution of the accessory helix, relieving the inhibition and inducing fusion (Tang et al., 2006). Once the synaptic vesicles have fused with the presynaptic nerve terminal membrane, the neurotransmitters can diffuse across the synaptic cleft and subsequently bind to specific receptors on the postsynaptic membrane. Also after fusion the SNARE complex is dismantled by NSF, an ATPase from the AAA family, and SNAPs in order to be recycled for another round of fusion (Mohrmann et al., 2010).

In response to neurotransmitter binding, ligand-gated receptors undergo a conformational change that leads to opening of an ion channel. Binding of neurotransmitters to G protein-coupled receptors triggers signalling pathways including, depending on the receptor subtype, adenylate cyclase, protein kinase C, and G-protein-coupled potassium channels. For ligand-gated ion channels, depending on their ion selectivity, the postsynaptic membrane will either be depolarized (cations) or hyperpolarized (anions). If the ligand-gated ion channel is cation-permeable, as is the case for ionotropic AMPA, kainate or NMDA glutamate

receptors, the postsynaptic current is depolarizing. If it is large enough it will induce an action potential in the post-synaptic cell (Figure 1.3.1).

Synaptic transmission is a dynamic process. Repeated use of synapses can either cause synaptic facilitation or depression. Synaptic facilitation has been shown to be presynaptic in origin with short-term enhancement dependent on presynaptic intracellular calcium (Brain and Bennett, 1995; Kita and Van der Kloot, 1974). It is thought that Ca^{2+} acting at sites distinct to the fast low-affinity site triggering exocytosis (Delaney and Tank, 1994; Regehr et al., 1994) is responsible for synaptic enhancement, via a number of potential mechanisms. In the 'buffer saturation' model, initial calcium influx to the first action potential is buffered, but subsequent action potentials result in increased Ca^{2+} targeting release sites as the buffer saturates. Another theory based on Ca^{2+} diffusion simulations suggests that the slow residual Ca^{2+} kinetics govern length of synaptic enhancement. One muted sensor for residual calcium has been Syt7 (Jackman et al., 2016) as it is a presynaptic protein with high affinity and slow kinetics. Synaptic depression is likely secondary to decrease of neurotransmitter release upon a period of elevated activity as a result of depletion of the ready release pool of vesicles (Zucker and Regehr, 2002)

After exocytosis vesicles undergo endocytosis and recycle and refill with neurotransmitter for a new round of exocytosis in a "trafficking cycle" (Sudhof, 2004). This recycling process is important as small presynaptic nerve terminals only contain a few hundred vesicles on average and an efficient recycling process is necessary to preserve synaptic transmission and synaptic morphology (Klingauf et al., 1998;

Rothman et al., 2016). A number of different mechanisms of synaptic vesicle recycling have been proposed. These include (1) so-called “kiss and stay” whereby vesicles are re-acidified and refilled with neurotransmitter without undocking (van Kempen et al., 2011), (2) “kiss and run” where vesicles undock and recycle locally to re-acidify and refill with neurotransmitter via a transient pore between the synaptic membrane and the vesicle (Ceccarelli et al., 1973; Harata et al., 2006; Klingauf et al., 1998; Richards et al., 2005), and (3) a process by which vesicles endocytose via clathrin–coated pits and then refill with neurotransmitters either immediately or via an endosomal intermediate (Sudhof, 2004).

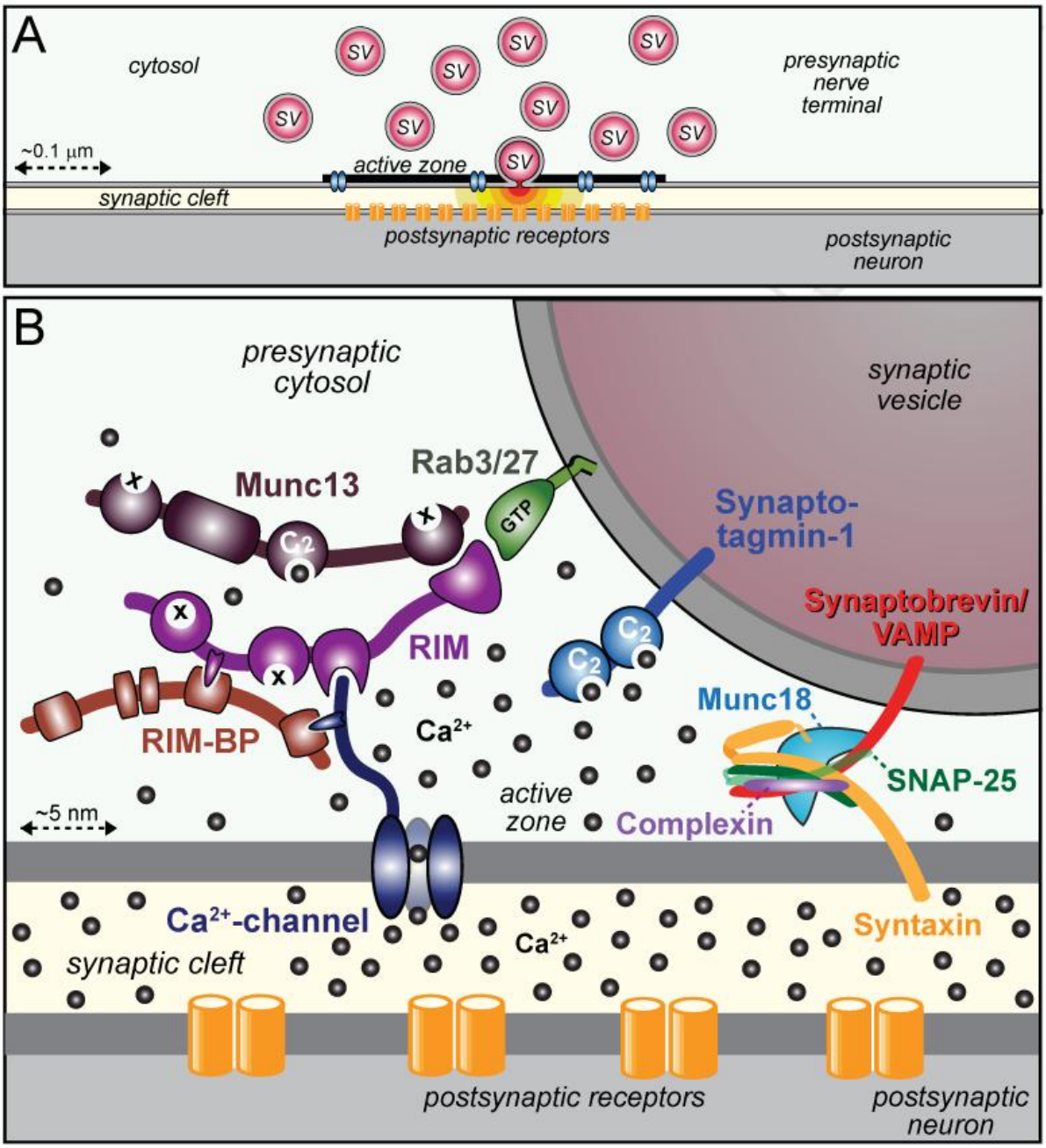

Figure 1.3.1 Schematic of the molecular machinery involved in Ca^{2+} evoked vesicle fusion. (A) A synapse with Ca^{2+} channels in blue and vesicles denoted SV. (B) A summary of the fusion process as described above. Taken from (Südhof, 2013).

1.4 The evolution of voltage gated channels

Ion channels are broadly characterised as either ligand-gated (also known as ionotropic receptors) or voltage-gated. Ion channels of both types are multimeric proteins, generally glycosylated on their extracellular segments. Although there are some homomultimers, the majority of channels are assembled from a number of subunits, each one coded for by a separate gene (heteromultimers).

Voltage-gated channels are constituted of one or more pore forming subunits (α subunit) and variable numbers of accessory subunits (β,γ… subunit). They mainly respond to membrane potential depolarization by opening, although some mixed cation permeable channels open, in contrast, upon hyperpolarization. The subunits determine ion selectivity and mediate the voltage-sensing functions of the channel. I will concentrate on the voltage gated sodium, potassium and calcium channels (VGSCs, VGKCs and VGCCs) as they are the focus of my experiments.

1.4.1 Voltage gated sodium channels

The voltage gated sodium channel (VGSC) gene family consists of nine homologous members (*SCN1A* to *SCN11A*) that code for the sodium selective ion channels $Na_V1.1$ to $Na_V1.9$ (Table 1.4.1). *SCN6A* and *SCN7A* encode the Nax channel, which is structurally related to other VGSCs but activated by change in sodium concentration rather than membrane depolarisation. VGSCs are composed of a

large α subunit (~260 kDa) containing four homologous domains, each of which consists of six transmembrane segments. Only one α subunit alone is necessary to form a functional channel, but α subunits also combine with β-subunits (β1-4 encoded by *SCN1B* to *SCN4B*), which modulate the biophysical and trafficking properties of the channel (Eijkelkamp et al., 2012). The transmembrane domains S1-S4 in each domain of the VGSC constitute the voltage sensor domain (VSD) and S5-S6 arrange to form the sodium selective pore (Catterall et al., 2005) (Figure 1.4.1a). The selectivity filter, the narrowest part of the channel's open pore, is lined with amino acid residues that specifically interact with the permeating ion, plays a major role in determining sodium selectivity. Different sodium channels have different selectivity filters, which vary in the symmetry, number, charge, arrangement, and chemical type of the metal-ligating groups and pore size. As mentioned above (**Section 1.2**) VGSCs are generally closed at resting membrane potential, and require membrane depolarisation to be activated, generating the upstroke in the AP. VGSCs inactivate within milliseconds of activation or faster, terminating the AP upstroke and helping to initiate its downstroke (Figure 1.4.1b). VGSC activation is thought to occur via the movement of the S4 segment in the VSDs of domains I-IV. The S4 segments contain a repeated pattern of positively charged amino acids (typically arginines) interleaved by two or three hydrophobic residues, arranged in an α helix. Outward movement of S4 segments in domains I-III results in a conformational change in the protein, opening the ion channel pore. Inactivation closes the channel and prevents it from reopening until there has been sufficient time for recovery, which helps to determine the frequency of action potential firing. VGSCs exhibit both fast and slow inactivation. Fast inactivation occurs by a 'ball-and-chain' or 'hinged lid' mechanism, in which a cytoplasmic region (the inactivating

particle) occludes the pore by binding to a region nearby (the docking site). The inactivating particle consists of a portion of the cytoplasmic linker connecting domains III and IV, with the crucial region centring on a four amino acid stretch consisting of isoleucine, phenylalanine, methionine and threonine (IFMT) (Figure 1.4.1b). The docking site consists of multiple regions including the cytoplasmic linkers connecting segments 4 and 5 (S4-S5) in domains III and IV and the cytoplasmic end of the S6 segment in domain IV. Slow inactivation is a separate process that does not involve the III-IV linker inactivation particle. It is likely that slow inactivation involves a significant conformational change of the channel that includes a rearrangement of the pore, but the actual mechanism that prevents ionic flow is still unknown (Goldin, 2003).

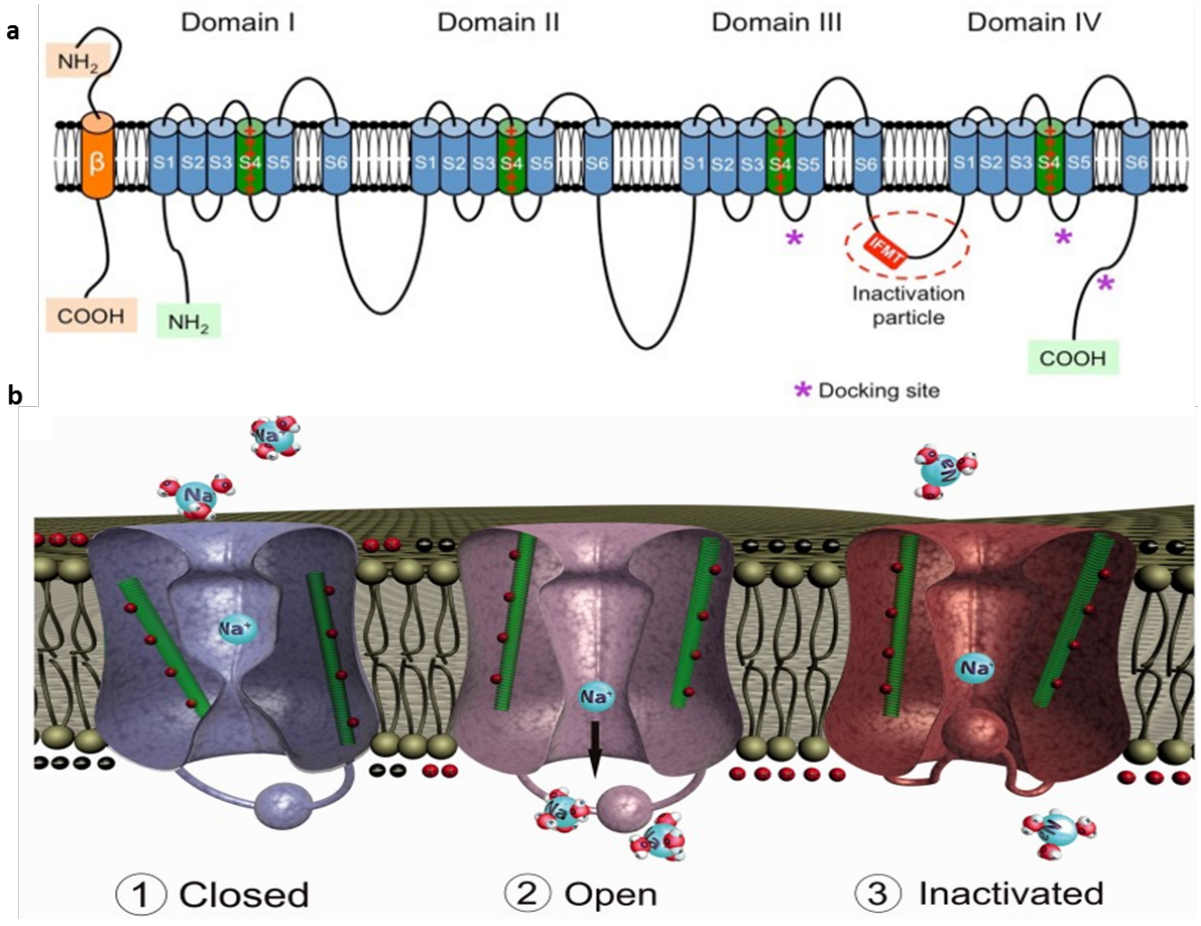

Figure 1.4.1 (a) **Schematic representation of the α- and β-subunits of the VGSC**. The four homologous domains (I–IV) of the α-subunit are represented; S5 and S6 are the pore-lining segments and S4 is the core of the voltage sensor. In the cytoplasmic linker between domains III and IV the IFMT (isoleucine, phenylalanine, methionine, and threonine) region or 'inactivation gate' is indicated (b) Mechanism of voltage sensitive gating of VGSCs. The left channel represents a VGSC in a deactivated (closed) state. A small depolarization of the membrane potential causes a movement of the positively charged S4 voltage-sensor domain (green) leading to a conformational change in the protein and opening of the pore (middle channel). Following activation, the pore is rapidly occluded by the inactivation gate, resulting in inactivation of the sodium channel (right channel) (Savio-Galimberti et al., 2012)

Gene	Na_V channel type	Distribution
SCN1A	$Na_V1.1$	Central neuron cell bodies 'Brain type I'
SCN2A	$Na_V1.2$	'Brain type II' central neurons Mainly unmyelinated/premyelinated axons
SCN3A	$Na_V1.3$	Central neuron cell bodies (embryonic);
SCN4A	$Na_V1.4$	Skeletal muscle
SCN5A	$Na_V1.5$	Denervated skeletal muscle
SCN8A	$Na_V1.6$	Somatodendritic distribution in cerebellar/ cerebral cortex/hippocampal output neurons. Purkinje cell – cerebellar granule cell layer; astrocytes and Schwann cells; DRG; CNS/PNS Nodes of Ranvier;
SCN9A	$Na_V1.7$	DRG neurons; sympathetic neurons, Schwann cell; neuroendocrine cells
SCN10A	$Na_V1.8$	DRG neurons (Verkerk et al., 2012)

SCN11A	$Na_V1.9$	DRG c-type neurons (nociceptive)
SCN7A	Na_X	Neurons of DRG, hippocampus, thalamus, cerebellum, median preoptic nucleus;

Table 1.4.1 summarises the genes that encode the known Na_V channel types and their cellular expression. Adapted from (Savio-Galimberti et al., 2012) DRG: dorsal root ganglia; CNS: central nervous system; PNS: peripheral nervous system;

1.4.2. Potassium channels

Potassium channels represent the most diverse group of ion channels for a number of reason including the large number of genes coding for potassium channel subunits, with further possibility conferred by alternative splicing, heteromeric assembly of different subunits, possible RNA editing and posttranslational modification (Coetzee et al., 1999). During development, potassium (K^+) currents are the first voltage-gated currents to appear in neurons (Veh et al., 1995). The channel expression varies substantially among different types of neurons. Hippocampal neurons possess a distinct pattern of potassium channels, which are sorted to the axonal or dendritic compartment in a cell-specific manner (Prüss et al., 2010). The time-dependent K^+ channel appearance during development suggests profound regulatory mechanisms linked to synaptogenesis and synaptic activity (Frotscher et al., 2000; Maletic-Savatic et al., 1995).

Over 100 different subunits of distinct types of potassium channels have been identified, including voltage gated, ligand-activated potassium channels, inward rectifiers, and “leak” potassium channels. The standard potassium channel clusters four subunits to create the ion permeation pathway across the membrane. Two transmembrane helices (2TM) with a short loop between them (termed the P loop) is a universal feature of all potassium channels. Indeed potassium subunits can be divided broadly into four groups depending on the number of transmembrane domains they possess; either six (voltage gated potassium channels, ligand-activated potassium channels), four (“Leak” potassium channels), two (inward rectifier potassium channels) or eight with 2 P loops (8TM/2P that are hybrids of 6TM/P and 2TM/P and first identified in yeast) (Figure 1.4.2).

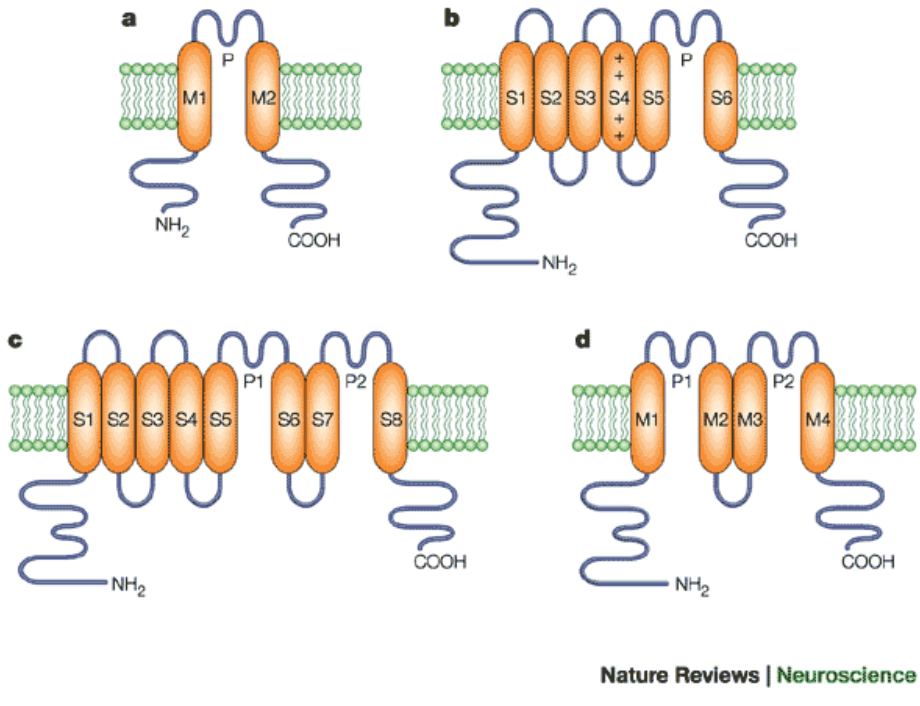

Figure 1.4.2. (a) 2TM/P channels exemplified by inwardly rectifying K^+ channels (b) 6TM/P channels, which are exemplified by ligand-gated and voltage-gated

K^+ channels (c) 8TM/2P channels (d) 4TM/2P channels, which consist of two repeats of 2TM/P channels and exemplified by “leak” channels. S4 is marked with plus signs to indicate its role in voltage sensing in the voltage-gated K^+ channels (Taken from (Choe, 2002).

Inward rectifying (Kir) channels were first identified by expression cloning. To date there are seven subfamilies of Kir (Kir1 – Kir7). The “inward-rectifying” property enables positive charge moves more easily into the cell than out of the cell, suggesting a role for stabilising resting membrane of potential of a cell. Although postulated by Hodgkin and Huxley, the existence of “leak” potassium channels were proven relatively recently in *Saccharomyces cerevisiae* and *Caenorhabditis elegans* (Ketchum et al., 1995). “leak” or Two−P potassium channels demonstrate a voltage-independent portal with Goldman-Hodgkin-Katz rectification. There are 15 known members of the Two−P channel family ($K_{2P}1.1$ – $K_{2P}18.1$ channels) (Goldstein et al., 2005).

Potassium channels are highly selective. Ion selectivity takes place at the narrowest part of the ion-permeation pathway, known as the selectivity filter (Bezanilla and Armstrong, 1972). The crystal studies of the bacterial potassium channel KcsA estimated the filter as ≈ 12 Å long and ≈ 2.5 Å in diameter and showed that the main constituents of the filter are carbonyl oxygens from the amino-acid residues Thr–Val–Gly–Tyr–Gly, which are characteristic of the P loop (Doyle et al., 1998). From this evidence it appears the selectivity process is a series of stereochemical checkpoints, with each checkpoint consisting of four oxygen atoms that form the corners of a

square. This would allow the hydration shell of the potassium ions to be replaced with pore oxygens as they enter the channel. Six potassium binding sites have been identified along the selectivity filter; four internal (P1 – P4) and two external (P0 – P5). P1 – P4 are found between two adjacent oxygen squares, to provide eight oxygen atoms that can coordinate a potassium ion. P0 is at the external entrance and P5 is at the internal entrance to the filter. It is this configuration that provides a low energy barrier and therefore greater selectivity for potassium ions compared with other cations; such as sodium ions where the energy barrier is ≈ 1000 time greater (Bernèche and Roux, 2001).

1.4.2.1 Molecular properties of VGKCs

Molecular characterisation of K_V channels has been a difficult process, mainly due to the diversity of K_V channel α subunits and their potential for oligomerisation. The first breakthrough came from isolating cDNAs encoding the K_V channel α subunit at the *Shaker* gene locus in the fruit fly *Drosophila melanogaster (Kamb et al., 1987; Papazian et al., 1987)*. This work proposed that the K_V α subunit was analogous to one of the four internally repeated homologous domains of a Na_V or Ca_V channel, and that K_V channels were functional tetramers of individual α subunits. Other potassium channel genes were then identified; *Shab* encoding K_V2, *Shaw* encoding K_V3 and *Shal* encoding K_V4 channels. From the first isolation of mammalian $K_V1.1$ cDNA, the remaining *Shaker*-related members, $K_V1.2$ – $K_V1.7$ (corresponding to the KCNA1 – 7 genes) were isolated. Heterologous cell expression demonstrated distinct functional properties between the K_V1 subunits, and that different K_V1

subunits could coassemble to form heterotetrameric channels with functional properties different to their homotetrameric equivalents.

VGKCs are composed of four homologous α subunits. Each subunit contains six transmembrane segments (S1–S6), linked by extracellular and intracellular loops. Both N- and C-termini are cytoplasmic (Figure 1.4.2b). The specific 2TM/P domain is flanked by cytoplasmic protein interacting domains, including a conserved amino – terminal tetramerization domain. Flow rate through these channels is approximately equivalent to the diffusion limit of the cation. To determine the conductivity of VGKCs a gating mechanism is present. One of the transmembrane segments (S4) has several positively charged amino acids, and spectroscopic studies have shown that this S4 helix undergoes conformational change upon membrane depolarization on a timescale equivalent to voltage activation of the channel (Glauner et al., 1999). In the closed state of the channel, the positive residues associated with the S4 helix lie within a narrow space that is open to the intracellular solution. As the channel opens, S4 rotates anticlockwise and tilts leaving the charged residues now exposed to the extracellular side (Cha et al., 1999). This movement underlies voltage-dependent channel activation (opening of the ion pore). Fast inactivation (or closure in the face of continued depolarization) occurs through an inactivation ball that resides at the amino – terminal end of the protein and can physically plug the pore. Despite there being four identical balls, only one inactivation peptide is required to inactivate the channel. Figure 1.4.2 represents the phylogenetic tree of 6 transmembrane domain channels and Table 1.4.2. summarises the distribution and function of known K_V subtypes. Heterologous studies have indicated that K_V1 α subunits can generate either transient (K_V1.4) or sustained (K_V1.1 – K_V1.3, K_V1.5, K_V1.6) currents.

In addition to the four α subunits, voltage-gated potassium channels of the K_V family also contain accessory cytoplasmic β subunits. The majority of K_V1 channel complexes in the mammalian brain have associated $K_V\beta$ subunits. Four $K_V\beta$ genes have been identified in humans with the possibility for many more isoforms via alternative splicing. The inclusion of $K_V\beta$ alters the functional properties of the channel; for example inclusion of $K_V\beta1.1$ in $K_V1.1$ or $K_V1.2$ containing channels significantly alters gating properties from delayed-rectifier type to rapidly inactivating or A-type. Accessory subunits for K_V4 channels are two types of proteins, calcium binding KChIPs and dipeptidyl-peptidase-like protein (DPPX) (An et al., 2000; Nadal et al., 2003). In addition "electrically silent" α subunit-like polypeptides have been reported (Patel et al., 1997) although their function and expression is unclear.

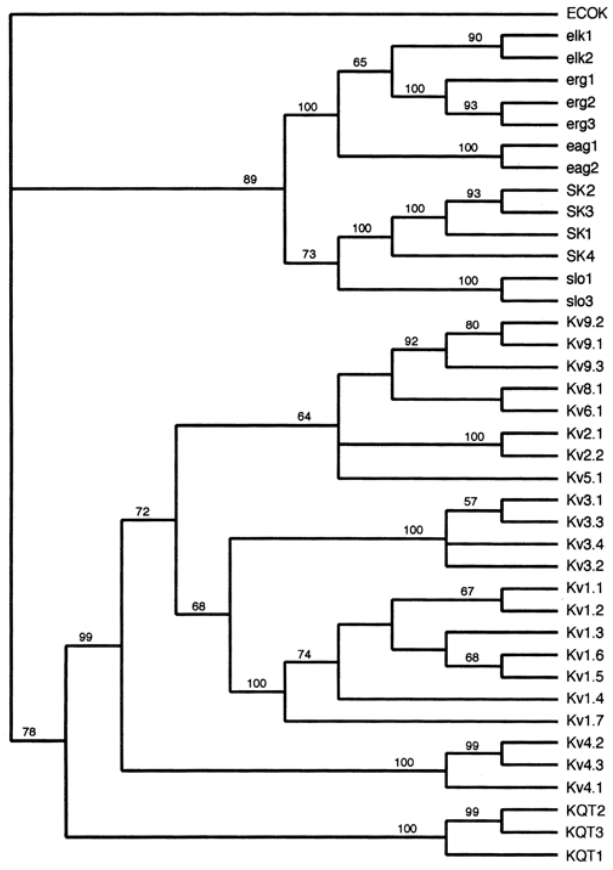

Figure 1.4.2.1 Phylogenetic tree of 6TMD voltage-gated and calcium-activated K^+ channels generated by parsimony. Bootstrap values generated using PAUP 3.1.1 are shown on the tree when available, and they represent a measure of node robustness (Trimmer and Rhodes, 2004)

K_V channel type	Gene	Main localisation	Function
K_V1		Axon	
$K_V1.1$	*KCNA1*		Controlling AP waveform Setting firing rate in layer II/III pyramidal neurons
$K_V1.2$	*KCNA2*		Intracortical processing in layer V pyramidal neurons
$K_V1.3$	*KCNA3*		
$K_V1.4$	*KCNA4*		Regulate Ca^{2+} influx and neurotransmitter release in mossy fibre axons
$K_V1.6$	*KCNA6*		"D" current in interneurons
K_V2		Soma, proximal dendrite	Delayed rectifier channels
$K_V2.1$	*KCNB1*		
$K_V2.2$	*KCNB2*		
K_V3			High frequency firing in neocortex and hippocampus
$K_V3.1$	*KCNC1*	Axon (3.1b) somatodendritic (3.1a)	3.1a/b splice variants of 3.1
$K_V3.2$	*KCNC2*	Soma, dendrite	
$K_V3.3$	*KCNC3*	Axon	Shaping depolarising events in cerebellum Purkinje cells
$K_V3.4$	*KCNC4*		
K_V4		Soma, dendrite	A-type K_V channels
$K_V4.1$	*KCND1*		
$K_V4.2$	*KCND2*		
$K_V4.3$	*KCND3*		
K_V7			Slowly activating and noninactivating M current that suppresses neuronal firing
$K_V7.2$	*KCNQ2*	Axon	
$K_V7.3$	*KCNQ3*	Axon, soma, dendrite	
$K_V7.5$	*KCNQ5*	Soma, dendrite	

Table 1.4.2. Identification of potassium channel α-subunits thus far. GP – Globus pallidus; SNpr – substantia nigra pars reticulata; IN – interneuron; DG – Dentate granule cell; PC – pyramidal cell; PV – parvalbumin; SOM – somatostatin; Cal – Calbindin. Adapted from (Vacher et al., 2008).

1.4.3 Voltage-gated calcium channels

Neuronal calcium currents are classified into L-, N-, P-, Q-, R- and T-type – all of which demonstrate unique physiological and pharmacological properties (Bean, 1989; Catterall, 2000; Dolphin, 2006; Hess, 1990; Llinás et al., 1992; Reuter, 1967; Tsien et al., 1988). The main pharmacological features of Ca^{2+} channels are governed by the pore-forming α_1 subunit of 190 kDa. The α_1 subunit amino acid sequence contains four highly homologous domains in tandem analogous to the VGSC, each of which resembles a voltage-gated potassium channel α subunit. They probably evolved through two duplications of a potassium channel, and are phylogenetically older than sodium channels. Each domain contains six transmembrane segments in the same way as the potassium channels, and movement of the four S4 segments governs activation. Only one α_1 subunit is thus required to form a channel. Table 1.4.3 below illustrates the roles of the different calcium channel α_1 subunits. Four highly conserved glutamate residues line the selectivity filter of calcium channels. Of importance to my project is the P/Q subtype. The P-type was found in cerebellar Purkinje cells, and blocked by the peptide ω - agatoxin IVA, a constituent of the venom produced by the *Agelenopsis aperta* or American funnel web spider. Q-type channels found in cerebellar granule cells, are

physiologically analogous to P-type but with a lower affinity for ω -agatoxin IVA. It is currently thought that the P- and Q-type channels either have different configurations of subunits (Richards et al., 2007) or more likely are splice variants of the same gene (Bourinet et al., 1999).

Calcium channels are associated with accessory $\alpha_2\delta$, β, and γ subunits with the typical subunit composition being $\alpha_1\alpha_2\beta\gamma$ in a 1:1:1:1: ratio (Catterall, 2000). Heterogeneity among the Ca_V accessory units is important in determining expression level, localisation and function of the Ca_V α1 subunit (Hofmann et al., 1994). Both $\alpha_2\delta$ and β promote channel trafficking to the plasma membrane and modulate voltage-dependent gating.

α_1 code	Ca^{2+} channel name	Current type	Gene	Main Localisation	Function
α_{1C}	$Ca_v1.2$	L	*CACNA1C*	Neurons	Gene regulation
α_{1D}	$Ca_v1.3$	L	*CACNA1D*	Neurons	Gene regulation
α_{1A}	$Ca_v2.1$	P/Q (Llinas et al., 1989; Randall and Tsien,1995)	*CACNA1A*	Nerve terminals, dendrites	Neurotransmitter release
α_{1B}	$Ca_v2.2$	N (Nowycky et al., 1985)	*CACNA1B*	Nerve terminals, dendrites	
α_{1E}	$Ca_v2.3$	R	*CACNA1E*	Nerve terminals, dendrites, cell bodies	Neurotransmitter release
α_{1G}	$Ca_v3.1$	T (Llinas and Yarom,	*CACNA1G*	Neurons	Repetitive firing

		1981)			
α_{1H}	$Ca_v3.2$	T	*CACNA1H*	Neurons	Repetitive firing
α_{1I}	$Ca_v3.3$	T	*CACNA1I*	Neurons	Repetitive firing

Table 1.4.3. Identification of calcium channel α-subunits in neurons thus far. DHP: 1,4-dihydropyridine; ω -aga: ω -agatoxin; ω -ctx: ω –conotoxin

1.5 Neurological channelopathies

Several neurological diseases including neuromuscular disorders, movement disorders, migraine, and epilepsy can be caused by ion channel disruption. Channelopathies can be divided into three main types. The first is genetic, where specific mutations of genes encoding ion channels of muscle, nerve or glia alter cellular, organ or circuit function (Griggs and Nutt, 1995; Lehmann-Horn and Jurkat-Rott, 1999). The second type is autoimmune, in which autoantibodies against ligand- or voltage-gated ion channels cause disorders of the central and peripheral nervous system (Vincent et al., 2006). Recent studies have provided growing evidence for the existence of a third type - transcriptional channelopathies - which result from changes in the expression of non-mutated channel genes. An example is some forms of peripheral nerve injury, which lead to altered expression of some sodium channels in spinal sensory neurons, affecting the excitability of these cells and possibly contributing to neuropathic pain (Waxman, 2001).

The genetic neurological channelopathies offer an unprecedented insight into the diversity of cellular mechanisms underlying the abnormal function of neuronal circuits. Indeed, the breakthroughs in understanding these diseases have raised expectations that the causes of far commoner idiopathic neurological diseases, in particular primary generalized epilepsy, will soon be understood. Due to their wide distribution, ion channel mutations can affect any aspect of the nervous system, causing a variety of different symptoms including paroxysmal disturbances of brain, spinal cord, peripheral nerve or skeletal muscle function. Indeed the list of these

channelopathies is expanding rapidly, as is the phenotypic range associated with each channel. Heterologous expression studies have shed light on the consequences of these mutations for ion channel assembly and electrophysiological function. However, to further understand channelopathies and their paroxysmal nature, knowing the biophysical changes caused by the mutation on the channel is not sufficient. It is also necessary to know where the mutant channel is expressed, and to define the effect of channel disruption on neuron or myocyte function, and on the circuit it operates in. Explaining the symptoms the patient experiences is therefore a substantial challenge.

Most currently known channelopathies are dominantly inherited and as such a positive family history of the disorder is common. A striking feature of many channelopathies is that patients often experience discrete paroxysms (seizures, migraine, paralysis, ataxia, dyskinesia) with preserved neurodevelopment and normal function in between attacks. Paroxysms may become less marked with age. Possible explanations for this phenomenon include changes in the expression of individual channels, maturation and compensatory alterations in circuit function. It is important to note, however, that different mutations of the same gene can lead to a range of phenotypes, and conversely, a given phenotype can be caused by mutations of different ion channels.

Epilepsy: Channelopathies can cause both focal and generalised seizures ranging from benign neonatal convulsion conditions to more severe epileptic encephalopathies associated with development regression. Mutations in the *KCNQ2*

and *KCNQ3* genes affect the potassium channel subunits K_V7.2 and 7.3 respectively, clinically manifesting as Benign Familial Neonatal Seizures (BFNS) and Early Onset Epileptic Encephalopathy (EOEE). Mutations of the *SCN1A*, *SCN2A* and *SCN1B* genes affect the sodium channel subunits Na_V1.1, Na_V1.2 and Na_Vβ1 respectively, clinically manifesting (in most cases) as Generalised Epilepsy with Febrile Seizures (GEFS), Severe Myoclonic Epilepsy in Infancy (SMEI) or Dravet syndrome, and Benign Non-Familial Infantile Seizures (BNFIS). More recently *de novo* mutations in the *SCN8A* gene that encodes Na_V1.6 (**Chapter 1.2**) have been identified in patients with two types of disorders, epileptic encephalopathy and intellectual disability (O'Brien and Meisler, 2013) Mutations of the *GABRA1* and *GABRG2* genes affect the α1 and γ2 $GABA_A$ receptor subunits and are also associated with GEFS in addition to Childhood Absence Epilepsy. Mutations of the *CHRNA2*, *CHRNA4*, *and CHRNB2* genes affect the acetylcholine receptor subunits α2, α4, β2 respectively, and clinically manifest as Autosomal Dominant Nocturnal Frontal Lobe Epilepsy.

Neuromuscular disorders: Channelopathies can either decrease or increase muscle fibre excitability. Periodic paralysis manifests as episodes of hypotonia and global weakness. Mutations in the *SCN4A* sodium channel gene and *CACN1A* calcium channel gene are responsible for the most common periodic paralyses. Myotonia is associated with increased muscle excitability and manifests as muscle stiffness. Mutations to the *CLCN1* chloride channel gene causes myotonia congenita (muscle stiffness alleviated by exercise) and mutations to the *SCN4A* gene causes paramyotonia congenita (muscle stiffness caused by exercise or cold temperature). Mutations in the *SCN9A* gene cause Primary Erythromelalgia, a rare neurovascular

peripheral pain disorder. A gain of function mutation in the *SCN10A* gene causes small fibre neuropathy, likely caused by Dorsal Root Ganglia hyperexcitability (Han et al., 2014). Mutations in the *KCNJ2* gene, which codes for the inward rectifier potassium channel $K_{ir}2.1$, cause Anderson-Tawil syndrome, which manifests as cardiac arrhythmias, periodic paralysis and dysmorphic features. The transient receptor potential vanilloid 1 and ankyrin 1 (TRPV1 and TRPA1, respectively) demonstrate high calcium permeability and have an integral role in pain, neurogenic inflammation and sensory nerve activation (Fernandes et al., 2012). A range of congenital myasthenic syndromes have been identified that affect either presynaptic function that present in infancy (*CHAT* and *COLQ* mutations), post synaptic function including acetylcholine receptor kinetics that present with predominant bulbar and respiratory weakness (*CHRNE, CHRNA, CHRNB, CHRND* mutations) or acetylcholine receptor aggregation that present with proximal muscle weakness (*DOK7* mutation).

Cerebellar ataxia will be discussed in more detail later in this chapter. Excessive startle to stimulus or hypereplexia is caused by mutations to the glycine receptor genes *GLRA1* and *GLRB*.

1.5.1 Episodic Ataxias

Episodic Ataxia Type 1 (EA1)

EA1 was first described in 1975 by Van Dyke et al. as an inherited disorder characterized by persistent myokymia as well as discrete episodes of cerebellar incoordination, manifesting as tremor of the head, arms, and legs, and loss of coordination and balance (VanDyke et al., 1975). The disease is due to dominantly inherited mutations of the *KCNA1* gene (Browne et al., 1994). Distinct mutations are associated with variable manifestations including, in some patients, cramps, contractures, titubation and seizures (Eunson et al., 2000; Zuberi et al., 1999). EA1 usually presents in the first or second decade with patients experiencing disabling attacks of midline cerebellar dysfunction, manifesting as truncal and limb ataxia, dysarthria, and visual symptoms such as oscillopsia and visual blurring. These are normally brief, lasting between seconds and minutes. The attacks can be triggered by emotional stress, startle and sudden postural changes (Rajakulendran et al., 2007). Another predominant feature is the presence of continuous interictal motor activity in the form of myokymia, a result of peripheral nerve hyperexcitability. This most commonly manifests as fine rippling in perioral or periorbital muscles.

Brain MRI and routine laboratory blood tests including serum concentration of creatine kinase and electrolytes are usually normal. Electromyogram may display a pattern of either rhythmically or arrhythmically occurring singlets, duplets, or multiplets. In specialized centres, electrophysiological assessments of motor nerve

excitability performed according to the TROND protocol (using Qtrac© software; UCL Institute of Neurology) allows differentiation of individuals with EA1 from normal controls with high sensitivity and specificity (Tomlinson et al., 2010). Muscle biopsy is usually not helpful in establishing the diagnosis, although bilateral calf hypertrophy, enlargement of type 1 and type 2 gastrocnemius muscle fibres, and variable glycogen depletion have been observed (Demos et al., 2009; Kinali et al., 2004; VanDyke et al., 1975). Nevertheless, these changes have not been consistently reported among individuals with EA1. A diagnosis of EA1 can be established by finding a heterozygous variant in *KCNA1* via Sanger or next-generation sequencing. It is not known if copy number variants also manifest as EA1.

A multi-gene panel can be sought if considering differential diagnoses. These include Episodic Ataxia type 2 (discussed below) and even more rarely EA3, 4, 5, 6, 7 and 8 and Spastic Ataxia Type 1 (SPAX1). Other differential diagnoses include Paroxysmal Kinesigenic Dyskinesia (PKD), Paroxysmal Non-Kinesigenic Dyskinesia (PNKD), and Isaac's Syndrome or acquired neuromyotonia.

No single medication has been proven to be very effective. Acetazolamide, a carbonic-anhydrase inhibitor, may reduce the frequency and severity of the attacks in some but not all affected individuals. The mechanism by which acetazolamide reduces the frequency and severity of the attacks is unclear. Chronic treatment may result in side effects including tiredness, paraesthesias, rash, and formation of renal calculi (D'Adamo et al., 2015; Graves et al., 2014). Antiepileptic drugs (AEDs) may significantly reduce the frequency of the attacks in responsive individuals; however,

the response is variable and some individuals are particularly resistant to drugs (Eunson et al., 2000). Phenytoin has been shown to improve muscle stiffness and motor performance (Kinali et al., 2004); carbamazepine and lamotrigine have also been used (Eunson et al., 2000).

1.5.2 Episodic Ataxia Type 2 and other $Ca_V2.1$ channelopathies

Different mutations of the *CACNA1A* gene encoding the pore-forming subunit of voltage-gated $Ca_V2.1$ (P/Q-type) Ca^{2+} channels (Ophoff et al., 1996) can cause clinically distinct conditions, including Familial Hemiplegic Migraine (FHM)(Inchauspe et al., 2012), Episodic Ataxia Type 2 (EA2), and Spinocerebellar Ataxia Type 6. Autoantibodies directed against the same channel cause Lambert-Eaton myasthenic syndrome. EA2 is an autosomal dominant paroxysmal cerebellar disorder, characterized by acetazolamide-responsive attacks of cerebellar ataxia and migraine-like symptoms, interictal nystagmus, and cerebellar atrophy (von Brederlow et al., 1995). It usually presents in the second decade and is commonly caused by nonsense, frame-shift or splice-site mutations (Denier et al., 2001), or deletions, resulting in a loss of channel function (Guida et al., 2001; Kullmann, 2010). How this leads to ataxia is not clear, but it has been suggested that loss of $Ca_V2.1$ leads to an impairment of inositol 1,4,5−triphosphate receptor type 1 (ITPR1)−dependent plasticity in Purkinje cells (Rajakulendran et al., 2010).

1.6. Pharmacological and genetic models for assessing K_V1 channel function

The role of potassium channels in influencing AP repolarisation and repetitive AP generation has historically been investigated using pharmacological blockers. Initial identification of two potassium currents, A- and D- currents, were dissected using 4-aminopyridine (4-AP) and dendrotoxin (Wu and Barish, 1992). 4-AP is a non-selective potassium channel blocker. Tetraethylamminium (TEA) is another often used voltage-gated potassium channel blocker.

Dendrotoxins are a class of presynaptic neurotoxins produced by mamba snakes (*Dendroaspis*) that act as reversible inhibitors of K_V1 channels in neurons. Dendrotoxins are ~7kDa proteins consisting of a single peptide chain of approximately 57-60 amino acids. It is thought the mode of action involves electrostatic interactions between the positively charged amino acid residues in the cationic domain of dendrotoxin and the negatively charged residues in the ion channel pore. There are three main dendrotoxin subtypes. α-Dendrotoxin is isolated from *Dendroaspis angusticeps* snake venom (Benishin et al., 1988). α-Dendrotoxin blocks $K_V1.1$ and $K_V1.2$ channels (IC_{50}= 0.4 to 4 nM, and 1.1 to 12 nM, in oocytes respectively, with higher values for mammalian cells). In addition the toxin was shown to block also $K_V1.6$ (IC_{50}= 9-25 nM) (Harvey, 2001). The role of presynaptic K_V1 channels in spike broadening in hippocampal mossy fibre boutons was investigated using α-DTX at 1 μM (Geiger and Jonas, 2000). Dendrotoxin–I is isolated from *Dendroaspis polylepis* snake venom (Schweitz et al., 1990). Dendrotoxin-I blocks $K_V1.2$ and $K_V1.1$ channels (IC_{50}=0.13 and 3.1 nM in oocytes

respectively) as well as heteromultimeric channels containing these, with other K_v1 isoforms. The role of K_V1 in action potential waveform in cortical axons has been studied using 50-100 nM DTx-I (Kole et al., 2007a).

Dendrotoxin-K (molecular formula: $C_{294}H_{462}N_{84}O_{75}S_6$.) is also isolated from *Dendroaspis polylepis* snake venom (Schweitz et al., 1990). It blocks mainly $K_v1.1$ (IC_{50}= 2.5 nM for homomers) but also $K_v1.2$ channels. The K26 and W25 residues from the β-turn and the K3 and K6 residues in the 3_{10}-helix are important for DTx-K binding to $K_V1.1$ containing channels. Residues in the 3_{10}-helix are crucial for recognition of K_V1 channels by DTx-K. K3 and K26 are around 14 Å apart, which is compatible to the estimated width (22-34 Å) for the outer vestibule of potassium channels. Low threshold potassium currents in the medial nucleus of the trapezoid body were investigated using DTx-K at 100nM (Dodson et al., 2002). DTx-K was used at 100 nM to explore the roles of potassium channels in action potential shape in cerebellar basket cells (Begum et al., 2016). Due to the selectivity of DTx-K for $K_V1.1$ containing channels, this toxin was used for our experiments (see **Section 6.1**).

In addition to pharmacological blockade of $K_V1.1$, genetic deletion of $K_V1.1$ in mouse models provide complementary insights into the normal roles of $K_V1.1$ and effects of mutations on neuronal properties. The *KCNA1* gene encodes the potassium channel subunit $K_V1.1$. $K_V1.1$ is widely expressed throughout the nervous system, most notably in the presynaptic terminals of cerebellar basket cells, but also in the axons of hippocampal neurons. $K_V1.1$ assembles with other K_V1 members to form heterotetrameric channels (Wang et al., 1993). $K_V1.1$-containing channels exhibit

variable kinetics depending on the other pore-forming subunits and associated cytoplasmic subunits (Lai and Jan, 2006; Rettig et al., 1994). The functional consequences of *KCNA1* mutations have been examined by expression of mutant and/or wild-type (WT) K_V1.1 in non-neuronal cells (Adelman et al., 1995; Boland et al., 1999; Bretschneider et al., 1999; D'Adamo et al., 1998; Eunson et al., 2000; Rea et al., 2002; Zerr et al., 1998; Zuberi et al., 1999). Most mutations confer a loss of K_V1.1 function through altered kinetics or reduced current density, in some cases with impaired trafficking (Manganas et al., 2001; Rea et al., 2002). The variable clinical severity of distinct mutations correlates imperfectly with their in vitro consequences (Eunson et al., 2000; Rea et al., 2002).

The two models I used were a homozygous knock-out mouse (*Kcna1a*$^{-/-}$) (Smart et al., 1998) and a heterozygous knock-in EA1 mouse (*Kcna1a*$^{V408A/+}$) (Herson et al., 2003). The homozygous null mouse has a phenotype different from EA1, and is characterized by focal seizures and temperature-dependent "shivering". Heterozygous mice do not have a detectable phenotype.

The EA1 mouse expresses a heterozygous V408A mutation in *Kcna1*. This is one of several mutations clustered at the cytoplasmic end of S6 that have been identified in EA1. Whilst the majority of EA1 mutations lead to a loss of function, heterologous expression of some mutations such as E325D and V408A, residing near the cytoplasmic ends of S5 and S6 of K_V1.1, can confer a both a loss of function by inducing an unstable open state compared to wild type (WT) resulting in a tenfold increase in the deactivation rate, and a paradoxical gain of function by the slowing of

β1-induced N-type inactivation with a tenfold increase in recovery from N-type inactivation (Adelman et al., 1995; Maylie et al., 2002). The extent to which the paradoxical gain of function associated with the V408A mutation outweighs the loss of function is unclear but appears to be dependent on which subunits are assembled with K_V1.1. This is illustrated in Figure 1.6. The effects of V408A are conferred on heteromeric channels formed with wild-type K_V1.1 or K_V1.2 subunits, roughly in proportion to the number of V408A subunits incorporated into the tetrameric channel (D'Adamo et al., 1998; Zerr et al., 1998).

Phenotypically, the V408A knock-in mouse recapitulates a human EA1 mutation and is more severe than the gene deletion, consistent with a dominant-negative effect on other K_V1 potassium channel family members. However this dominant-negative effect has not been demonstrated in heterologous studies to date. Homozygous *Kcna1a*$^{V408A/V408A}$ mice die after embryonic day 3. *Kcna1a*$^{V408A/+}$ mice exhibit stress-induced loss of motor coordination that improves with acetazolamide, analogous to human with EA1. Juvenile animals were used (typically E18 to P1 pups) with hippocampi extracted to make primary dissociated neuronal cultures.

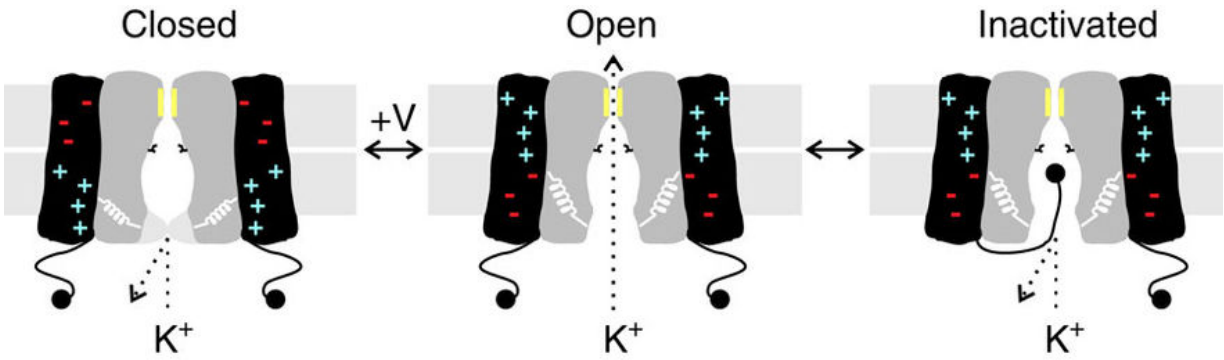

Figure 1.6 **Gating mechanisms of K_V1 channel.** In response to depolarisation K_V1 opens an intracellular gate (open) allowing K^+ to pass at rates close to diffusion.

However open channels can be directly blocked by an N-terminal inactivating gate (inactivated) (Gonzalez et al., 2011).

K_V1 channels modulate neuronal firing and neurotransmitter release. In mossy fibre boutons, a major excitatory synapse in the hippocampus, cumulative inactivation of Kv1 channels contributes to activity-dependent spike broadening. This leads to an increase in calcium ions entering the synaptic terminal per action potential and thus facilitation of evoked excitatory post synaptic currents (EPSC) in CA3 pyramidal neurons (Geiger and Jonas, 2000). More recently it has been recognised that K_V3 and BK_{Ca} channels in addition to K_V1 play an important role in AP repolarisation at the mossy fibre bouton (Alle et al., 2011). Relatively little is known of the effects of EA1-associated Kv1.1 mutations on presynaptic APs. Lentivector- mediated overexpression of the C-terminus-truncated R417 stop mutation, which is associated with severe drug-resistant EA1, in rat hippocampal neurons in culture leads to increased neuronal excitability and neurotransmitter release (Heeroma et al., 2009). Overexpression of wild type Kv1.1 had the opposite effects.

In fast spiking cells, a prominent subtype of GABAergic interneurons, K_V1 channels and in particular $K_V1.1$ in the AIS have been implicated in suppressing near-threshold excitability and AP threshold, which accounts for at least some of the firing pattern diversity observed within the FS cell class (Goldberg et al., 2008).

1.6.1 Recording of presynaptic action potential morphology and modulation to date

K_V1.1 is found predominantly in the axonal and presynaptic compartment. To understand the role of K_V1.1 in action potential morphology and modulation, direct electrophysiological recording of the axonal/presynaptic compartment was required. However conventional patch-clamp recordings of neuronal cultures rely on diffraction-limited optical microscopy to navigate the patch-clamp pipette to the target structure. The smallest cellular structures successfully targeted using differential interference contrast (DIC) optics, such as hippocampal mossy fibre boutons (~2–5 µm diameter) (Bischofberger et al., 2006; Ruiz et al., 2010) are an order of magnitude larger than the optical diffraction limit (~200 nm). Recordings from narrow axons have recently been obtained using pipettes coated with fluorescently conjugated albumin; however, this method only allows cell-attached recordings of AP waveforms (Sasaki et al., 2011). Indirect methods such as extracellular or cell-attached patch-clamp recording from axons of cerebellar Purkinje cells (Kawaguchi and Sakaba, 2015) do not allow the action potential shape to be measured directly. Presynaptic voltage-sensitive fluorescence measurements or loose patch clamp of fluorescent-dye loaded axons may not detect sub-millisecond differences in action potential shape, although major parameters like action potential peaks have been shown to be reduced by K_V3.1b and K_V1 in small CNS nerve terminals using this method (Hoppa et al., 2014).

Investigations of presynaptic spike modulation have relied heavily on recordings from blebs that form after axons have been transected (Kim, 2014; Kole et al., 2007a; Shu et al., 2006, 2007a). A potential pitfall of this method is that the ion channels present in blebs may not be representative of the normal complement of channels at an unperturbed bouton. A further difficulty is that the attenuation of voltage with distance from the soma is likely to be smaller than when recording from an intact axon. Indeed, classical cable theory predicts that steady-state somatic voltage should decrease by approximately 63% at one length constant if the axon is represented by an infinite cable, but only by ~35% if it is sealed at the same point (Rall, 1959). The discrepancy increases as the axon is made shorter: if the axon is cut at half a length constant, the attenuation of steady-state voltage at its termination is only ~29% of that predicted for an infinite cable. Given that the length constant of unmyelinated axons in the CNS has been estimated in the range of 400 – 600 μm (Alle and Geiger, 2006; Jackson, 1993; Scott et al., 2008; Shu et al., 2006), this implies that the modulation of action potential shape by passively propagating subthreshold somatic depolarization may have been greatly overestimated.

Modulation of action potentials at mossy fibre boutons (Fig 1.6.1a) and large calyceal synapses have been demonstrated (Awatramani et al., 2005a; Steinert et al., 2011). However the modulation demonstrated in these specialised synapses may not apply to the far more abundant small presynaptic boutons of the forebrain (Fig 1.6.1b), arguing the need for alternative recording methods to resolve the role of spike broadening.

We have adapted a method called Scanning Ion Conductance Microscopy (SICM), which overcomes the optical diffraction limit. It allows a topographical image to be obtained of small synapses in neuronal culture at a resolution down to 50nm in 3D, and also allows one to obtain direct electrophysiological data from such structures.

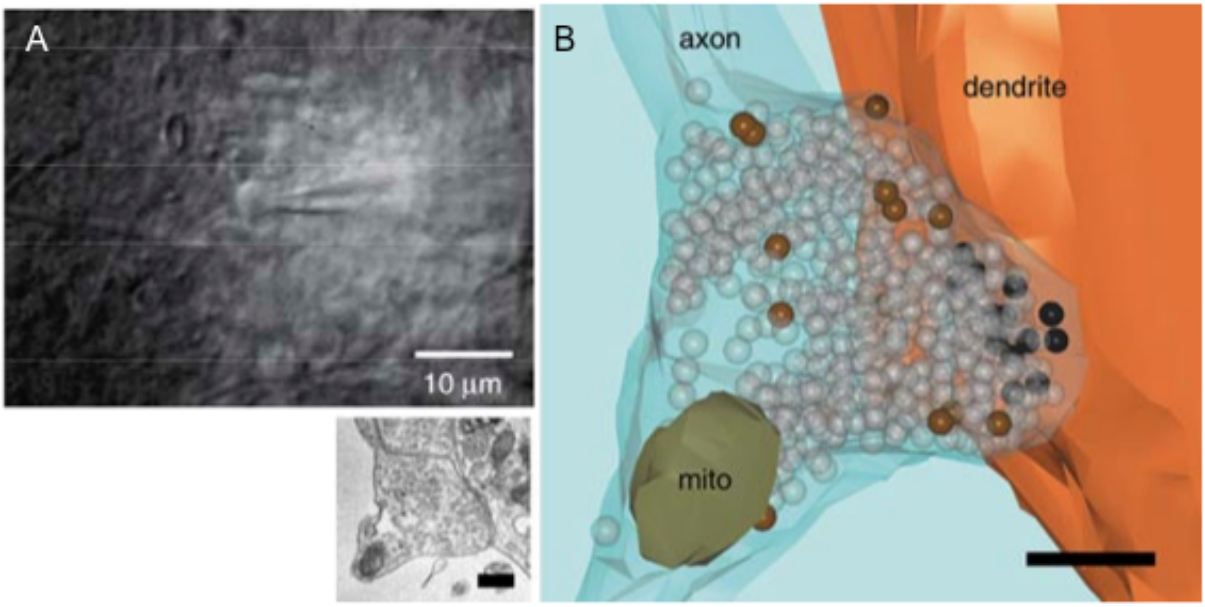

Figure 1.6.1. **Different glutamatergic synapses in the CNS**. (a) Patch clamp of a mossy fibre bouton in a mouse brain slice (Bischofberger et al., 2006) (b) Reconstruction of a small hippocampal bouton, using serial electron microscopy data (inset). Adapted from (Schikorski and Stevens, 2001); scale bar 0.1 µm.

Originally developed to image the topography of nonconducting surfaces (Hansma et al., 1989), SICM was further refined by the Korchev group (Novak et al., 2009) to enable live imaging at sub-micrometre resolution, and in collaboration we have optimised its application in patch-clamp recording from small CNS synapses (diameter ~1µm) that predominate throughout the mammalian brain. This semi-automated approach allows precise targeted recordings from small synaptic

terminals in cultured hippocampal neurons in all four configurations of the patch-clamp method (cell-attached, inside-out, whole-cell, and outside-out). I will further describe this technique in the methods section.

2.0 Hypotheses

Although the consequences of the *KCNA1* mutations for ion channel kinetics are known, there are several unanswered questions about their effects on synaptic function, and so the disease mechanisms of EA1 remain incompletely understood. Key to progress is to examine the kinetics of the pre-synaptic action potential, because this is what determines how calcium channels open and how calcium influx triggers exocytosis of neurotransmitter vesicles.

Parallel work from the laboratory produced direct evidence for increased action potential width by recording from cerebellar basket cell terminals in EA1 knock in mice (Begum et al., 2016). However, it is not known whether this holds for forebrain synapses, nor whether particular patterns of activity lead to excessive neurotransmitter release as a result of action potential broadening. Because K_V1.1 assembles with other potassium channel subunits in different combinations, and these have different kinetic properties, it is not possible to extrapolate from heterologous expression studies to predict the effects on action potential shape. Indeed, abundant evidence exists for homeostatic compensation for the effects of chronic pharmacological blockade of neuronal ion channels and synaptic receptors (Turrigiano and Nelson, 2004). It remains possible therefore, that dysfunction of K_V1.1 is compensated for by changes in expression of other ion channels.

Subthreshold membrane potential fluctuations at the cell body also spread passively along the axon and affect the shape of action potentials invading presynaptic terminals (‘analogue signalling’) and consequently calcium influx and neurotransmitter release (**Section 1.2.4**). Inactivation of axonal Kv1 family channels

contributes to ‘analogue’ signalling by broadening presynaptic action potentials (Bialowas et al., 2015; Kim, 2014; Kole et al., 2007a; Shu et al., 2007a). Although this phenomenon has been investigated in transected axons or highly specialized presynaptic terminals, the role of K_V1.1 in small presynaptic terminals has not been studied.

The recent development of SICM now makes it possible addressing the following hypotheses:

1. Deletion or pharmacological blockade of Kv1.1, or the V408A mutation in the EA1 mouse model, prolongs the action potential repolarization phase at glutamatergic synapses in the hippocampus.

2. Loss of Kv1.1 or the V408A affect sub-threshold signalling in the axon, because K_V1.1 activates and inactivates at relatively negative potentials.

3.0 Methods

3.1 Animals and preparation

Newborn (P0) Sprague Dawley rats from UCL Central Biological Unit were used to produce primary rat hippocampal neuronal cultures. All animal procedures were carried out in adherence to Home Office regulations under the UK Animal (Scientific Procedures) Act 1986. Animals were kept under controlled environmental conditions (24−25°C; 50−60% humidity; 12 hour light/dark cycles) with free access to food and water.

Two mutant mouse strains were used - (*Kcna1a*$^{-/-}$) (Smart et al., 1998) and knock-in (*Kcna1a*$^{V408A/+}$) (Herson et al., 2003) – the latter a kind gift from the Maylie lab. Litters were weaned at three weeks and ear-tagged in order to ascertain genotype (PCR based genotyping was performed by Dr. Stuart Martin of the Biosciences Huxley Building Molecular Biology Facilities). For the knockout mice *Kcna1*$^{+/-}$ was bred with *Kcna1*$^{+/-}$ to generate homozygous-null pups. For the knockin mice *Kcna1a*$^{V408A/+}$ female mice were crossed with wild-type C57/BL6 mice.

3.2 Hippocampal neuronal cultures

The technique of culturing neuronal tissue was first described by Ross Harrison in 1910 (Harrison, 1910). Since then this technique has advanced considerably and is

a useful tool in investigating synaptic function and development (Banker and Goslin, 1988; Kaech and Banker, 2006; Vicario-Abejón, 2004; Viesselmann et al., 2011).

Dissociated neuronal cultures were suitable for my experiments for a number of reasons. Due to their low three-dimension spatial density as compared with intact neural tissue (such as brain slices); external factors such as temperature and extracellular bathing solution can be easily controlled. The two dimensional architecture of neuronal cultures is easy to view with light microscopy and lends itself to patch clamp experiments due to its easy accessibility. Currently SICM is not possible in hippocampal slices, although it is being trialled in organotypic cultures. The exposed nature of dissociated neuronal cultures permit the facile perfusion of drugs and toxins, which will be used to pharmacologically dissect action potential shape and whole cell currents in the following experiments.

One of the limitations of dissociated neuronal cultures is that physiological neuronal connections are lost during dissociation, and this may in turn affect neuronal function. However as juvenile animals are used (typically E18 to P1 pups), normal dendritic arborisation is incomplete at the time of preparation. In addition these cultures form extensive synaptically-connected networks after several days (Friedman et al., 2000).

The hippocampus is a very popular model for investigation of brain function. This is mainly due to its relatively simple layered structure when compared with other brain

regions, with few cell types and morphologically distinct excitatory (pyramidal) and inhibitory (interneurons) cells (Benson et al., 1994; Buchhalter and Dichter, 1991; Grosse et al., 1998; Miyawaki and Hirano, 2011). Hippocampal neuronal cultures are rich in small synaptic boutons (around 1μm), which are the regions of interest for my experiments. 90% of synaptic boutons are glutamatergic in hippocampal cultures (Benson et al., 1994).

Instead of primary neuronal cultures, co-cultures with glial cells were developed. Contact between neurons and glial cells is important for neuronal survival (Lasek et al., 1977), axonal and dendritic growth (Gasser and Hatten, 1990; Piontek et al., 2002), synaptogenesis (Hama et al., 2004) and synaptic efficacy (Pfrieger and Barres, 1997).

3.2.1 Preparation of hippocampal neuronal cultures

Although for the majority of the project senior laboratory technician Dr Marife Cano prepared neuronal cultures, initially I was involved in their production. The protocol used was derived from that outlined in Dr Felicity Alder's PhD thesis (Alder, 2011), which I will summarise.

The protocol has three main stages:

1. Preparation and expansion of cortical glial cells

2. Preparation of coverslips and plating of the glial cell feeding layer
3. Isolation of hippocampal neurons

3.2.2 Hippocampal dissection and preparation of cortical astroglial cells

P0 rat pups were culled and decapitated. The heads were rinsed in 70% ethanol, washed four times in 30ml of wash solution (comprised of 500ml HBSS and 5ml 10mM HEPES), and placed onto a 10cm. dissection plate containing wash solution. The skin of the head was removed using Dumont No. 5 forceps, the skull pierced at the lambda and the parietal bones removed, exposing the brain.

The brain was removed from the skull vault and placed onto a 6cm. dissection plate, filled with wash solution. Under microscope guidance, the cerebral hemispheres were separated from the brainstem using Dupont 55 forceps. All meninges were removed with fine forceps, leaving the hippocampus exposed. Cerebral hemispheres and hippocampi were transferred to separate plates containing dissection solution (comprised of 40ml wash solution and 10ml 20% FBS) and finely chopped using small dissection scissors.

Ice cold solutions were used in all preceding steps up to trypsinisation. The pieces of cerebral hemisphere were placed in a 50ml. tube containing 9.5ml CMF-HBSS,

1.5ml 2.5% trypsin and 1.5ml DNAse (10mg/ml). The tube was incubated for 5 minutes at 37°C in a water bath. The tissue was triturated through a 10ml. pipette ten times in order to prevent clumping of cells, before being returned to the water bath for a further ten minutes. A further trituration using a 5ml pipette was performed until the suspension was homogeneous. The cell suspension was filtered through a 70µm filter, into a 50ml tube containing 15ml of glial medium (comprised of 500ml MEM, 6.7ml D−glucose, 5ml 1% penicillin-streptomycin, 50ml 10% horse serum, 5ml 1% L−Glutamine). This suspension was centrifuged for ten minutes at 2000RPM to remove the enzyme and lysed cells. The supernatant was removed and the pellet resuspended in 20ml of glial medium. Cells were plated at a density of 7-10 x 10^6 cells per T75 flask, and topped up to a final volume of 12ml with glial medium. The flasks were transferred to an incubator at 37°C, 5% CO_2. The following day, medium was exchanged in order to remove dead cells, and thereafter media were changed every 3 days, until cells reached 90−95% confluence.

When confluent, the glial cells were split with each T75 flask divided into 8 to amplify the colony. The cells were rinsed with 10ml of warmed CMF-HBSS, and treated with 2ml of trypsin/EDTA to dislodge the cells. The trypsin/EDTA was then inactivated by 8ml GM, and the cells pelleted (10 minutes at 2000RPM). The pellet was resuspended in GM and again divided between 8 flasks. This process was repeated to multiply cell numbers.

The cells were frozen in cryotubes and stored in liquid nitrogen to provide an accessible stock of glia. They were defrosted two weeks prior to neuronal

preparation to form a feeding layer on glass coverslips. One tube was defrosted and resuspended in ice cold glial medium, before pelleting to remove DMSO. The pellet was then suspended in warmed glial medium and plated in T75 flasks. As before, medium was exchanged the following day and cells grown to attain near 100% confluence over several days.

3.2.3 Preparation of coverslips

18mm glass coverslips were stacked in ceramic racks and submerged in 70% nitric acid for three days. They were rinsed four times for two hours in ddH_20 before being baked overnight at 225°C. The coverslips were placed in 12 well plates (6 coverslips per plate) and coated with 100µl PLL solution. They were incubated overnight, and rinsed twice the following morning with ddH_20.

Glial cells were dislodged with trypsin/EDTA, resuspended in glial medium and plated onto coated coverslips at a density of 60K per cm^2. Media was exchanged the day after, and cells left to form a monolayer before the neuronal preparation was applied.

3.2.4 Preparation of rat neuronal cultures

Dissected hippocampi (**Section 3.1.3**) were placed in a 60mm dish with dissection buffer (comprised of 40ml wash solution and 10ml 20% FBS) and transferred to a 15ml centrifuge tube and washed five times in 5ml wash buffer. The hippocampal tissue was transferred to a tube containing digestion mix (comprised of 25mg Trypsin, 2.5ml Digestion solution and 10µl DNAse) and incubated for ten minutes at 37°C. The enzyme was then inhibited by 5ml of dissection buffer, before being rinsed twice with 5ml of dissection buffer and twice with 5ml of wash buffer. The digested tissue was triturated in 2ml dissociation mix (comprised of 2.5ml Dissociation solution and 12.5µl DNAse) for five strokes with a half-diameter fire-polished, cotton-plugged Pasteur pipette. 1ml of cell solution was removed to a 15ml tube (to minimise cell death by mechanical trituration), then the remnant triturated with a third-diameter, fire-polished Pasteur pipette. The remaining cell solution was then added to the 15ml tube. 10ml dissection solution was added and cells centrifuged for five minutes at 2000RPM.

The supernatant was discarded and the cell pellet was disrupted. Cells were resuspended in Complete Neurobasal A (NB) and counted using a haemocytometer. Glial medium was removed from the glial cell coated coverslips and 1ml NB added instead to each well. The cell solution was diluted to a concentration of 30K cells per ml and 1ml added to each well (ending with a density of around 10K cells/cm^2). The cell density was important for reasons explained in **Section 4.2.** Cells were returned to the incubator and stored at 37°C and 5% CO_2. On day 7 post plating 1ml of

medium was removed from each well and 1ml of fresh medium applied. Cultures were then used 14-18 days after plating, because synaptogenesis generally is attained by day 14.

3.2.6 Mutant mouse cultures

As mice tended to produce smaller litters (around 6-12 pups) and their hippocampi when dissected were smaller, a few alterations were made to the above process. The genotype was established via PCR (by Stuart Martin) on tail clippings post culturing. Six to eight pups were dissected at one sitting, with surgical instruments cleaned between each with 70% ethanol to prevent cross contamination of genotypes. Four coverslips were plated per pup. After genotyping heterozygous knockouts were discarded. Wild type and knockout were compared in one set of experiments performed on the same day to control for differences in development; wild type and knockin were compared in another set of experiments performed on the same day.

3.3 Electrophysiology − The patch clamp

Much of what we know about the properties of ion channels in cell membranes stems from experiments using voltage clamp. Broadly, the method allows ion flow across a cell membrane to be measured as an electric current, whilst the membrane voltage is held under experimental control with a feedback amplifier. Thus with a controlled voltage over an area of membrane, it is much easier to record information about channel behaviour especially as the opening and closing of most ion channels are affected by the membrane potential.

In order to isolate a patch of membrane electrically from the external solution and to record current flowing into the patch, a fire polished glass or borosilicate pipette filled with an electrolyte solution is pressed against the surface of a cell. The result is a seal whose electrical resistance is greater than 1GΩ and at this point the glass pipette and cell membrane are less than 1nm apart (Ogden, 1994). In this *cell-attached* state recording of single channels can be performed and information about the unitary conductance and kinetic behaviour of ion channels can be obtained. Much work is done using patch clamp in the cell-attached mode, but the resting potential of the cell is unknown and neither intra- nor extra-cellular ionic concentrations can be manipulated. To overcome this, other configurations are possible (Figure 3.2). The *inside-out* configuration is achieved by pulling the membrane patch off the cell into the bath solution. The *whole-cell* configuration is achieved by destroying the membrane patch via suction in order for the cell, whose interior now is exposed to the solution of the pipette, to be voltage- or current-

clamped. The *outside-out* configuration is created by pulling the pipette away from the cell after achieving the whole-cell mode, thus resulting in a patch of membrane whose intracellular face is in contact with the pipette solution.

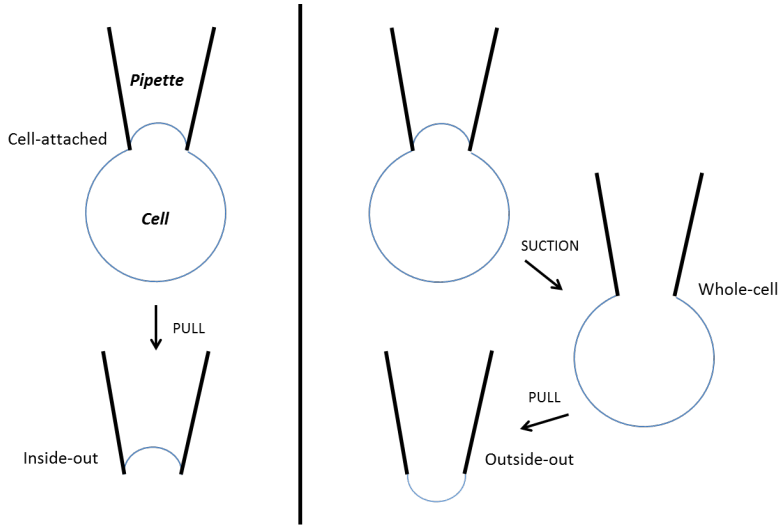

Figure 3.2 Schematic illustrating the four configurations of patch-clamp. Adapted from (Ogden, 1994)

3.3.1 Scanning Ion Conductance Microscopy

There is a great interest in developing methods to image live cells at sub-micron resolution. Scanning probe microscopy (SPM) is one approach to this problem and both atomic force microscopy (AFM) and scanning electrochemical microscopy (SECM) have been used to image live cells (Dufrêne, 2008; Sun et al., 2008). However, deformation of the soft cell by the AFM cantilever, particularly when imaging eukaryotic cells, is a significant limitation for AFM. SECM involves no physical contact with the sample, but true topographic imaging of the convoluted surface of living cells with nanoscale resolution has not been reported.

SICM relies on an electrolyte-filled glass nanopipette sensing the proximity of a cell surface via changes in the pipette current for a constant command voltage. In conventional SICM, a nanopipette is mounted on a three-dimensional piezoelectric translation stage and automatic feedback control moves the pipette up or down to keep the pipette current constant (the set point) while the sample is scanned in x and y directions. The 3D resolution is determined by the inner radius of the nanopipette. Thus, a pipette-sample separation, typically equal to the pipette's inner radius, is maintained during imaging (Figure 3.3d).

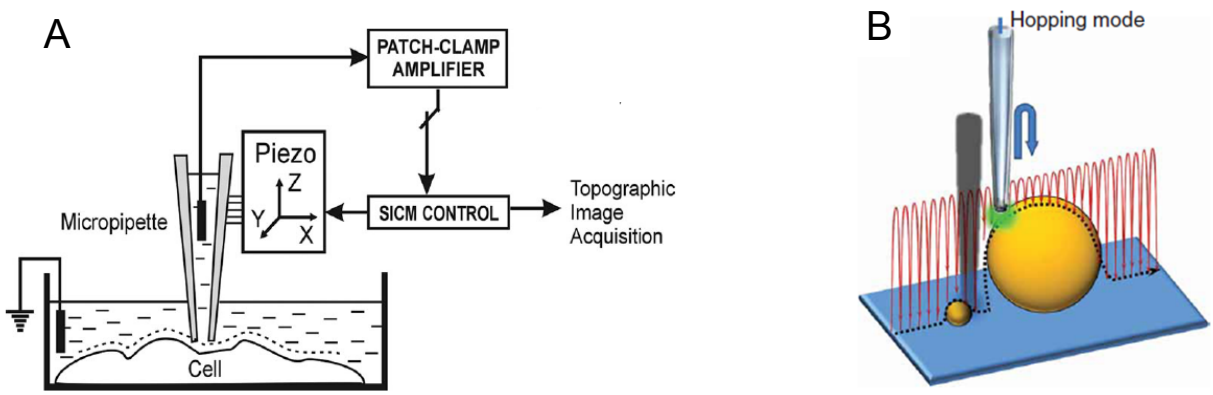

Figure 3.3. (a) Schematic of the SICM process. The feedback loop allows to control the distance between the pipette tip and cell surface (b) Schematic of the hopping mode used in HPICM

However the main limitation with conventional SICM was crashing of the pipette into 'suspended' structures such as axons during scanning, as the automatic feedback was not able to maintain a constant pipette – sample distance. This led to image distortions when scanning these structures (Novak et al., 2009). To overcome this, hopping probe ion conductance microscopy (HPICM) was developed, which does

not use continuous feedback. The speed of adaptive HPICM generates a snapshot of axons, dendrites and boutons in complex live networks such as hippocampal culture, and is not affected by the relatively slow migration of cells that occur in this preparation. At each imaging point, the pipette approaches the sample from a starting position that is above any of the surface features. The reference current is measured while the pipette is far from the surface. The pipette then approaches until the current decreases by a predefined amount, usually 0.25–1%. The position of the z-dimension actuator when the current achieves this reduction is recorded as the height of the sample at this imaging point. The z-dimension actuator then withdraws the pipette to a position well above the surface and the sample is moved laterally to the next imaging point (Figure 3.3b). This method is capable of reproducing the three-dimensional topography of live cells in culture at nanoscale resolution (≤ 20 nm) (Novak et al., 2009).

In order to determine the resolution limits of HPICM, fixed specimens of the mechanosensitive stereocilia of the auditory hair cells in cultured organ of Corti explants were used, and HPICM images were compared with scanning electron microscope images. HPICM was able to resolve links between the stereocilia to a diameter of 16 nm. After subtraction of the platinum coat thickness, scanning electron micrograph images resolved the diameter of the same stereocilia links to 12 nm., thus confirming agreement between the two imaging techniques (Novak et al., 2009).

3.3.2 Integrating HPICM with other parts of the experimental setup

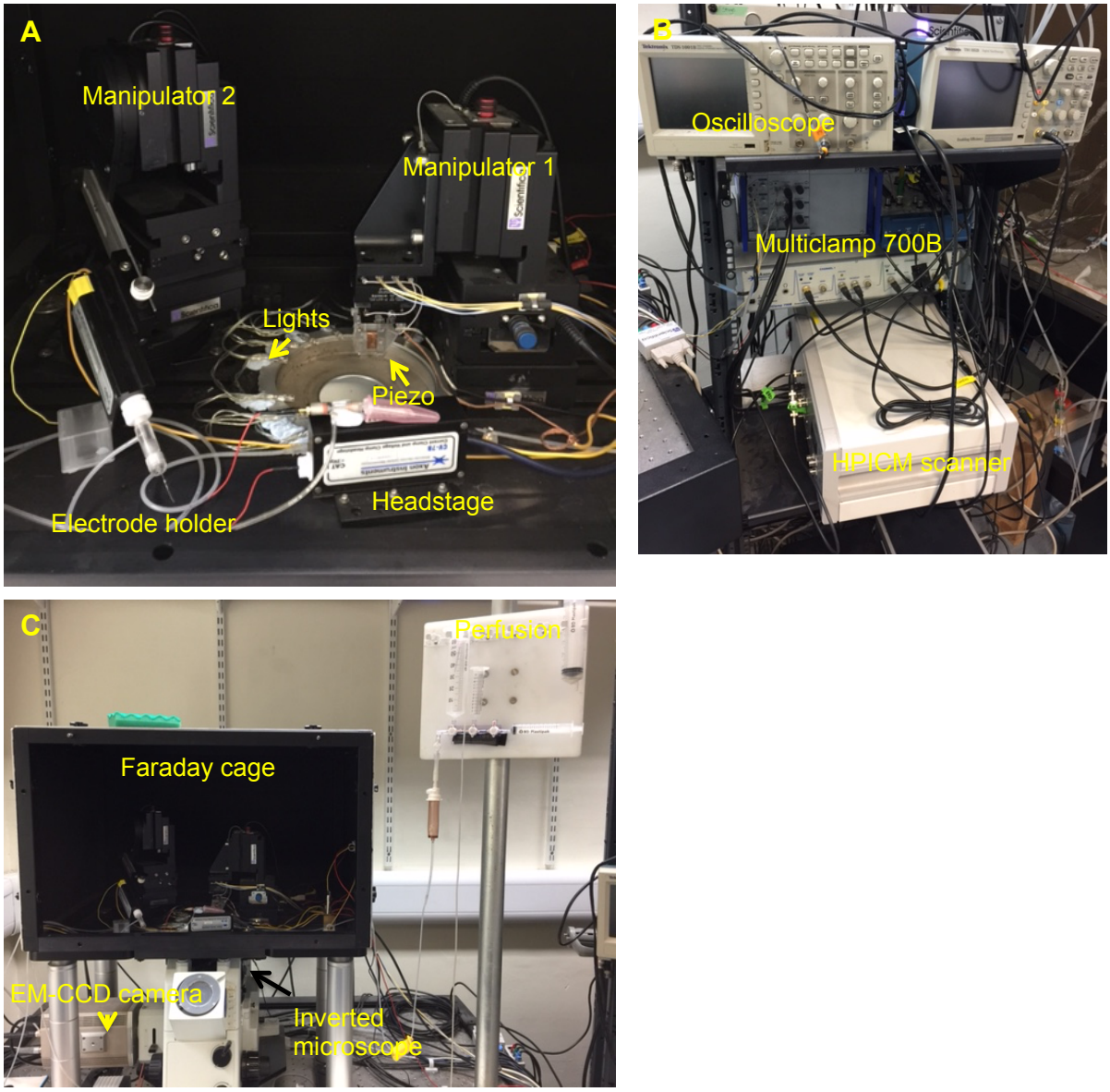

Figure 3.3.1 **The experimental rig**. (a) Inside the Faraday cage (b) the stack (c) zoomed out image of rig

Due to the unique way HPICM operates, a number of considerations were taken into account in order to integrate the method with existing electrophysiological and

conventional microscopy methods. There were three micromanipulators (Scientifica), two that directed separate headstages (Axon instruments) and one that directed the microscope objective. Having one headstage for soma recording and one headstage for HPICM would permit paired patch clamp recordings. This would be housed in a Faraday cage to electrically isolate the apparatus. All components within the cage were grounded. The cage rested on an air table (TMC) to isolate vibrations for steady imaging (Figure 3.3.1a). The headstages would be connected to an external amplifier (Multiclamp 700B). The HPICM sample scanner (Ionscope) was below in the stack and received input from the amplifier and communicated with Piezo controller. The oscilloscope (Tektronix) was used to view the 'hopping' produced by the HPICM scanner (Figure 3.3.1b).

The recording chamber housed 18 mm. glass coverslips that were secured using a rubber O-ring to prevent leakage of the extracellular buffer. A silver/silver chloride ground pellet was used to complete the electrical circuit. The coverslip was perfused with fresh extracellular buffer during experiments via the in- and outflow (Figure 3.3.2). The bottom plate of the chamber was magnetic and fitted securely onto a corresponding sized trough at the base of the Faraday cage.

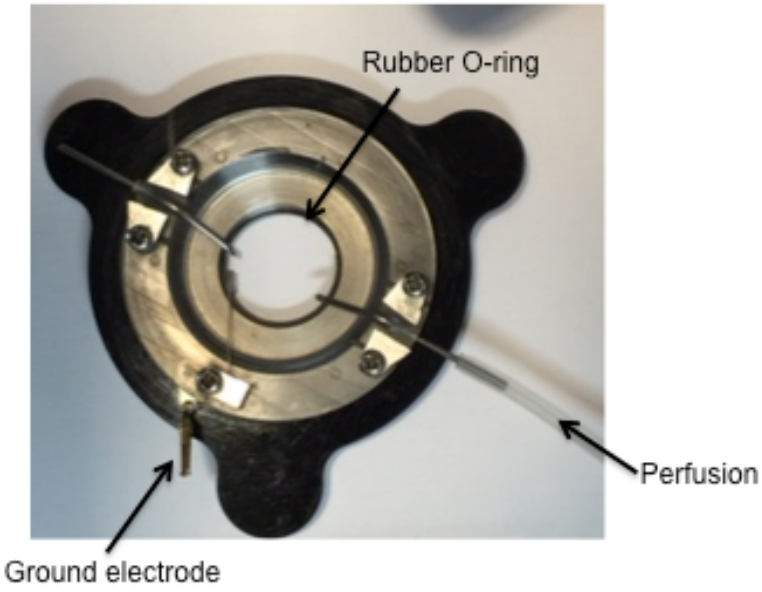

Figure 3.3.2 **The recording chamber**

With conventional bright field microscopy, light from a halogen source or LED is dispersed via a condenser onto the specimen, and then passes through an objective lens to a camera or to the experimenter's eye. Objects in the light path because natural pigmentation or stains absorb light differentially, or because they are thick enough to absorb a significant amount of light despite being colourless. In an inverted microscope the light source and condenser are above the specimen stage pointing down and the objectives are below the stage pointing up. As shown in Figure 3.3a the scanning nanopipette is held vertically so that x and y dimensions can be locked. This meant that the scan head was mounted on an inverted microscope (IX71, Olympus). However the position where the condenser would be expected was occupied by the piezo translational stage (PI instruments) and mounted nanopipette (Harvard apparatus). Therefore an alternative light source arrangement for the microscope was required. Initially a single LED attached to the piezoelectric translation stage was trialled, but this limited the wide field illumination

needed for locating the pipette and choosing a suitable cell. Similarly an LED source suspended from the top of the Faraday cage had similar results (Figure 3.3.3a). The best illumination was provided by using a string of LED lights in series arranged in a circle around the bath chamber. In order to prevent shadows of the pipette tip being viewed in the bright field image created by the multiple light sources, one of the LEDs protruded beyond the others, acting as a dominant source (Figure 3.3.3b). This LED arrangement was supplied by a USB cable, which would need to be grounded when not in use to prevent noise during electrophysiological recording.

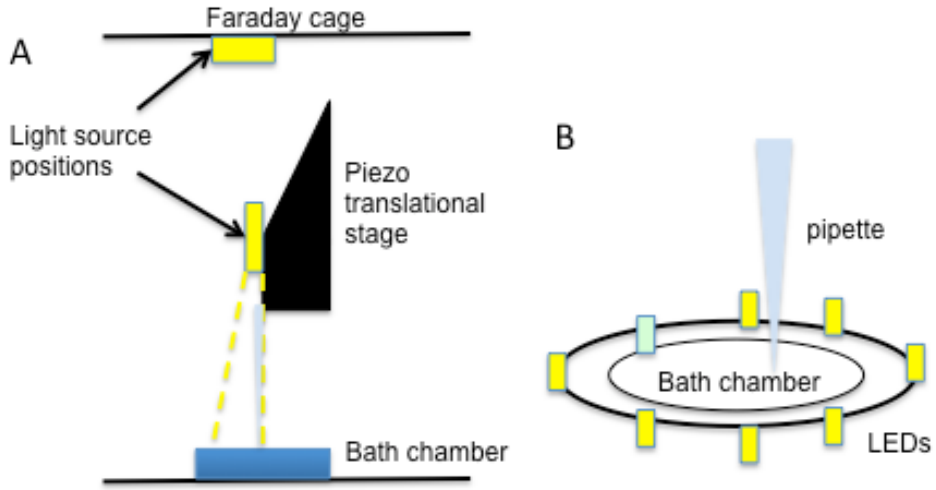

Figure 3.3.3 (a) Previous positions trialled for light source within rig (b) Distribution of LEDs around bath chamber; green LED dominant

As the scanning nanopipette had to be held vertically, it could not be connected directly to the headstage as it was already part of the piezoelectric translational stage. To overcome this a thin insulated wire was fashioned with pins on either end as a connector between the headstage and nanopipette. Importantly this did not change the impedance of the circuit. The SICM software only functioned in a 32-bit

system, thus a way to simultaneously use it with the 64-bit software (LabView, QCapturePro, Multiclamp) was required. We installed a 32-bit virtual machine (VM Ware) to run the SICM software, which communicated with the Ionscope controller via a USB port, which did not retard either topographic or electrophysiological data acquisition.

To integrate epifluorescence imaging in the set-up, blue LED illumination (and longpass dichroic mirror with 505nm cut-off wavelength) and green LED illumination (and longpass dichroic mirror with 560nm cut-off wavelength) were installed (OptoLED). The images were obtained using a high-sensitivity EM-CCD camera (Evolve).

Previous experience from the laboratory indicated that constant perfusion of the neuronal culture once in the chamber achieved longer cell viability than with static medium. In addition the application and washout of drugs and toxins would require a perfusion system (Figure 3.3.1c). The perfusion system we set up worked by gravity with a pump (Easyload II) at it lowest point to recycle the solution. A perfusion rate of 1ml per minute was adopted for bathing the cells in extracellular buffer. In order to estimate the time required for a drug to adequately perfuse the cells, the following control experiment was performed. After perfusing an empty coverslip with extracellular solution at the usual rate of 1ml/minute to reach a steady state, the perfusing fluid was switched to extracellular solution containing Alexa Fluor488 dye. A timer was started and the coverslip was viewed under blue LED illumination until

the fluorescence was detected and the timer was stopped. An average time of 90 seconds was recorded and subsequent analysis used this time window.

3.3.3 Recording solutions

All recordings were conducted at ambient temperature (23°C–26°C) 12–19 days after plating. The standard extracellular solution used in all experiments contained 125 mM NaCl, 2.5 mM KCl, 2 mM $MgCl_2$, 2 mM $CaCl_2$, 30 mM glucose, and 25 mM HEPES (pH 7.4). AMPA, NMDA, $GABA_A$, and $GABA_B$ receptors were routinely blocked with 10 μM 2,3-dihydroxy-6-nitro-7-sulfamoyl-benzo[f]quinoxaline- 2,3-dione, 50 μM (2R)-amino-5-phosphonovaleric acid, 100 μM picrotoxin, and 1 μM CGP 52432. APV was from Ascent. All other compounds were from Tocris.

Active synapses were labelled in **Section 4** with 20 mM (bath concentration) FM1-43 (Invitrogen) or 200 mM SynaptoRed C1 (SRC1, Biotium) by incubation in the extracellular solution, with 90 mM NaCl replaced by 90 mM KCl for 90 s followed by a 10–15 min wash in the original solution.

3.3.4 Patch clamp

The use of filamented borosilicate glass was based on previous experience from our collaborators at the Korchev lab (Imperial College London). Initially a filament puller

was used to pull the pipettes. However this resulted in substantial variability in pipette resistance and taper. Resolving individual synaptic boutons and axons on 3D topographical images requires reproducibly high-resistance pipettes with a small inner tip diameter (~100 nm; (Novak et al., 2009; Sánchez et al., 2008). To achieve this, a horizontal laser−based puller was used (Sutter P-2000). Furthermore, pipettes deteriorated over several days of storage, thus affecting the quality of HPICM images, increasing the likelihood of pipette blockage, and decreasing the success of bouton patching. Placing the pipettes in a desiccator to prevent the tips from being affected from moisture did not prevent the above complications from occurring. Thus nanopipettes were made each morning prior to experimenting.

For high resolution scanning and cell−attached recordings (**Section 4**) pipettes pulled from borosilicate glass (OD 1 mm, ID 0.5 mm, Sutter Instruments) were used. The pipette resistance was in the range of ≈ 80–110 MΩ, corresponding to an estimated inner tip diameter of ≈ 90–125 nm. The pipette resistance of widened pipettes used for whole-cell recordings in small synaptic boutons (described in detail in **Section 4.2**) was within the range 35 to 45 MΩ, corresponding to an inner tip diameter of ≈ 350–450 nm. For paired recordings (**Section 7**) the soma was patched under light microscopy using a 3–5 MΩ conventional patch pipette and the HPICM nanopipettes were the same as above.

Cell−attached Ca^{2+} recordings (**Section 4.3**) were performed using a pipette solution that contained 90 mM $BaCl_2$, 10 mM HEPES, 10 mM TEA-Cl, 3 mM 4-aminopyridine, adjusted to pH 7.4 with TEA-OH and zeroed cell membrane potential

by switching the bath solution after obtaining a gigaseal to 120 mM KCl, 3 mM $MgCl_2$, 5 mM EGTA, 11 mM glucose, and 10 mM HEPES (pH 7.4). Whole-bouton Na^+ current recordings (**Section 4.3**) were performed using the standard extracellular solution without Ca^{2+} in the bath and a pipette solution containing 135 mM $CsMeSO_4$, 2 mM $MgCl_2$, and 10 mM EGTA (pH 7.4 with CsOH). Whole-cell K^+ current recordings (Figures 4H–4J) were performed with a Ca^{2+}-free extracellular solution containing 1 mM tetrodotoxin and a pipette solution containing 135 mM $KMeSO_4$, 10 mM HEPES, 10 mM Na-Phosphocreatine, 4 mM $MgCl_2$, 4 mM Na_2ATP, and 0.4 mM Na_2GTP. Whole-bouton Ca^{2+} current recordings were performed in the standard extracellular solution (containing 2 mM $CaCl_2$) supplemented with 1 mM tetrodotoxin. The pipette solution contained 145 mM $CsMeSO_4$, 2 mM $MgCl_2$, 2 mM Na_2ATP, 0.3 mM Na_2GTP, 10 mM HEPES, 10 mM EGTA, and 5 mM Na-creatine phosphate (pH 7.4 with CsOH). Confirmation that recorded Ca^{2+} currents were mediated by VGCCs in some experiments was demonstrated by adding 0.1 mM $CdCl_2$ to the extracellular solution. In outside-out experiments, the extracellular solution was replaced by buffer containing 135 mM CsGluconate, 20 mM $BaCl_2$, and 10 mM HEPES (pH 7.4 with CsOH).

For paired soma/bouton recordings (**Section 6.0 −7.0**) the internal solution for soma pipette was 130 mM K gluconate, 10 mM KOH-Hepes, 1 mM KOH-EGTA, 10 mM KCl, 4 mM Mg-ATP, 0.5 mM Na-GTP (pH 7.35 with KOH). The nanopipette used for HPICM contained the same internal solution supplemented with 200 µM Alexa Fluor 568 (Invitrogen). DTx−K (20nM) was added to the extracellular solution to block

K_V1.1 channels and UK-78282 (200 nM) was added to block Kv1.3 and Kv1.4 channels. DTx-K and UK-78282 were from Alomone Labs.

Fluorescence dye	Ex/Em wavelength (nm)	Stock conc.	Final conc.	Storage	Supplier
SynaptoRed C1 (SRC1)	558/734	20mM	200μM	−20°C	Biotium, USA
Alexa Fluor 488	490-525	20mM	200μM	−20°C	Thermo Fisher Scientific
Alexa Fluor 568	578-603	20mM	200μM	−20°C	Thermo Fisher Scientific

Table 3.3.6 Dyes for identifying presynaptic boutons

3.3.5 Data Acquisition and statistical analysis

Single-channel currents (**Section 4.3**) were recorded under voltage-clamp, filtered at 1 kHz and sampled at 20 kHz. Data acquisition and analysis were done using pCLAMP 9.2 (Molecular Devices). For whole-cell currents the membrane

capacitance was not actively compensated and the specific ion-channel currents free of capacitive transients were obtained using a P/N leak subtraction protocol implemented in the pCLAMP 9.2 and LabVIEW acquisition software. Action potentials (**Section 6.0 – 7.0**) were recorded in current-clamp mode and either elicited by directly injecting current into the bouton, or by injecting current into the soma and recording passively from the bouton, Recordings were filtered at 5 kHz, digitized at 10 kHz, and acquired and analysed off-line with custom LabVIEW (National Instruments) software. Cells where action potentials did not exceed 0 mV were discarded. The spike take-off point was estimated from the peak of the second time derivative of voltage, and spike half-width was measured at the half-way voltage between take-off and peak (discussed in greater detail in **Section 5.0.5)**. Where several spikes were elicited, only the first was analyzed.

Statistical analysis was performed using SigmaPlot (Systat Software) and Microsoft Excel.

4.0 Imaging presynaptic boutons and recording ion currents using HPICM

4.0.1 Identifying active presynaptic boutons and obtaining a high resolution topographic image with HPICM

In order to identify active synapses in the complex network of hippocampal neuronal cultures, I labelled active synapses with the dye SynaptoRed C1. The coverslip was then transferred to the recording chamber of the rig and perfused with EC solution at a rate of 1ml/min. A suitable area rich in axons was chosen under light microscopy using a 60x objective. Under blue LED illumination I could identify isolated bouton-rich fields of interest, which fluoresced as red (Figure 4.1a). The pipette was lowered into the bath using the coarse manipulator. Pipette resistance was calculated with the 5mV seal test and the pipette tip potential was offset to zero. The pipette was then lowered to the level of the neurons using the fine manipulator. Once the pipette was 3000nm above the cell surface two images were taken, light transmitted and fluorescence, and these were co-registered using the SICM software. The area of interest was then scanned in nanoscale resolution using the HPICM method (Figure 4.1b). The hop amplitude (i.e. prescan pipette – sample separation distance) can be controlled depending on the structure being scanned; I chose an amplitude of 4000nm when scanning cell bodies and 2000nm when scanning axons and dendrites. Once the initial scan was completed, a higher resolution scan of the bouton of interest was then performed (Figure 4.1c). Height-coded topographical images (in which z coordinates are represented by shades of grey) were initially obtained (Figure 4.1c, e1, e2) and allowed direct identification of the exposed presynaptic boutons. These images could then be rendered to produce slope coded topographical images (Figure 4.1f1, f2) where the gray scale intensity of each pixel

was determined by calculating the local slope using the function sourceΦ =arctan(dz/dx) on data from the height coded image, giving the visual appearance of illumination from the right.

This approach also enabled us to estimate the morphological size of live synaptic varicosities resting on dendritic surfaces (Figure 4.1g, h – data from Pavel Novak). The volume of identified synaptic boutons (V = 0.14 ± 0.11μm^3, mean ± S.D., n = 41) was in agreement with previous electron microscopy estimates (V = 0.12 ± 0.11μm^3) (Schikorski and Stevens, 2001).

4.1 Properties of presynaptic boutons

Once SICM maps out the cell topography, the same pipette can be returned precisely to any point on the surface to obtain a cell-attached recording, which we have termed ‘smart patch-clamp’ (Novak et al., 2013). One important factor to consider is that although epifluorescence imaging may identify an active synapse, it may not be amenable to patch-clamp and so must be co-registered with SICM topography. This is illustrated in Figure panels 4.1 d1 and d2 as both boutons demonstrated fluorescence; however the bouton in 4.1 e1, f1 is exposed to the pipette and amenable to patch-clamp, but the bouton in 4.1 e2, f2 is obstructed by an overlying dendrite and not amenable to patch-clamp.

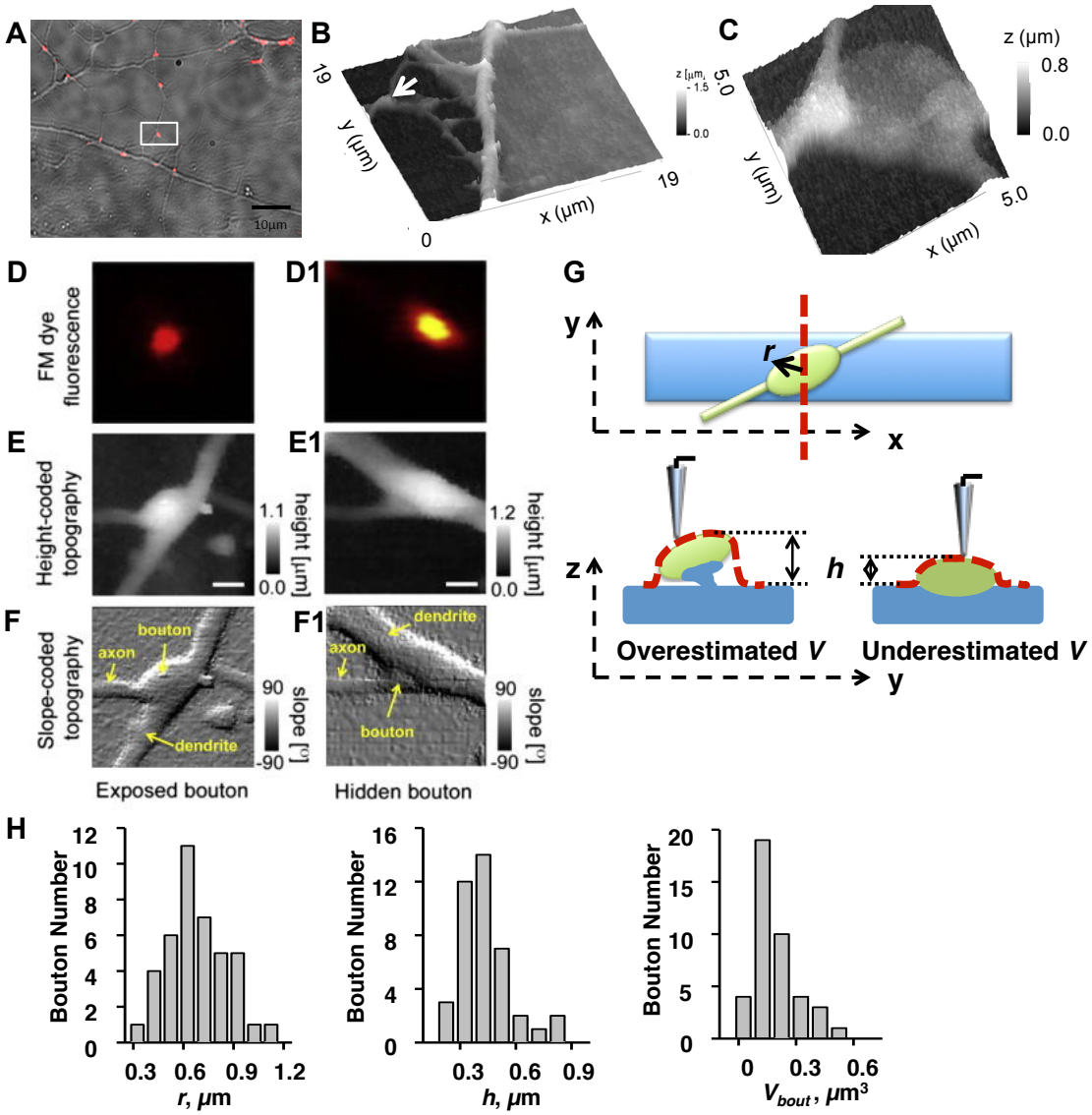

Figure 4.1. **HPICM imaging of synaptic boutons**. (a) Merged image of neuronal network in culture. Grey – transmitted light image. Red – SynaptoRedC1 (SRC1) labelled synaptic boutons. (b) SICM image of boxed area of interest in (a). Arrow depicts bouton. (c) SICM image of the bouton magnified (my data) (d1,d2) FM dye fluorescence identifying active boutons. Height coded topography of amenable bouton (e1) and obstructed bouton by overlying dendrite (e2) Scale bars all 1 µm. (f1,f2) Slope coded topography of e1 and e2 (g) Schematic illustrating estimate for presynaptic bouton size and geometry. Volume was estimated by direct integration of the planar scans over x, y and z. Due to variability in synaptic organisation, SICM

may either overestimate (bottom left) or underestimate (bottom right) the true volume. (h) Distributions of the radius r = 0.63 ± 0.18μm (left), height h = 0.38 ± 0.14 μm (middle) and volume V = 0.135 ± 0.11μm^3 (right) measured for 41 boutons (data from Novak, Gorelik and Korchev).

4.2 Controlled widening of scanning nanopipette to allow whole-cell patch clamp recording

A major limitation of smart patch clamp is its restriction to the exposed membrane directly accessible to the vertically oriented nanopipette. Ion channels in and near the active zone (AZ) are hidden from the patch pipette; meaning currents mediated by these channels cannot be recorded. In order to test the hypotheses stated in **Section 3**, detailed analysis of the AP waveform at the bouton would be required, and thus far only cell-attached recording (where AP morphology can only be inferred) of boutons was possible. In principle both above scenarios could be resolved by rupturing the membrane patch of the terminal and enter the whole-cell patch-clamp configuration. Resolving individual synaptic boutons and axons on 3D topographical images, however, requires high-resistance pipettes with a small inner tip diameter as explained above. Therefore, in practice, we could not break the presynaptic cell membrane and obtain whole-cell patch-clamp recordings when using the original scanning nanopipettes.

To overcome this limitation, the Korchev group, Imperial College London, optimized a method to widen the ultra-fine pipette tip after the completion of the high-resolution

3D topography scan by breaking it against the glass coverslip (Böhle and Benndorf, 1994; Novak et al., 2013), using programmable feedback control of the HPICM scanner controller. The nanopipette tip-breaking procedure consisted of three steps (Figure 4.2a). First, the pipette was navigated to a previously identified area of the coverslip free of any processes. Second, the fall rate (the rate at which the pipette repeatedly approaches the surface during "hopping") was increased from the standby rate (typically 60 nm/ms) by approximately one order of magnitude (to ~500 nm/ms). At this fall rate, the noncontact mode of HPICM could no longer be preserved because of the inherent latency of the z axis piezo feedback control. As a result, the pipette repeatedly crashed into the coverslip, breaking its tip and increasing its diameter because of the conical shape of the pipette. During initial trials of the procedure only the fall rate could be manipulated, leading to the positive feedback of the increased fall rate overcoming the noncontact mode in most cases and resulting in broken pipette tips. However with our collaboration the chopping procedure was further refined to terminate automatically once the baseline current increased by a pre-determined percentage. This, together with the fall rate, enabled much more control in pipette tip breaking and resulted in reproducible stepwise decreases of the pipette resistance (red arrows in Figure 4.2b). This stepwise breaking of the pipette also ensured that the tip itself was smooth, thereby increasing the likelihood of a good seal when attempting whole-cell configuration. To prove this was the case electron micrographs of the pipette tip were taken before and after pipette breaking (Figure 4.2c,d). The breaking was automatically stopped by returning the fall rate to baseline (60 nm/ms) once the pipette current reached a desired level. This process could be repeated to fine-tune the desired pipette tip

diameter in steps as small as 10% by varying the stop criteria for current increase, duration, and “breaking” fall rate (Figure 4.2e).

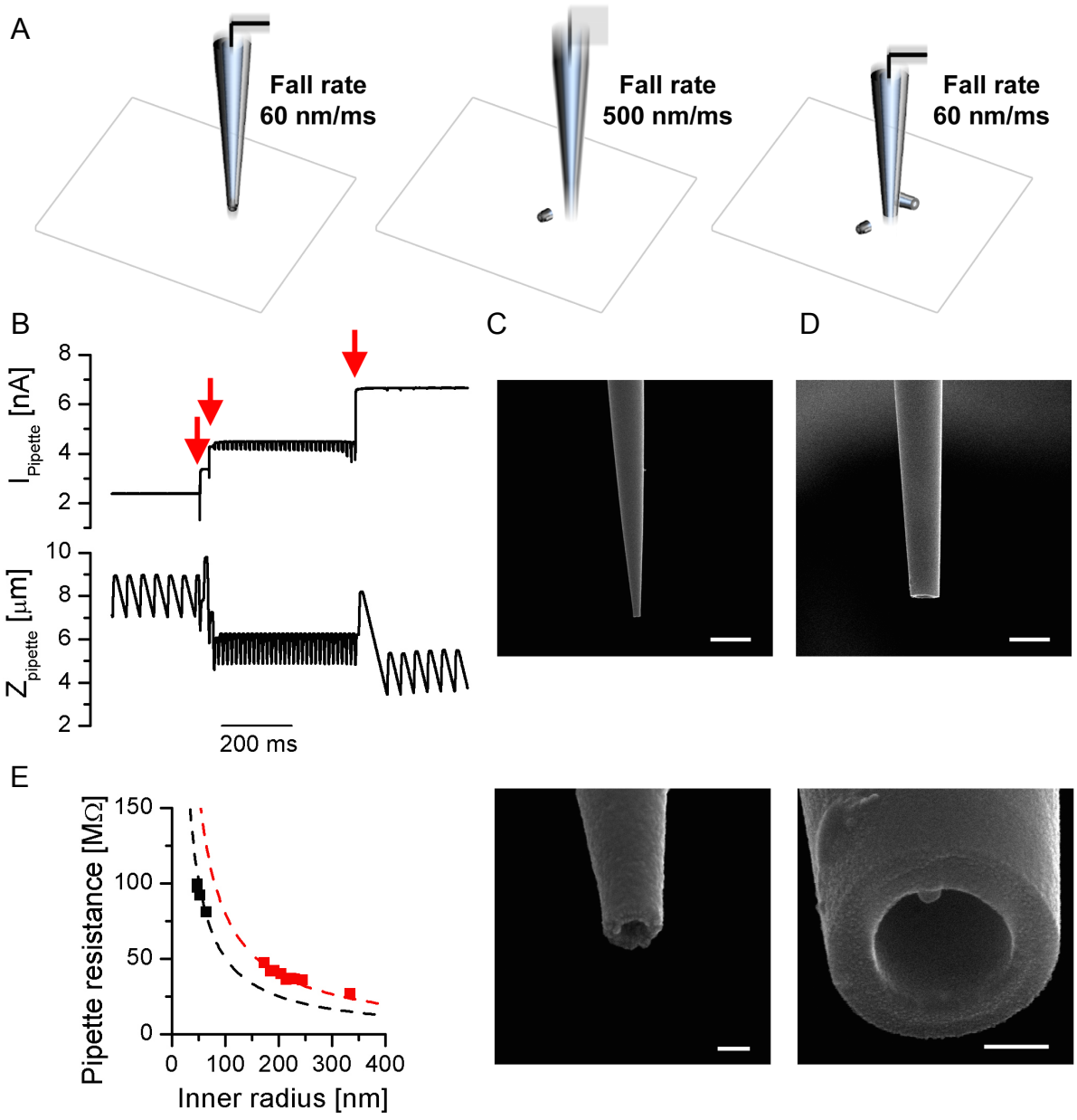

Figure 4.2 (a) Schematic illustrating the pipette widening procedure (b) Traces of pipette z position and pipette current during the breaking procedure. Every time a small fragment of the pipette tip is chopped off, the pipette current increases (red arrows). The holding pipette voltage was kept constant at 200 mV. (c and d)

Scanning electron microscopy images of two representative nanopipettes pulled from the same capillary, one of which was widened using the controlled breaking procedure. Side views of the intact pipette (c) and widened pipette (d) at low (top) and high (bottom) magnification. Scale bars represent 1 μm in top of (c), 100 nm in bottom of (c), 1 μm in top of (d), and 200 nm in bottom of (d). (e) Relationship between pipette resistance and inner tip diameter for intact pipettes (black) and widened pipettes (red) (Data from Pavel Novak).

4.2.1 Attaining whole cell configuration of a presynaptic bouton using SICM

The method was identical to **Section 4.0** up to the acquisition of a high resolution scan of the bouton. The pipette was filled with KGluc intracellular solution (Table 3.3.4) and the morphological fluorescent tracer AlexaFluor 488 (50 μM). Once a high resolution image of the bouton was acquired, the pipette was directed to any empty area of coverslip. Crucially as the broken pipette was held vertically at all times, the x and y co-ordinates of the pipette did not alter, meaning that the pipette could be navigated exactly to the targeted bouton to achieve a Gigaseal. The membrane was clamped to a holding potential of -70mV, and once a Gigaseal was established the fast and slow capacitance transients were cancelled via the amplifier interface (Multiclamp Commander). The presynaptic membrane was ruptured by applied suction to obtain a whole-bouton configuration. The configuration is recognised by the characteristic capacitance transients seen on the passive current trace (Figure 4.2.1a). The AlexaFluor 488 in the pipette solution allowed us to verify fluorescence

in the patched bouton and adjacent axon and boutons (Figure 4.2.1b,c). This process also gave us an insight into the morphology of axons in neuronal culture (Figure 4.2.1d).

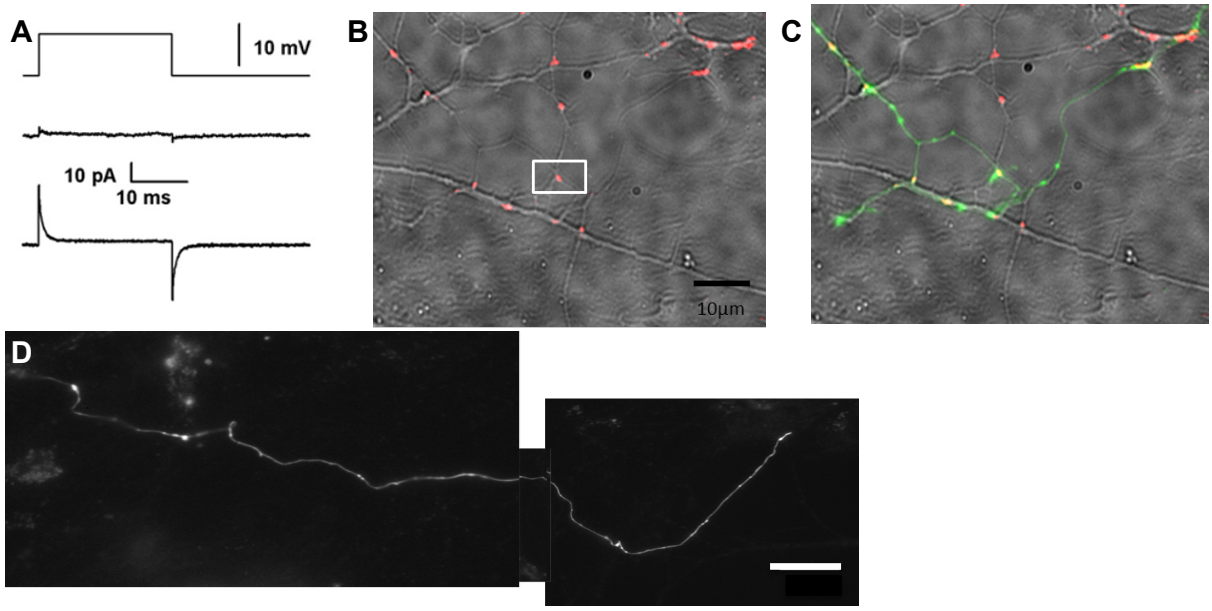

Figure 4.2.1 **Whole-bouton recording** (a) A typical passive current response to a 10mV square voltage command (top) in bouton-attached configuration (middle) and then whole-bouton configuration (bottom). (b) Overlay of SRC1−stained active synaptic terminals (red puncta) with transmitted-light image of neuronal culture. White arrow marks the bouton where whole-cell was subsequently obtained. (c) The same area as in (a) showing labelling with AlexaFluor488 (green channel) of the patched bouton and adjacent axon. (d) An en passant bouton and associated axon loaded with AlexaFluor488; scale bar 10 µm

4.3 Na^+, K^+, and Ca^{2+} whole cell current recordings in presynaptic boutons

4.3.1 Introduction

As previously discussed, action potentials are generated near the action initial segment, propagate down the axon and reach the pre-synaptic terminals where they evoke neurotransmitter release (Hille, 2001; Katz and Miledi, 1967). However the mode of this propagation and how it couples to neurotransmitter release is unclear. Previous experiments at the amphibian neuromuscular junction demonstrate a passive process of AP invasion into pre-synaptic terminals (Dreyer and Penner, 1987; Lindgren and Moore, 1989). However, action potentials propagate with high reliability in axons bearing en-passant boutons (Cox et al., 2000; Engel and Jonas, 2005). Moreover, outside-out patches of central synapses, hippocampal mossy fibre boutons, have shown a high presynaptic Na^+ channel density of ~ 2000 channels per bouton, with rapid inactivation onset and recovery kinetics. In addition, computational analysis suggests that Na^+ channels amplify the pre-synaptic AP to increase Ca^{2+} inflow as opposed to axonal Na^+ channels which determine the speed of AP propagation (Engel and Jonas, 2005). However MFBs are large and highly specialised synapses, not representative of the majority of pre-synaptic terminals.

VGCCs form variable sized clusters in the active zone of the presynaptic terminal (Holderith et al., 2012; Nakamura et al., 2015; Sheng et al., 2012) corresponding with their central role in exocytosis enabling reliable coupling of Ca^{2+} entry and

neurotransmitter release. Direct recordings from giant terminals indicate that evoked exocytosis is dependent on Ca^{2+} entry near release sites in the active zone (Sheng et al., 2012). However the sensitivity of neurotransmitter release in central synapses to intracellular Ca^{2+} buffering suggests that a proportion of Ca^{2+} sources are distant to the Ca^{2+} sensors triggering exocytosis (Eggermann et al., 2012; Ohana and Sakmann, 1998). If this were true then the relative contribution of these sources to Ca^{2+} entry in the micrometre sized boutons we are studying would be significant, even if they occurred in a low surface density. These 'ectopic' VGCCs would have a prominent role in AP-evoked release of vesicles and short term synaptic plasticity (Nadkarni et al., 2012).

4.3.2 Main aims

- Verify that sodium and potassium currents can be recorded from small presynaptic boutons
- Identify the site of calcium channels in presynaptic boutons

4.3.3 Results

Na^+ currents

Current traces were recorded by voltage-clamping at -80mV and then providing a 50ms prepulse to -120mV followed by voltage commands ranging from -70mV to + 70mV in 10mV 5 ms steps (n=7) as previously used by Engel and Jonas, (Engel and Jonas, 2005). In order to isolate the Na^+ current of the solitary bouton from the rest

of the axon, I performed an outside-out patch clamp recording (achieved by slowly withdrawing the pipette from the bouton once whole-cell was completed, n=3). As expected that had a reduced peak amplitude (mean and SEM of -30.5 ± 0.65pA compared with -74.5±7.6pA) (Figure 4.3c).

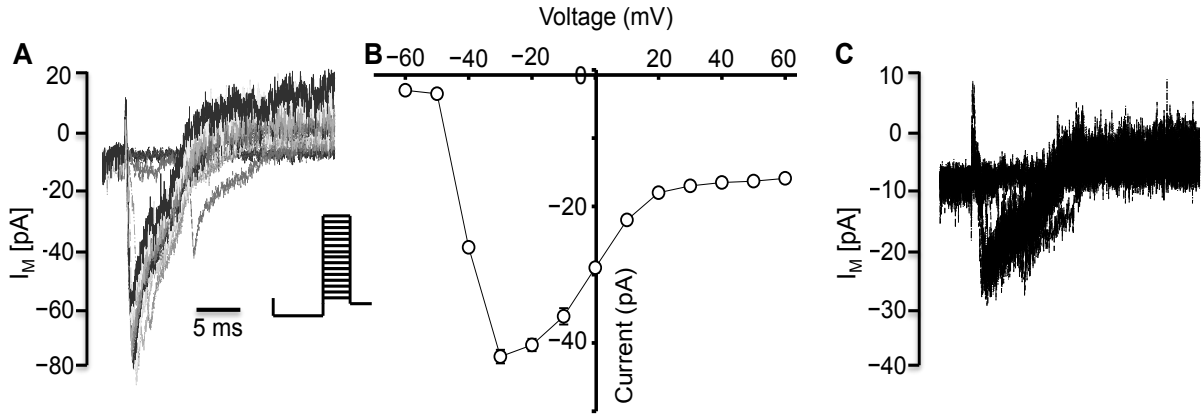

Figure 4.3. **Whole-bouton sodium traces** (a) Example of pre-synaptic whole-bouton Na^+ recording with inset of pulse protocol (b) associated IV curve (c) Example of outside-out Na^+ recording (n=3)

K^+ currents

Current traces were recorded by voltage-clamping at -80mV and then providing a voltage commands ranging from -70mV to + 70mV in 10mV 400 ms steps (n=5) (Figure 4.3.1 a,b).

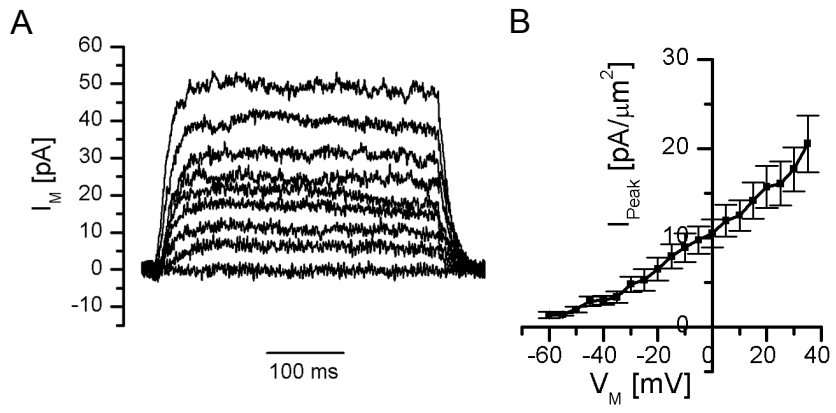

Figure 4.3.1 (a) Example of pre-synaptic whole-bouton potassium trace with (b) associated IV curve (n=5) (Data from Pavel Novak)

Ca^{2+} recordings

To assess properties of VGCCs in small presynaptic boutons, we first attempted HPICM-targeted cell-attached recordings from the exposed bouton surface. Our collaborators (Korchev, Gorelik and Novak) performed 44 bouton cell-attached patches with unmodified scanning nanopipettes and 21 patches with a broken (~300nm) pipette at different parts of the exposed bouton (n=65). In these recording no evidence of VGCC activity was found (Figure 4.3.2 a).

In order to access the whole presynaptic membrane including the active zone a whole-cell configuration was required. Once a whole-cell configuration was attained, the perfusion was switched to also include the potassium channel blocker tetraethylammonium chloride (20mM). Currents consistent with VGCC activity were

obtained in whole cell mode (Figure 4.3.2 b). To verify that these were mediated by VGCCs, the broad spectrum blocker cadmium was then applied after one minute of recording. This uniformly abolished the current (n=5) (Figure 4.3.2 c). To further dissect the presynaptic calcium current, ω-Agatoxin, a specific blocker of the P/Q calcium channel subtype, was added in a single experiment (Figure 4.3.2 e). This decreased the calcium current peak amplitude by 48%.

A possible explanation for the discrepancy between whole cell recordings, which revealed a robust calcium current, and cell-attached recordings that failed to reveal single channel activity, is that the VGCCs are confined to the active zone, which is inaccessible to the pipette used for cell-attached recordings. Consistent with this hypothesis, in a separate experiment, whole-bouton Ca^{2+} currents were abolished when proceeding from whole-cell to outside-out configuration (Figure 4.3.2 f).

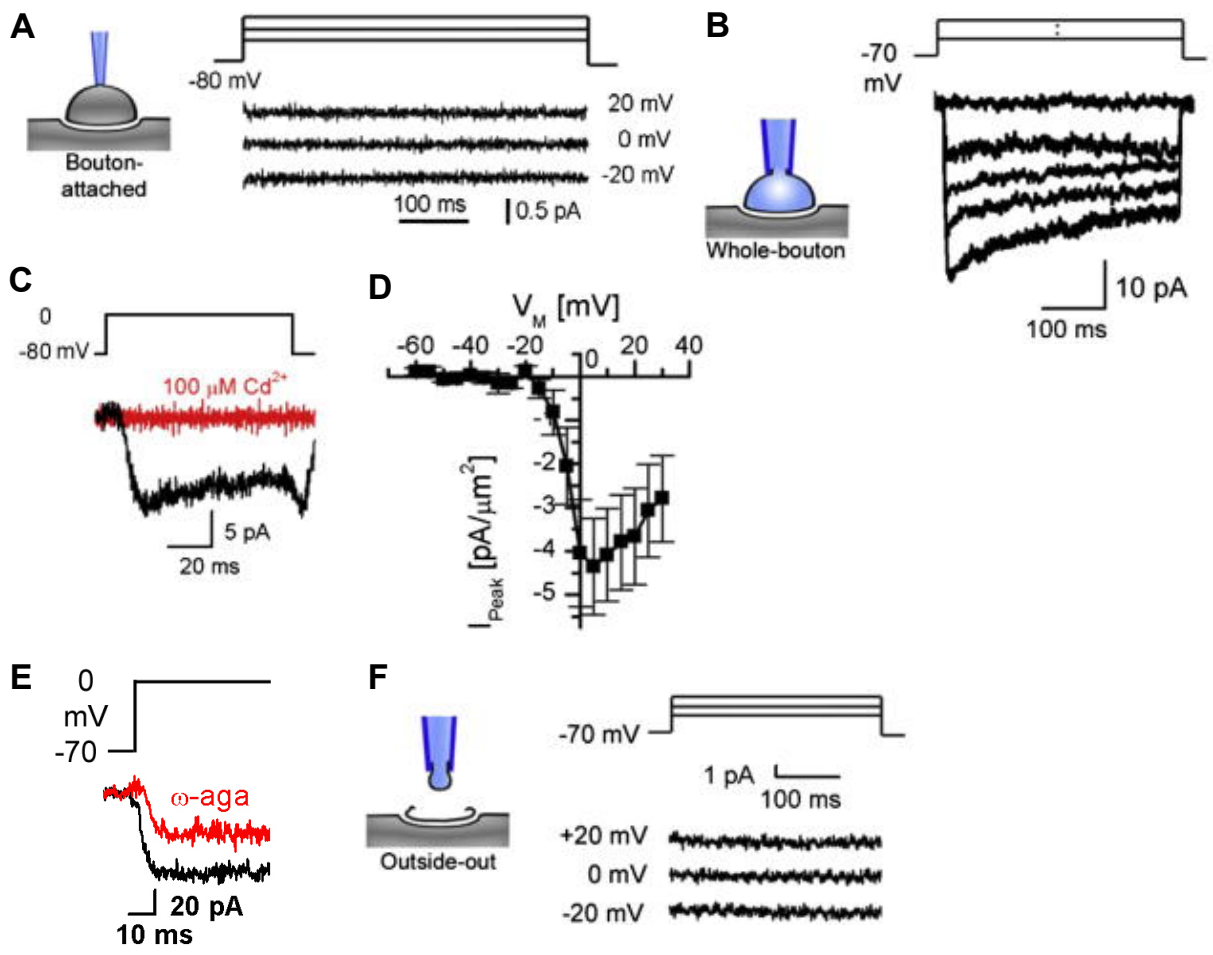

Fig 4.3.2 **Recording VGCC activity in presynaptic boutons** (a) Cell-attached recordings showing no VGCC activity on the exposed surface of the presynaptic bouton (b) Example of pre-synaptic whole-bouton Ca^{2+} current (c) Example of a whole-bouton Ca^{2+} recording before (black) and after (red) cadmium application (n=6) (d) associated IV curve for Ca^{2+} current. (e) Whole-bouton Ca^{2+} before (black) and after (red) the application of ω -agatoxin (f) Absence of VGCC recording in outside-out patch (Novak et al., 2013).

4.3.4 Conclusions

Using HPICM in addition with the novel pipette 'breaking' technique all four configurations of patch-clamp: cell-attached, inside-out, whole-cell and outside-out are possible, giving unprecedented information into the presynaptic physiology of small synapses. In this experiment, whole-bouton sodium currents and potassium currents were recorded and demonstrated the typical kinetics seen in larger central synapses (Engel and Jonas, 2005; Geiger and Jonas, 2000).

No VGCC activity was detected with the pipette cell-attached to the exposed surface of the presynaptic bouton. To obtain confidence estimates for channel density Monte-Carlo simulations were performed. With the assumption that channels are randomly found on the exposed cell surface, a probability of finding no channels can be derived based on the membrane area sampled (in this case the nanopipette tip area). By running the simulations numerous times for randomly selected channel densities it was estimated that the density of VGCCs on the exposed surface of axonal boutons was less than six channels per bouton (99% confidence interval) (Novak et al., 2013). However VGCC activity was found when the whole-bouton configuration was obtained. Although only seen in one experiment, the reduction of whole-bouton calcium current peak amplitude by 48% in the presence of ω -agatoxin is anecdotal evidence that about half the contribution to presynaptic calcium current in small boutons is supplied by P/Q channels, which is in agreement with previous work in larger cortical synapses (Ermolyuk et al., 2012; Holderith et al., 2012; Tottene et al., 2002). This activity was further abolished when the outside-out

configuration was achieved. The reason for this abolition was most likely because the active zone remained firmly attached to the post-synaptic density and therefore inaccessible to the outside-out configuration. This data strongly suggests that the vast majority of VGCC in central synapses are located near the active zone and are excluded from the surface membrane of the bouton.

A technical limitation of using high resistance pipettes is the quality of the voltage clamp. We estimated an upper limit for the access resistance (R_A = 156.1 ± 38.2 MΩ, mean ± SD, n = 10) by fitting the capacitive current transients generated by step command voltages using a sum of two exponential functions (Novak et al., 2013).. Thus the high series resistance (R_S) will have two detrimental effects. Firstly, it will introduce a voltage error or "IR" drop causing the cell membrane voltage (VM) to deviate from the desired clamping voltage. Secondly, it will lower the temporal resolution of the voltage clamp. Temporal resolution is approximated by the time constant, a product of R_S and cell capacitance (**Section 1.2.2)**, and so a high R_S will reduce the temporal resolution. The average time constants calculated from the capacitive current transients were t_1 = 0.074±0.024 ms and t_2 =1.3±0.5 ms (mean ± SD, n = 10), which corresponded to capacitances C_1 = 0.621 ± 0.226 pF, C_2 = 0.962 ± 0.655 pF. These values are significantly higher than would be expected from a single bouton, and so are likely to reflect the compound capacitances of the axonal arbor and possibly the cell soma.

Another limitation is that because the length constant of axons is of the order of

hundreds of microns, the currents obtained could have arisen from distant sources. An indication for this is the slow kinetics demonstrated in the whole-bouton Na^+ current (Figure 4.3). One would expect that the current would reverse i.e. pass 0 pA, at around +60 mV, which does not occur with our recordings. This has implications when localising calcium channels, as again the Ca^{2+} current could have arisen from several boutons. One way to overcome this would be to anatomically isolate the bouton by severing it from the rest of the axon once identified, for example with a laser. This bouton could then be patched onto to provide single bouton electrophysiological information.

5.0 Recording of presynaptic action potentials

5.0.1 AP recording in rat hippocampal cultures - Introduction

As discussed earlier the kinetics and more specifically the waveform of the action potential (AP) received at the pre-synaptic terminal, determines how calcium channels open and how calcium influx triggers exocytosis of neurotransmitter vesicles. It has been suggested that the AP waveform can be modulated depending on the geometry of axons and the activation state of voltage-gated ion channels (Debanne, 2004). Furthermore, broadened APs more efficiently activate calcium channels at presynaptic terminals and facilitate synaptic transmission to postsynaptic neurons (Awatramani et al., 2005a; Geiger and Jonas, 2000; Sasaki et al., 2011). To directly investigate the mechanisms underlying presynaptic AP waveform, we used HPICM to identify small intact boutons in rat and then mouse hippocampal neuronal cultures for patch clamp.

5.0.2 Main aims

To record an action potential waveform from a pre-synaptic bouton

5.0.3 Method

Once whole-cell configuration was achieved, the bouton was then current-clamped at 0 pA., with appropriate ‘bridge balancing’ and capacitance neutralisation

performed. A current pulse of 50pA was delivered over 10ms to elicit an action potential. Briefer current pulses (1ms, 2ms) did not elicit an action potential even up to currents of 800pA. Longer pulses (up to 100ms) also produced only a single action potential.

5.0.4 Results

In order to compare action potential waveform between cell soma and presynaptic bouton, action potentials were elicited from both in separate cells. Table 5.0.4 describes the results.

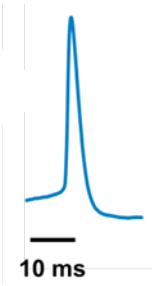

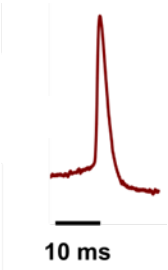

	Amplitude soma (mV)	AP half-width soma (ms)	Amplitude bouton (mV)	AP half-width bouton (ms)
	67.4	1.04	62	0.91
SEM	6.2	0.21	4.9	0.19
n	6		5	

Table 5.0.4 AP waveform comparison between spikes elicited at bouton and soma in rat hippocampal cultures

5.0.5 Conclusions

To our knowledge this is the first demonstration that action potentials can be elicited by current injection into a submicrometer sized presynaptic bouton. This argues that, despite the disruption to the cell membrane caused by the SICM patch pipette, there were still ample Na^+ channels present to generate action potentials. The technique could now be translated to the EA1 disease models.

In terms of technical considerations, a 'Bridge Balance' needed to be performed to accurately measure membrane potential deflections in response to current injection. This is because the current injected down the micropipette encounters both a series resistance between the micropipette and the cell, and a resistance between the intracellular solution and the bath. The bridge balance is used to compensate for the series resistance, providing a more accurate measure of the actual trans-membrane potential when a current is injected. Another consideration is microelectrode capacitance. The capacitance at the input of the headstage amplifier is due to the capacitance of the amplifier itself (C_{in1}) and that of the microelectrode and its connecting lead (C_{in2}). This capacitance in addition to microelectrode resistance acts as a low-pass filter for signals recorded at the tip of the electrode. Ideally microelectrodes with the lowest possible resistance would be used to minimise the contribution to microelectrode capacitance. However as previously discussed the pipette resistance post 'breaking procedure' (see **Section 4.2**) is around 30MΩ, an order of magnitude greater than usual patch pipettes. Thus any AP waveforms

recorded using this method may be distorted by the low-pass filter created, and affect measurement of AP width and amplitude. In addition if current pulses were used to elicit AP, the C_{in2} would act as a capacitance sink, where the injected current would act to charge the microelectrode tip in preference to the bouton membrane. As using a relatively high resistance pipette is necessary for scanning, a method for electrically reducing the effective magnitude of microelectrode capacitance has been incorporated by the Multiclamp system. Termed 'capacitance neutralisation', the technique passes a current exactly equal to the current that passes through C_{in2} to the ground. Control experiments were required beforehand. For a series of boutons, the whole-cell configuration was obtained and then the level of neutralisation was steadily increased from 0pF until oscillation occurred and the clamp was lost. It was found that 7pF was reliably the highest level of neutralisation that could be obtained before oscillation occurred, so this level was chosen for all subsequent experiments. Despite this incomplete capacitance neutralisation remained a possibility, and therefore filtering of AP signals recorded.

A number of different pulse protocols were attempted to elicit APs. Initially 300pA pulses of 1ms duration were used as described by Geiger in driving APs in mossy fibre boutons in hippocampal slices (Geiger and Jonas, 2000) but these did not elicit APs in submicrometer sized boutons. By elongating the pulse to 10ms, action potentials were faithfully evoked in these boutons, with 50pA being the minimum current needed. Only single APs were elicited using this protocol. Increasing the pulse current to 80pA, 100pA, or 150pA did not alter the AP amplitude or half width.

The spike take-off point was estimated from the peak of the 2nd time-derivative of voltage. Amplitude was calculated from the take-off point to the peak and spike half-width was measured at the halfway voltage between take-off and peak. It appeared that APs elicited at the soma had a larger amplitude and larger half-width than those elicited at the bouton. From these experiments I could devise criteria on AP waveform that I would accept in further experiments. Firstly that the resting membrane potential should not be less than -60mV when in current clamp and held at 0pA. Secondly the AP must pass 0mV. Thirdly, that the half-width of the AP could be used to characterise spike shape. If the half-width exceeded 2ms the recording was discarded, as this usually represented an unhealthy bouton.

5.1 AP recording directly from pre-synaptic boutons in EA1 models

In order to test the role of $K_V1.1$ in presynaptic action potential morphology in hippocampal pyramidal cells, both a pharmacological blocker of $K_V1.1$ called Dendrotoxin-K (**Section 1.6**) and genetic deletion models including a knock-out mouse (*Kcna1a*$^{-/-}$) (Smart et al., 1998) and a knock-in mouse harbouring an EA1 mutation (*Kcna1a*$^{V408A/+}$) (Herson et al., 2003) were used. Although it has been shown in mossy fibre boutons that K_V1 channels contribute to activity-dependent spike broadening, more recent work on K_V3 and BK_{Ca} channels have argued the importance of $K_V1.1$ for this particular role. Thus using HPICM to directly record presynaptic action potentials, we can investigate whether $K_V1.1$ contributes to AP shape. AP broadening has recently been demonstrated in cerebellar basket cell terminals from *Kcna1a*$^{V408A/+}$ mice (Begum et al., 2016), but it is not known whether

this holds for forebrain terminals. Although one would expect the *Kcna1* null mice to have a loss of function effect, it is known from heterologous expression studies that $K_V1.1$ co-assembles with other members of the K_V1 family and with beta subunits, making it difficult to predict the consequences of a given mutation (Imbrici et al., 2006; Maylie et al., 2002). The *Kcna1a*$^{V408A/+}$ model bypasses this limitation of heterologous expression.

5.1.1 Main aims

1. To determine whether the AP half width differs between *Kcna1a*$^{-/-}$ mice and their wild type littermates

2. To determine wither the AP half width differs between *Kcna1a*$^{V408A/+}$ mice and their wild type littermates

3. To ask whether blocking $K_V1.1$ channels with DTx-K prolongs action potential half width in wild type, *Kcna1a*$^{-/-}$ or *Kcna1a*$^{V408A/+}$ boutons

5.1.2 Method

Experiments on hippocampal cultures from *Kcna1a*$^{-/-}$ and their wild type littermates were performed on the same day in order to avoid confounding effects of differences in developmental stage. This was also the case for *Kcna1a*$^{V408A/+}$ and their wild type

littermates. Active synapses were identified and a high resolution HPICM image was acquired using the scanning nanopipette (**Section 4.0**). The desired bouton was subsequently patched in whole cell mode and action potentials elicited via the scanning nanopiette (**Section 4.2.1**). The perfusing fluid was then switched from extracellular solution to extracellular solution plus 20nM DTx- K. Bovine serum albumin (BSA) was used to line the tubing as previous experience with DTx-K was that it avidly adhered to tubing meaning little reached the neuronal culture.

5.1.3 Results

The half width of both the knockout and the EA1 knockin was larger than their wild type littermates (Figure 5.1.4). In the *Kcna1a*$^{-/-}$ mice the mean action potential half width (t/2) was 1.42 ± 0.12ms (mean ± s.e.m; n = 9) and in wild type littermates the mean t/2 was 0.89 ± 0.06ms (n = 13), a difference of 0.53ms or 59% (p=0.002 with unpaired t test). In the *Kcna1a*$^{V408A/+}$ mice the mean t/2 was 1.04 ± 0.1ms (n = 12) and in wild type littermates the mean t/2 was 0.83 ± 0.07ms (n = 16), a difference of 0.21ms or 25% (p=0.02, unpaired t test). The AP amplitude was not significantly different between genotypes.

In all wild-type littermates, application of DTx-K increased the mean t/2 from 1.06 ± 0.09ms to 1.19 ± 0.08ms, an increase of 18% (Figure 5.1.3a) (p<0.001 with paired t test; n = 23), In the *Kcna1a*$^{-/-}$ mice application of DTx-K caused a non-significant 2% increase in the mean t/2 from 1.39 ± 0.14ms to 1.42 ± 0.14ms (Figure 5.1.3b) (p =

0.09; n = 7). In the *Kcna1a*$^{V408A/+}$ mice application of DTx-K again led to a non-significant 2% increase in the t/2 from 1.1 ± 0.07ms to 1.12 ± 0.07ms (Figure 5.1.3c (p = 0.09; n = 8).

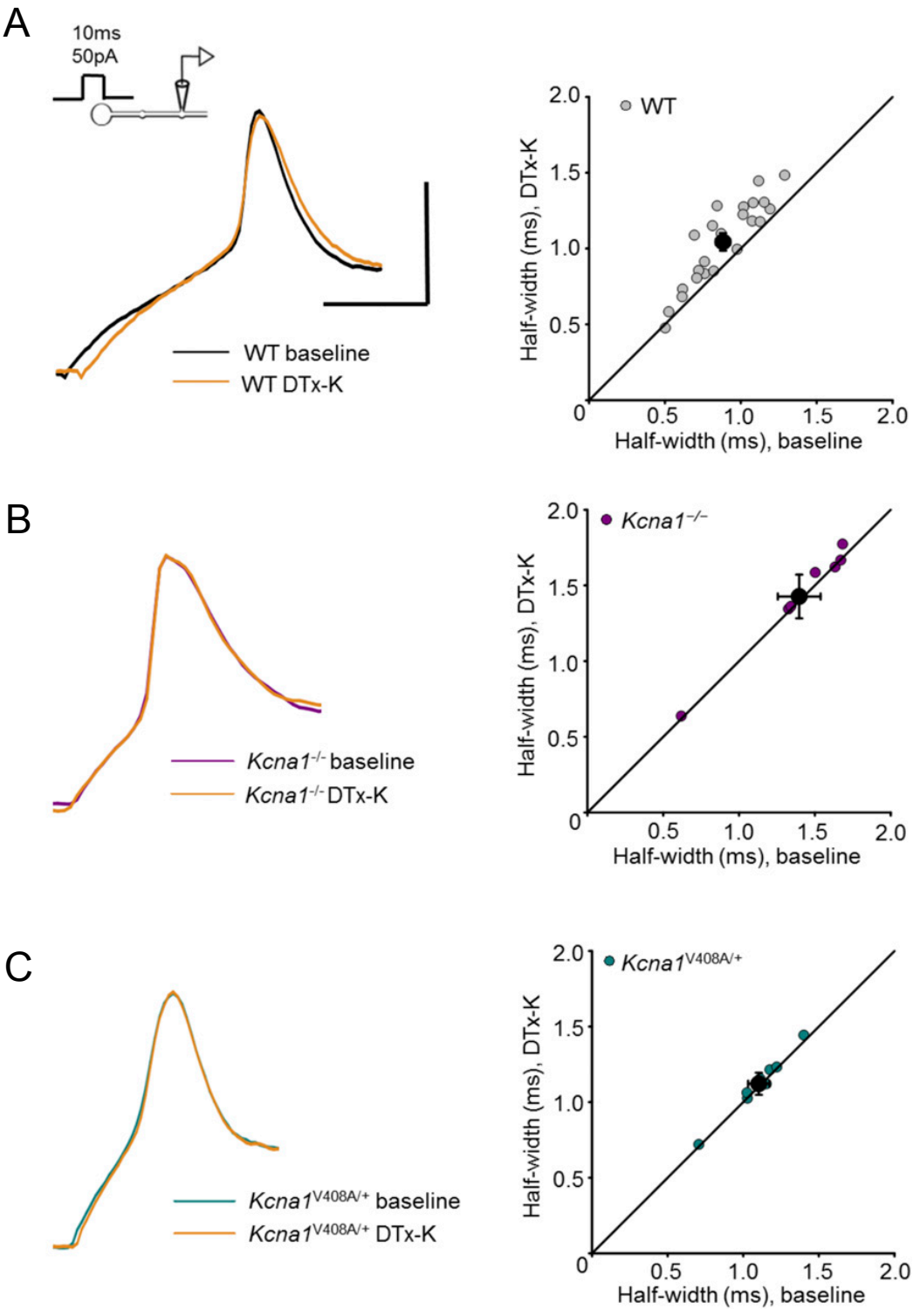

Figure 5.1.3. **Effect of DTx-K on spikes elicited at the bouton**. (A) Recordings from wild type neurons. Left, sample traces before and after 20nM DTx-K application. Right, presynaptic spike widths before and after DTx-K perfusion, showing 18 ± 3 % broadening (n = 23). Insert top left, schematics illustrating experimental paradigm with direct current injection into the recoded bouton. (B) Recordings from *Kcna1*$^{-/-}$ neurons. Left, sample traces from one neuron before and after DTx-K application. Right, DTx-K failed to broaden bouton spike width in Kcna1$^{-/-}$ neurons (n = 7). (C) Recordings from *Kcna1*$^{V408A/+}$ neurons. Left, sample traces before and after DTx-K. Right, DTx-K had no effect on bouton spike width in Kcna1V408A/+ neurons (n = 8). Scale bar in (A) applies to (B) and (C): 40 mV / 2 ms.

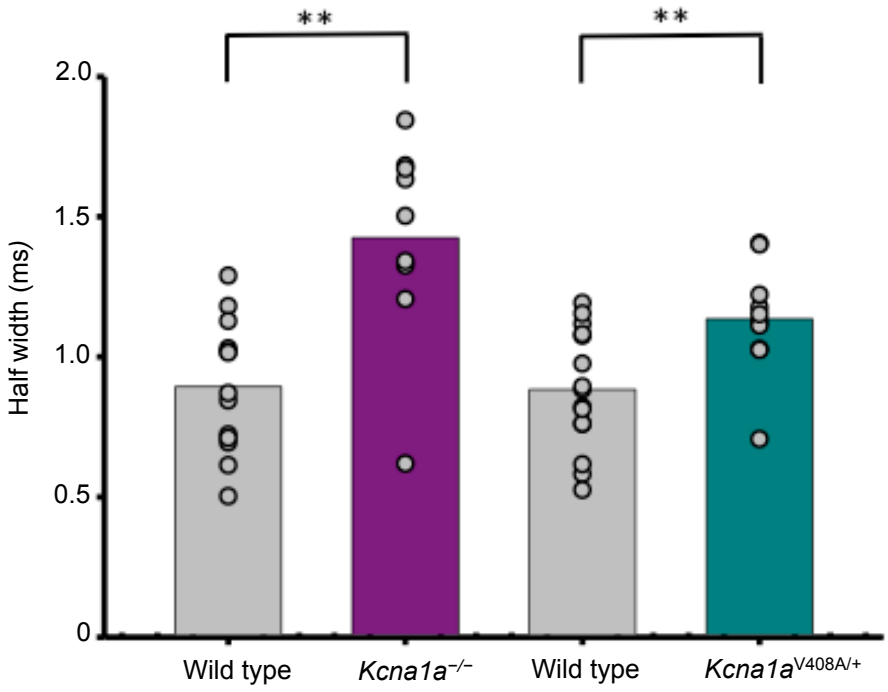

Figure 5.1.4 Action potentials recorded directly from presynaptic boutons of *Kcna1a*$^{V408A/+}$ and *Kcna1*$^{-/-}$ neurons were broader than in wild type neurons from the same mouse strains (unpaired t-test).

5.1.4 Conclusions

The AP half width in both EA1 knockout and knock-in were larger than in the wild type. This argues that K_V1.1 contributes to the repolarisation phase of the AP. This is an interesting finding, as K_V1.1 is not as strongly expressed in the forebrain as in the cerebellum (Begum et al., 2016; Smart et al., 1998). Although K_V1.1 is removed in the knockout, it is substituted by other K_V subunits such as K_v1.2 or K_V1.4. The results for the knock-in are interesting given that the mutation has not been shown to exert a dominant negative effect in heterologous studies and when expressed in *Xenopus* oocytes the V408A mutation has relatively subtle effect on current density, voltage threshold, activation kinetics and heterotetramerization (Adelman et al., 1995; Zerr et al., 1998). It is difficult to explain why the difference in *Kcna1a*$^{-/-}$ versus wild type is greater than *Kcna1a*$^{V408A/+}$ versus wild type, although small sample size (n = 9) may have contributed to this.

Dendrotoxin-K (Alamone labs) is a selective K_V1.1 blocker derived from *Dendroaspis polylepis* snake venom. The finding of DTx-K increasing wild type presynaptic t/2 by 18% is in agreement with other work on K_V1 in cerebellar basket cells, another region where K_V1.1 channels are richly represented (Begum et al., 2016). This increase is comparable to the 22% difference in t/2 seen between wild type and

Kcna1$^{V408A/+}$. The effect of DTx-K was abolished with either deletion of *Kcna1* or the heterozygous EA1 mutation.

Recording directly from the bouton has provided novel information about AP waveform and the role of $K_V1.1$ in small presynaptic terminals. However, a potential limitation of the technique is that it relied heavily on bridge balancing, and if the estimate of series resistance was incorrect, this could have distorted the recorded AP waveform. During analysis, defining the take-off point was also difficult because the initial depolarizing phase resulting from current injection was not always clearly demarcated from the regenerative depolarization at the spike onset.

In order to overcome these limitations the technique needed adapting to allow simultaneous recording from cell soma and bouton. Eliciting spikes at the soma whilst recording passively from boutons, would obviate any potential problems of improperly bridge balancing the bouton pipette. Furthermore, without an immediate voltage transient arising from local current injection may facilitate analysis of the spike shape. In addition other fundamental questions about AP transmission could be answered, such as

Is there a difference in AP amplitude between cell soma and bouton?

What factors affect how APs propagate along the axon when elicited at the soma?

Can we interpret the location of the spike initiation site from the data?

6.0 Simultaneous somatic and presynaptic bouton recordings in Kv1.1 mutant neurons

6.0.1 Method

In order to further investigate the presynaptic action potential waveform the above method had to be developed further. A conventional patch pipette for somatic recording (Ps) was identified using the larger 10x objective and lowered until it was near the culture surface. A putative pyramidal cell was chosen dependent on its morphology: large cell body (5 – 10 μm) with at least two dendritic arbours emanating from it. Then the objective was switched to 60x to obtain a whole cell patch clamp recording from the soma under light microscopy. An average access resistance of 35 MΩ (n = 53) was calculated (Figure 6.0.1a)

Once whole cell configuration of the cell soma was achieved I would wait for 5 minutes to allow the cell to be slowly dialysed with the tracer. After this period, I viewed the cell under blue LED illumination to find an associated axon that had been filled, which I could follow and locate a proximal bouton (Figure 6.0.1b). The transmitted light image and fluorescent image were then merged using Image J (Figure 6.0.1c), and imported into the SICM software. The chosen bouton was then scanned with the nanopipette (Pb) at high resolution using HPICM. The bouton was patched and whole cell configuration was attained (**Section 4.2.1**).

APs were elicited with a 200pA depolarizing somatic current pulse lasting 200ms. and simultaneously recorded at the bouton (Figure 6.0.3c). Only the first spike was

used for subsequent analysis. This experiment was performed in wild type neurons at first.

6.0.2 Results

As expected, finding the AP threshold was more straightforward in post-hoc analysis using the dual patch method. This is illustrated by the irregular dV/dt versus voltage plots for spikes directly elicited and recorded at the bouton (Figure 6.0.1d) compared with those elicited at the soma (Figure 6.0.1f) and recorded simultaneously at the bouton (Figure 6.0.1e). The dual patch technique also provided a direct comparison between somatic and bouton spikes, information which has not been recorded before in small presynaptic terminals. The amplitude for soma and bouton spikes in wild type neurons were similar (Figure 6.0.1g). Interestingly the resting membrane potential (when I = 0) had a trend of being depolarised at the bouton compared to the soma, but this did not reach significance; n = 22 (Figure 6.0.1h). The access resistance as expected was larger at the bouton (~350MΩ) compared with soma (~35MΩ) but was comparable to previous bouton-only recordings.

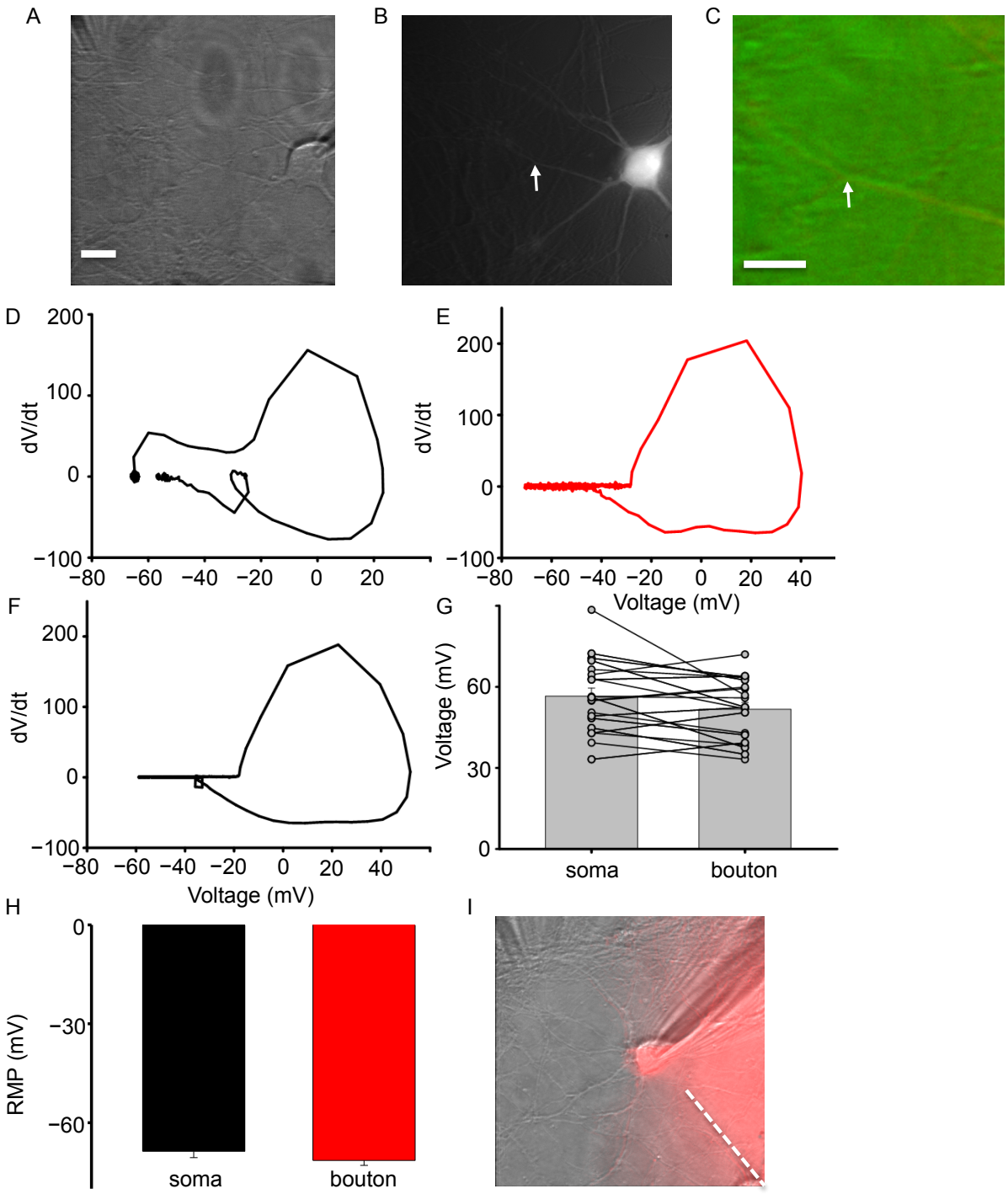

Figure 6.0.1 (A) Transmitted light image of patched cell soma (right) and bouton pipette (left); scale bar 10 µm. (B) Epifluorescence image under blue LED illumination showing filled axon and selected bouton (arrow) (C) Enlarged co-registered transmitted light (green) and epifluorescence image (red) identifying bouton; scale bar 5 µm. (D) dV/dt versus voltage plot for bouton only recording (E)

dV/dt versus voltage plot for bouton in dual patch (F) dV/dt versus voltage plot for soma in dual patch (G) Spike amplitude comparing wild type soma and bouton (H) Resting membrane potential of soma versus bouton (I) Adjusted composite transmitted light and fluorescence image showing flaring (dashed line)

6.0.3 Conclusions

Simultaneous patch clamp recordings of the cell soma and connected presynaptic bouton was successful in 24% of experiments once a somatic recording was achieved. This was due to a combination of unsuccessful attempts of whole bouton configuration, patching of bouton that was unrelated to the patched cell soma and patching of unhealthy boutons. A typical experiment would last between 30 minutes. Once whole-cell configuration of the soma was attained I initially allowed 15 minutes for dialysis of the cell. This would have enabled me to follow an axon to its terminal and simultaneously patch a terminal bouton and its soma. However experiments where this timeframe was used resulted in very low success for dual recordings. I subsequently reduced the time spent dialysing the cell to 5 minutes, meaning boutons identified were generally closer to the cell (within 100 µm). In CA3 pyramidal neurons, the AP initiation zone or axon initial segment (AIS) is located at 35–40 µm from the soma (Debanne et al., 2011). Thus boutons elected for simultaneous recording were usually situated close to the AIS. Methods for estimating of bouton – soma distance are discussed in **Section 6.2**. Another limitation was in the acquisition of the fluorescence images of the patched soma and associated axons under blue LED illumination. As fluorescent tracer was present in the somatic pipette, flaring of

the image in that region was unavoidable (Figure 6.1i). However this effect was somewhat minimised during co-registration with transmitted light image by post-hoc adjusting the brightness using Image J software.

In attempting to optimise the method by reducing the experiment time, I omitted the stage where the soma was filled with tracer. I randomly chose an area of attached dendrite with processes emanating from it. An HPICM scanning image of this region (boxed region Figure 6.0.3a) was then attained searching for nearby boutons (usually 12 x 12 μm). Once a suitable bouton it was scanned under higher resolution again with HPICM (usually 6 x 6 μm)(Figure 6.0.3b). The bouton was patched and whole-cell configuration attained. Surprisingly the success rate of finding an associated bouton and soma was comparable to the initial method described. That the bouton and soma belonged to the same cell was confirmed by APs elicited at the soma being simultaneously recorded at the bouton. Also Pb was prefilled with Alexa568 as before, and so the patched bouton and associated axon morphology could be confirmed post hoc under green LED illumination (Figure 6.0.3d).

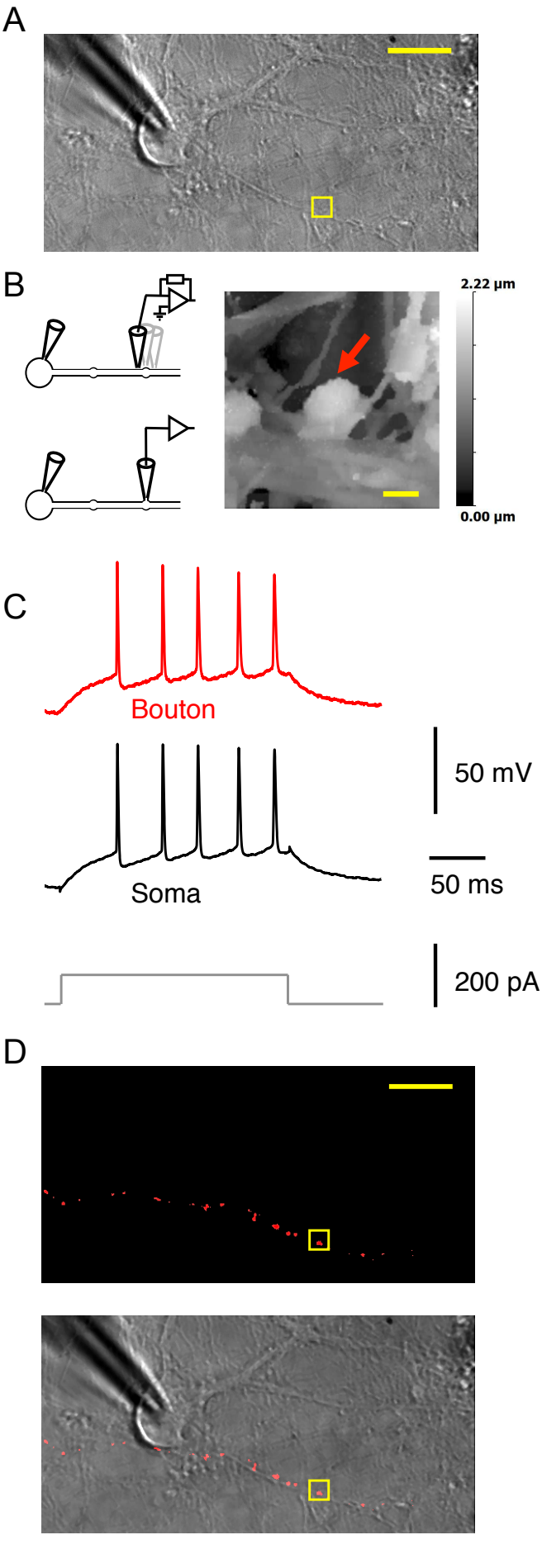
A
B
2.22 µm
0.00 µm
C
Bouton
Soma
50 mV
50 ms
200 pA
D

Figure 6.0.3 **Dual recordings from the soma and small presynaptic bouton of the same neuron. (A)** Transmitted light image of a neuron with somatic patch pipette, with a neighbouring 6 µm x 6 µm region selected for HPICM indicated with the square. Scale bar: 20 µm. **(B)** Left, Schematics indicating HPICM in voltage clamp mode (top) and whole-cell recording from presynaptic bouton (bottom). Right, height-coded image corresponding to highlighted area in (a), showing bouton (arrow) supplied by an axon adjacent to a dendrite. Scale bar: 1 µm. **(C)** Simultaneous somatic and presynaptic recordings of action potential train elicited by somatic current injection from the same cell as in (A). **(D)** Epifluorescence image overlaid on the transmitted light image, showing neighbouring boutons supplied by the same axon filled with Alexa Fluor 568 in the bouton pipette. The axon runs approximately horizontally through the image but typically could not be traced back to the soma.

6.1 Spike latency

Simultaneous recording from soma and presynaptic bouton gives us an insight into the spacial and temporal resolution of axonal transmission in hippocampal neurons. To estimate the distance between presynaptic bouton and soma in the dual patch experiments, we initially tried to analyse post hoc fluorescence images. As part of the experiment, the scanning nanopipette contained the fluorescent tracer AlexaFluor568. As whole bouton configuration was attained, the tracer labelled neighbouring boutons either side of the targeted structure, providing morphological confirmation of the axon identity, and showing that the axon was not transected. However due to the tortuosity of the axon, it was difficult to trace the axon all the way back to the soma (Figure 6.1a). Another way to estimate bouton – soma distance, is to look at axonal action potential latency relative to the soma. This can be determined by documenting latency (ta − ts) between the axonal spike (latency ta) recorded at the bouton, and the somatic spike (latency ts) (Scott et al., 2014). In layer 5 pyramidal cells, the shortest axonal AP latencies were recorded 30 – 60 µm. from the axon hillock, occurring about −100 µs. before the somatic AP (Kole et al., 2007a; Palmer and Stuart, 2006; Shu et al., 2006). This would be considered to be within the axon initial segment (see **Chapter 1.2**). From this region onwards, spike latency observed a positive linear relationship with distance down the axonal arbor (Figure 6.1b). We translated this approximation curve to the latencies we observed in hippocampal neurons.

6.1.1 Main aims

1. Estimate mean bouton-soma distance using the proxy of spike latency

6.1.2 Results and conclusion

The spike latency was non-significantly longer in the bouton than in the somatic recording when all genotypes were pooled together (average ± SD soma-bouton difference: 0.02 ± 0.10 ms., n = 53). This is consistent with action potential initiation at the axon initial segment and a mean axon length of 200 – 300 µm. There was no systematic relationship between normalised spike half width and latency in wild type or *Kcna1a*$^{V408A/+}$ neurons (as in **Section 7.1)** (Figure 6.1c). As with all previous experiments we only considered the first spike elicited.

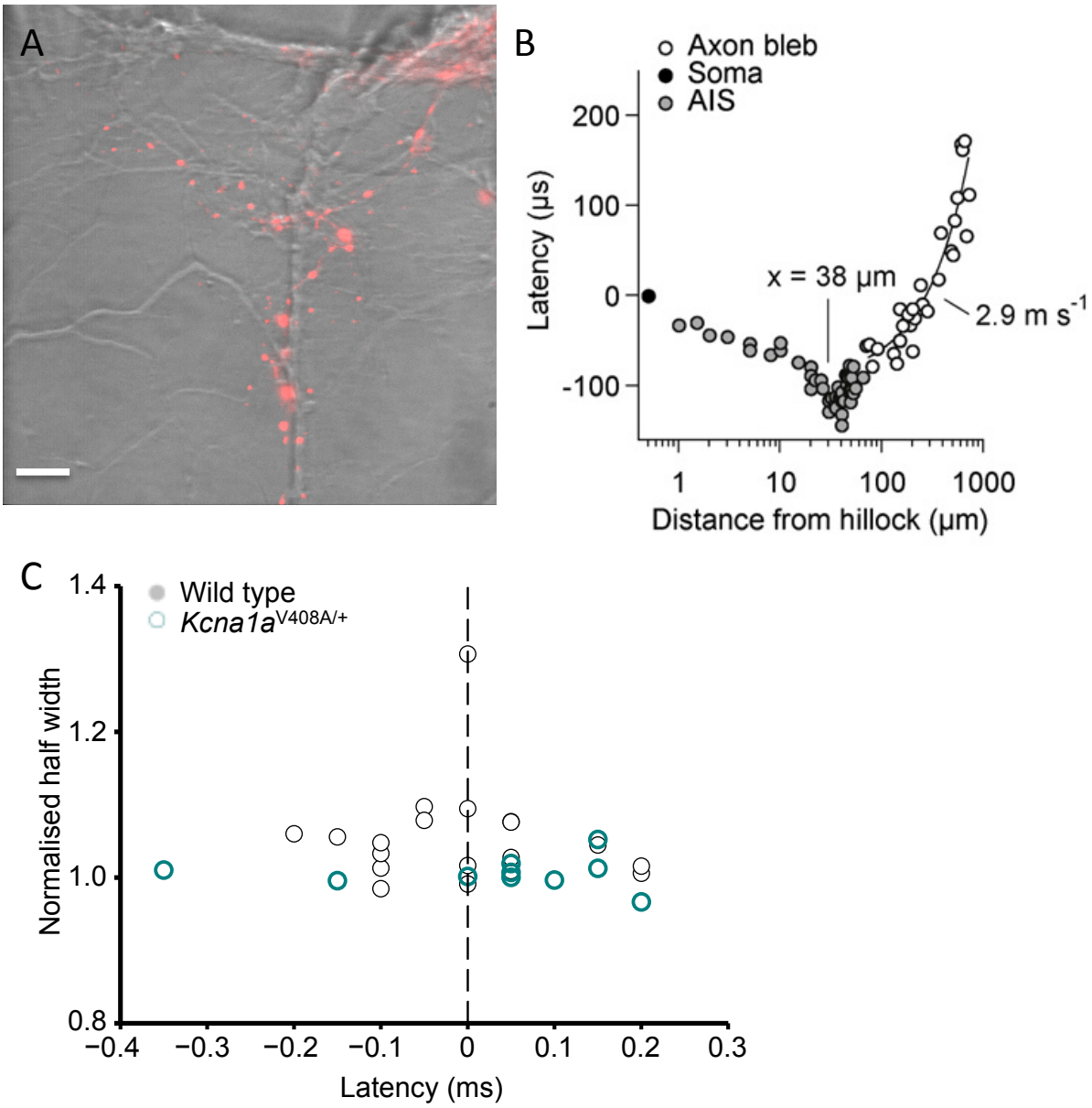

Figure 6.1 **Analysis of spike latency.** (A) Epifluorescence image (red) overlaid on the transmitted light image, showing neighbouring boutons supplied by the same axon filled with Alexa Fluor 568 in the bouton pipette. The axon typically could not be traced back to the soma due to it tortuous route; scale bar 10 microns. (B) Plot of AP latency relative to that of the somatic AP (black) for APs recorded in the AIS (gray circles, n = 45) and axon blebs (open circles, n = 22) versus recording distance from the axon hillock. Adapted from (Kole et al., 2007) (C) Normalised spike half width

plotted against latency for wild type (grey) and *Kcna1a*$^{V408A/+}$ (cyan) (wild type n = 19; *Kcna1a*$^{V408A/+}$ n = 9)

6.2 Simultaneous soma and bouton recordings in *Kcna1a*$^{-/-}$, *Kcna1a*$^{V408A/+}$ and wild type littermates

K_V1.1 appears to have an effect on AP morphology in forebrain presynaptic boutons as evidenced by the prolonged AP half-width in the knock-out and knock-in models of EA1. The broadened spike in the *Kcna1*$^{V408A/+}$ neurons is in agreement with similar experiments performed in cerebellar basket cells (Begum et al., 2016), another brain region rich in K_V1.1. But is this a solely presynaptic phenomenon? With the ability to now perform consistent simultaneous patches of soma and bouton from the same cell, we could now focus on AP morphology in pharmacological and genetic models of K_V1.1 deletion.

6.2.1 Main aims

1. What is the role of K_V1.1 at the bouton and at the soma?

6.2.2 Method

Experiments on hippocampal cultures from *Kcna1a*$^{-/-}$ mice and their wild type littermates were performed on the same day in order to make direct comparison. This was also the case for *Kcna1a*$^{V408A/+}$ mice and their wild type littermates. The

dual patch experiment (**Section 6.0**) was performed on each type of neuron and spikes elicited at the soma using the same 200pA current pulse. Thirty sweeps were recorded and then the EC solution was switched to one containing 20nM DTx-K with a further 30 sweeps recorded.

6.2.3 Results

In the *Kcna1a*$^{-/-}$ mice the mean bouton t/2 was 1.43 ± 0.09ms (n = 10) and in their wild type littermates the mean bouton t/2 was 1.17 ± 0.05ms (n = 13), a difference of 0.26ms (p = 0.01 with unpaired t test). Thus the difference in spike t/2 was ≈ 22%. When pooling all wild type littermates the difference was 0.31 ms (25%)(n = 27). In contrast the *Kcna1a*$^{-/-}$ mean soma t/2 was 1.36 ± 0.12ms and in their wild type littermates the mean soma t/2 was 1.26 ± 0.08ms, a non-significant difference of 0.1 ms (p = 0.5). In pooled wild type littermates the difference was 0.13 ms (10%). (Figure 6.2.4a).

In the *Kcna1a*$^{V408A/+}$ mice the mean bouton t/2 was 1.39 ± 0.06ms (n = 12) and in their wild type littermates the mean bouton t/2 was 1.1 ± 0.05ms (n = 14), a difference of 0.29ms (p = 0.001 with unpaired t test). Thus the difference in spike t/2 was ≈ 24%. In pooled wild type littermates the difference was 0.27 ms (25%)(p < 0.001, n = 27). Again in contrast, the mean *Kcna1a*$^{V408A/+}$ soma t/2 was 1.33 ± 0.09ms and in their wild type littermates the mean soma t/2 was 1.17 ± 0.08ms, a

non-significant difference of 0.16ms (p = 0.18). In pooled wild type littermates the difference was 0.1 ms (8%) (Figure 6.2.4a).

In the pooled wild type littermates, application of DTX-K increased the mean bouton t/2 from 1.12 ± 0.04ms to 1.27 ± 0.04ms, an increase of 13% (Figure 6.2.3a, b) (p=0.004 with paired t test). However the mean soma t/2 only changed from 1.24 ± 0.05ms to 1.25 ± 0.06ms, a non-significant increase of 1% (p=0.6) (Figure 6.2.3g). In the *Kcna1a*$^{-/-}$ mice, DTX-K increased the mean bouton t/2 from 1.44 ± 0.12ms to 1.49 ± 0.12ms, a small but significant increase of 4% (Figure 6.2.3c, d) (p=0.004). Mean soma t/2 remained unchanged at 1.37 ± 0.15ms (Figure 6.2.3g). In the *Kcna1a*$^{V408A/+}$ mice application of DTX-K had no significant effect on bouton t/2 (baseline: 1.39 ± 0.05ms; DTx-K: 1.41 ± 0.05ms; p=0.3) (Figure 6.2.3e, f) (p=0.3). Again mean soma t/2 remained unchanged at 1.33 ± 0.09ms (Figure 6.2.3g).

These results suggest that the contribution of $K_V1.1$ to spike width is not apparent from somatic recordings, but is robustly revealed by bouton recordings, consistent with an axonal localisation of the channel subunit.

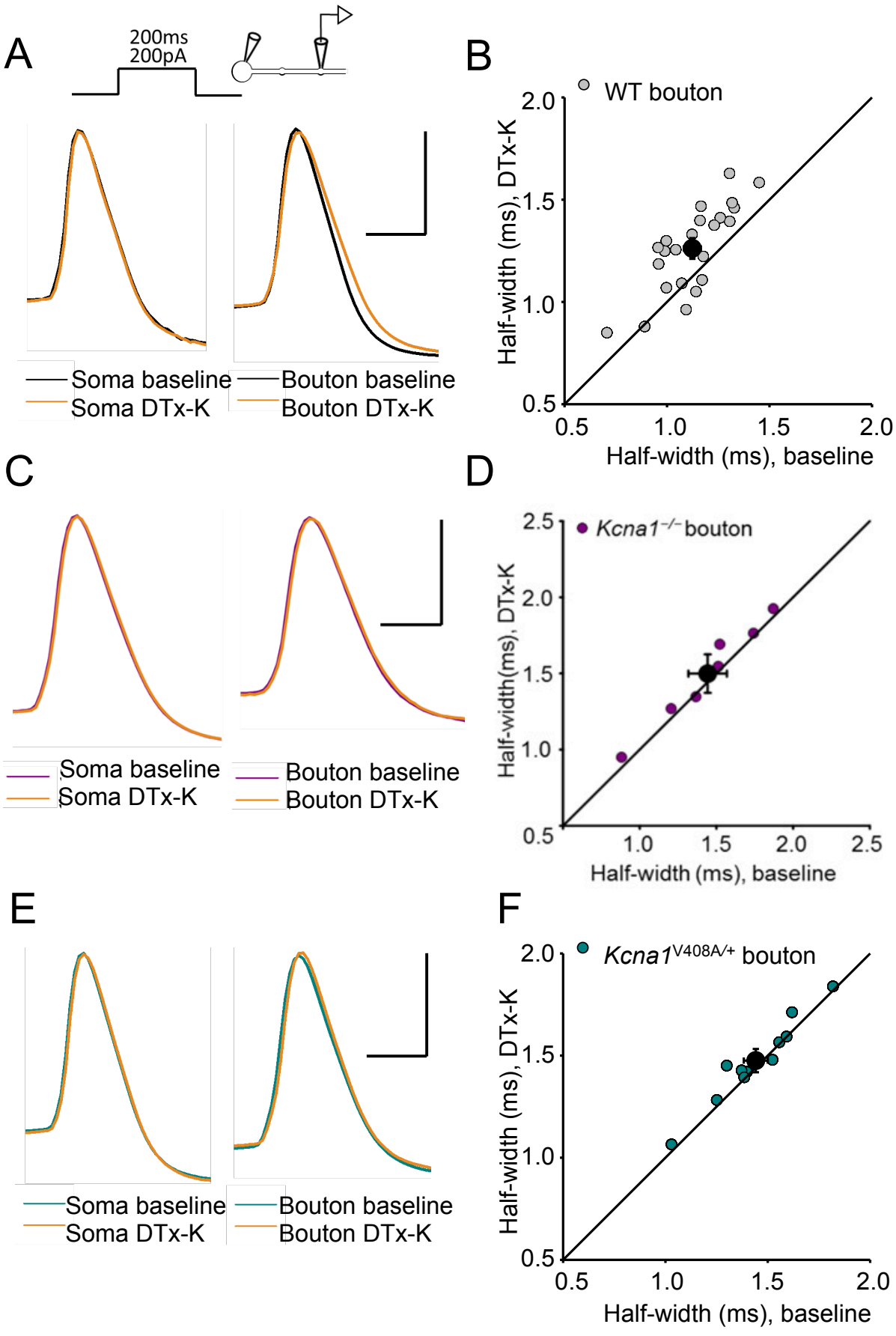
A
200ms
200pA
Soma baseline
Soma DTx-K
Bouton baseline
Bouton DTx-K
B
WT bouton
Half-width (ms), DTx-K
Half-width (ms), baseline
C
Soma baseline
Soma DTx-K
Bouton baseline
Bouton DTx-K
D
Kcna1−/− bouton
Half-width(ms), DTx-K
Half-width (ms), baseline
E
Soma baseline
Soma DTx-K
Bouton baseline
Bouton DTx-K
F
Kcna1V408A/+ bouton
Half-width (ms), DTx-K
Half-width (ms), baseline

G

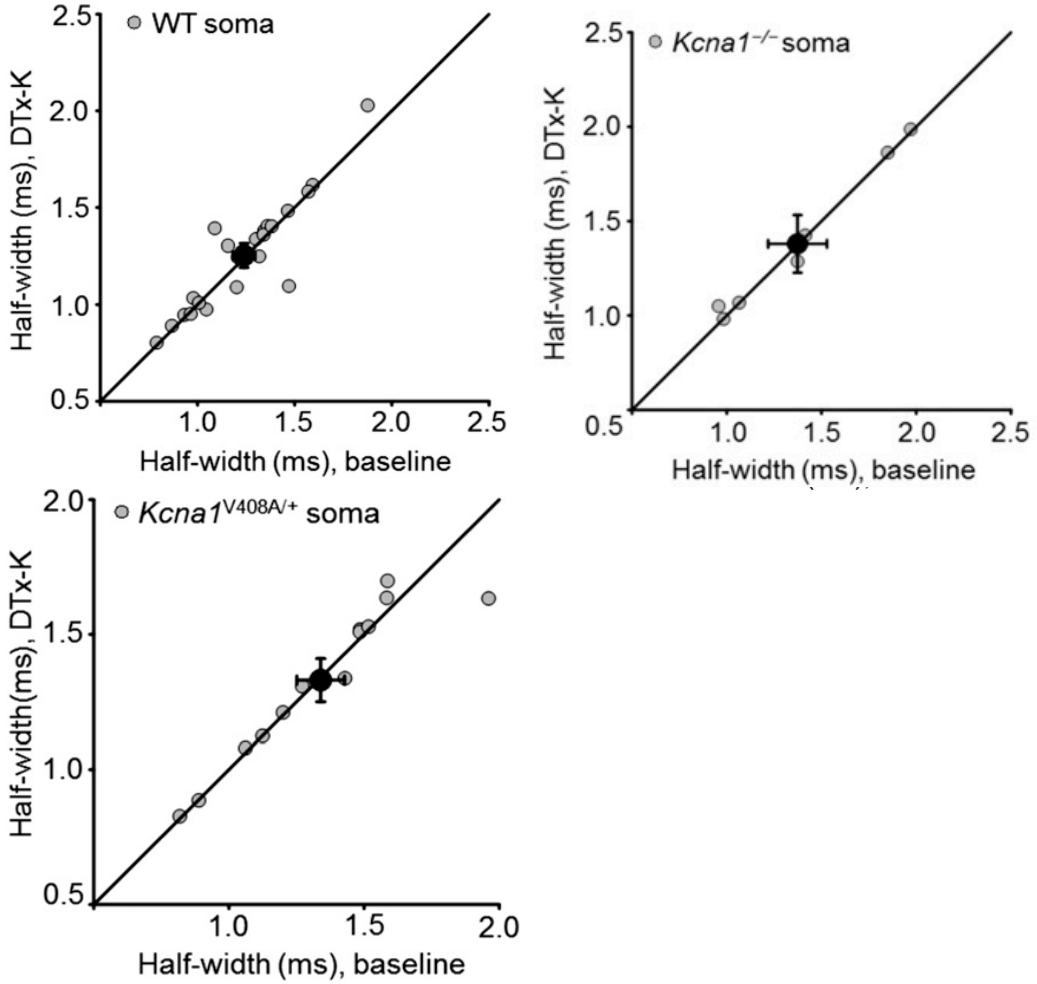

Figure 6.2.3 **K_V1.1 channels determine spike width. (A)** Example recordings from one neuron before and after 20 nM DTx-K application. This had no effect on somatic spikes but led to broadening of presynaptic action potentials**. (B)** Presynaptic spike widths elicited by somatic current injection before and after DTx-K perfusion, showing a significant broadening (*n* = 22 neurons, *p*<0.001, paired *t*-test). **(C)** Sample traces from one *Kcna1*$^{-/-}$ neuron showing simultaneously recorded somatic and presynaptic spikes before and after DTx-K application. (**D**) Summary data showing partial occlusion of presynaptic spike broadening by DTx-K in *Kcna1*$^{-/-}$ neurons (*n* = 7, *p* = 0.05, paired *t*-test). **(E)** Example traces showing failure of DTx-K to broaden either somatic or presynaptic spikes in a *Kcna1*$^{V408A/+}$ neuron. **(F)**

Summary data showing occlusion of presynaptic spike broadening by DTx-K and *Kcna1*$^{V408A/+}$ (*n* =12; *p* = 0.33). Scale bar in (A) and (D): 40 mV / 1ms. DTx-K had no effect on somatic spike half-width in wild type neurons (G) (*n* = 22; *p* = 0.6, paired *t*-test), *Kcna1*$^{-/-}$ neurons (H) (*n* = 7; *p* = 0.77), and *Kcna1*$^{V408A/+}$ neurons (I) (*n* = 12; *p* = 0.75).

Amplitude of spikes were measured from the take-off point to the peak (measured in mV). In the *Kcna1a*$^{-/-}$ mice the mean bouton AP amplitude was 53 ± 4mV; in the *Kcna1a*$^{V408A/+}$ it was 52 ± 1mV; and in the pooled wild type littermates it was 56 ± 3mV (p=0.58 and p=0.35 respectively with unpaired t test). The *Kcna1a*$^{-/-}$ mean soma amplitude was 63 ± 5mV; in the *Kcna1a*$^{V408A/+}$ it was 60 ± 3mV and in the pooled wild type littermates it was 51 ± 2mV, (p=0.03 and p=0.06 respectively) (Figure 6.2.4b).

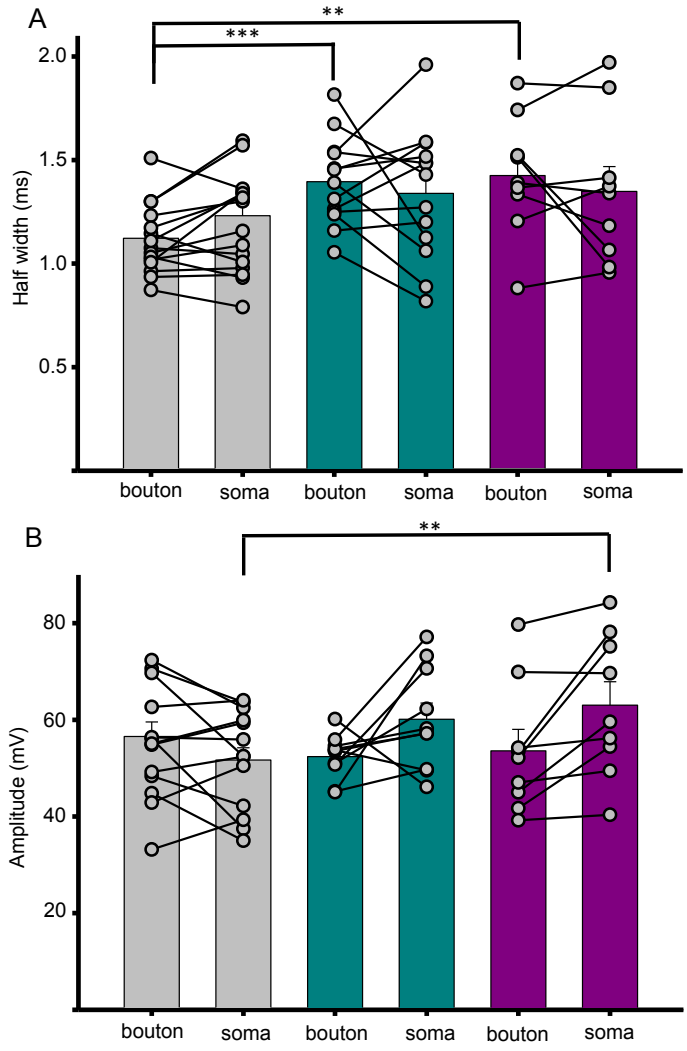

Figure 6.2.4. (A) **Spike half widths of bouton and soma from pooled wild type (grey), *Kcna1*$^{V408A/+}$ (cyan) and *Kcna1*$^{-/-}$ (purple) neurons**. Spikes recorded from boutons, but not somata, of *Kcna1*$^{-/-}$ and *Kcna1*$^{V408A/+}$ neurons were broader than in wild type neurons (*Kcna1*$^{-/-}$; **, p < 0.01; *Kcna1*$^{V408A/+}$, ***, *p* < 0.001 unpaired t-test). Spikes were also significantly narrower in boutons than somata in wild type (p < 0.05, paired *t*-test), but not *Kcna1*$^{V408A/+}$ neurons. (B) **Same data but for spike amplitude**. Action potentials recorded from somata, but not boutons of *Kcna1*$^{-/-}$ neurons had a larger amplitude than in wild type neurons. Action potentials recorded from boutons or somata of *Kcna1*$^{V408A/+}$ neurons were not significantly different in amplitude than in wild type neurons.

6.2.4 Conclusions

I have used the double patch method (recording AP propagation to the presynaptic bouton via depolarisation of the soma) to show that the AP t/2 is increased in both the $K_V1.1$ knockout mouse and in a knock-in model of Episodic Ataxia type 1. This was in agreement with AP recorded directly from the presynaptic boutons (**Section 6.0**), but perhaps more convincing evidence as there was a clearer identification of take-off point in analysis and correct bridge balance was not required. Although a role of $K_V1.1$ in determining action potential width has been proposed in previous studies, until now it has never been shown directly in submicrometer sized synapses, the most abundant type of synapse in the brain. Nor has it been studied with genetic (as opposed to pharmacological) manipulation of $K_V1.1$ channels. The double patch method also confirmed that the difference in t/2 is a solely presynaptic or axonal phenomenon, as t/2 not significantly increased in *Kcna1a*$^{-/-}$ and *Kcna1a*$^{V408A/+}$ somatic recordings. DTX-K affected wild type presynaptic spikes but had no effect on somatic spikes, supporting axonal targeting of the channel. In addition, either deletion of *Kcna1* or the heterozygous EA1 mutation occluded the effect of a specific $K_v1.1$ blocker.

There was a trend for the AP amplitude to be smaller at the soma than at boutons in the wild type neurons, and an opposite trend in the *Kcna1a*$^{-/-}$ and *Kcna1a*$^{V408A/+}$ neurons. However none of these differences reached 5% significance. The somatic

AP amplitude was however significantly different between wild type and *Kcna1a*$^{-/-}$. I would not wish to draw strong conclusions from this finding because it only emerged from post-hoc analysis of experiments designed to test a different hypothesis (namely, that presynaptic spike width differed). Moreover, the statistical test may not survive correction for multiple comparisons because only relatively few *Kcna1a*$^{-/-}$ cells were sampled (n = 9).

K_V1 channels are known to be densely clustered at subdomains of the axon, such as the distal region of the AIS (Inda et al., 2006; Lorincz and Nusser, 2008b; Van Wart et al., 2007). No change in latency was observed with subthreshold depolarisation in the wild type neurons. However we did not examine the temporal aspect of subthreshold excitation as all prepulses were 200ms; it has been shown it is rate of depolarisation rather than amount that reduces latency, thought to be a sodium channel effect (Scott et al., 2014). Latency also did not change with subthreshold depolarisation in *Kcna1a*$^{V408A/+}$ neurons, suggesting that AP waveform rather than AP latency is affected in the distal AIS when K_V1 function is abolished.

Due to technical limitation, the bouton chosen for double patch recording was electrically close, usually within 100 µm., to the soma. Therefore it is conceivable that the AP passively recorded at the bouton may have been a reflection of the AP at the action initial segment or even the soma. Indeed the mean AP half width at the bouton in wild type was 1.12 ms. with simultaneous recording, but 0.89 ms. when recorded directly at the bouton. The slower AP waveform at the bouton

demonstrated during double patch recording may suggest different underlying conductances.

7.0 ‘Analogue’ and ‘Digital’ signalling

7.0.1 Introduction

Recordings from large mossy fibre boutons avoid the pitfalls of recording from axon blebs. However, although depolarization by presynaptic $GABA_A$ receptors broadened spikes and action-potential evoked Ca^{2+} transients in one study (Ruiz et al., 2010), an increase in spike-evoked Ca^{2+}-dependent fluorescence transients was not detected in other studies which examined sub-threshold depolarization propagating from the soma (Alle and Geiger, 2006; Scott et al., 2008). Presynaptic recordings from calyceal synapses in the brainstem, furthermore, detected an increase in Ca^{2+} transients without change in spike shape upon depolarization, whether elicited by activation of presynaptic glycine receptors (Turecek and Trussell, 2001) or by direct current injection (Awatramani et al., 2005b). The principles governing analogue-digital modulation at large calyceal synapses may not, however, apply to far more abundant small presynaptic boutons of the forebrain, arguing the need for alternative recording methods to resolve the role of spike broadening. Presynaptic voltage-sensitive fluorescence measurements or loose patch clamp of fluorescent-dye loaded axons may not detect sub-millisecond differences in action potential shape.

7.0.2 Main aims

1. To devise a current protocol to investigate the role of analogue-digital signalling in hippocampal neuronal culture

2. To identify whether DTx - K affected analogue-digital signalling

3. To identify whether genetic knockout of $K_V1.1$ or the knock-in model of EA1 affected analogue-digital signalling.

7.0.3 Method

We used simultaneous somatic and bouton recording as described in **Chapter 6.1**. However instead of delivering one depolarising pulse of 200pA for 200ms, we now delivered four subthreshold prepulses at -100pA, -50pA, 0pA and 50pA lasting 200ms, immediately followed by a supra-threshold somatic depolarizing current of 200pA lasting 200ms. One sweep consisted of a cycle through each of the prepulses. 10 sweeps were recorded and then averaged for each prepulse. For the DTx-K experiments 10 sweeps were recorded prior to application of 20nM DTx-K to the EC solution and a further 10 sweeps were recorded. The first spike evoked by each of the +200pA pulses was used for subsequent analysis. Any recordings where the first spike occurred during a prepulse instead of the +200pA pulse were discarded. The experiments were performed in *Kcna1a*$^{-/-}$ neurons, *Kcna1*$^{V408A/+}$ neurons and the pooled wild type littermates of both EA1 models.

7.0.4 Results

In neurons from wild type mice the presynaptic action potential width showed a positive dependence on the pre-pulse (Figure 7.0.3A). This relationship persisted when spike width was plotted against the voltage of the bouton membrane prior to the somatic depolarizing pulse used to evoke spiking (Figure 7.0.3A_4). In order to quantify this dependence, we calculated the Spearman rank correlation coefficient ρ between the pre-pulse current (or bouton voltage) and the spike width in each experiment. The null hypothesis that ρ should be randomly distributed around 0 was rejected at p <0.005 (n = 20; Wilcoxon signed-rank test, Figure 7.0.3D). In parallel, in order to compare across neurons, we normalized the half-width measured with −100, −50, 0 or +50 pA prepulses by the average width measured with –100 and –50 pA prepulses. This showed a consistent upward-concave relationship. Spike broadening was not accompanied by a detectable change in spike height.

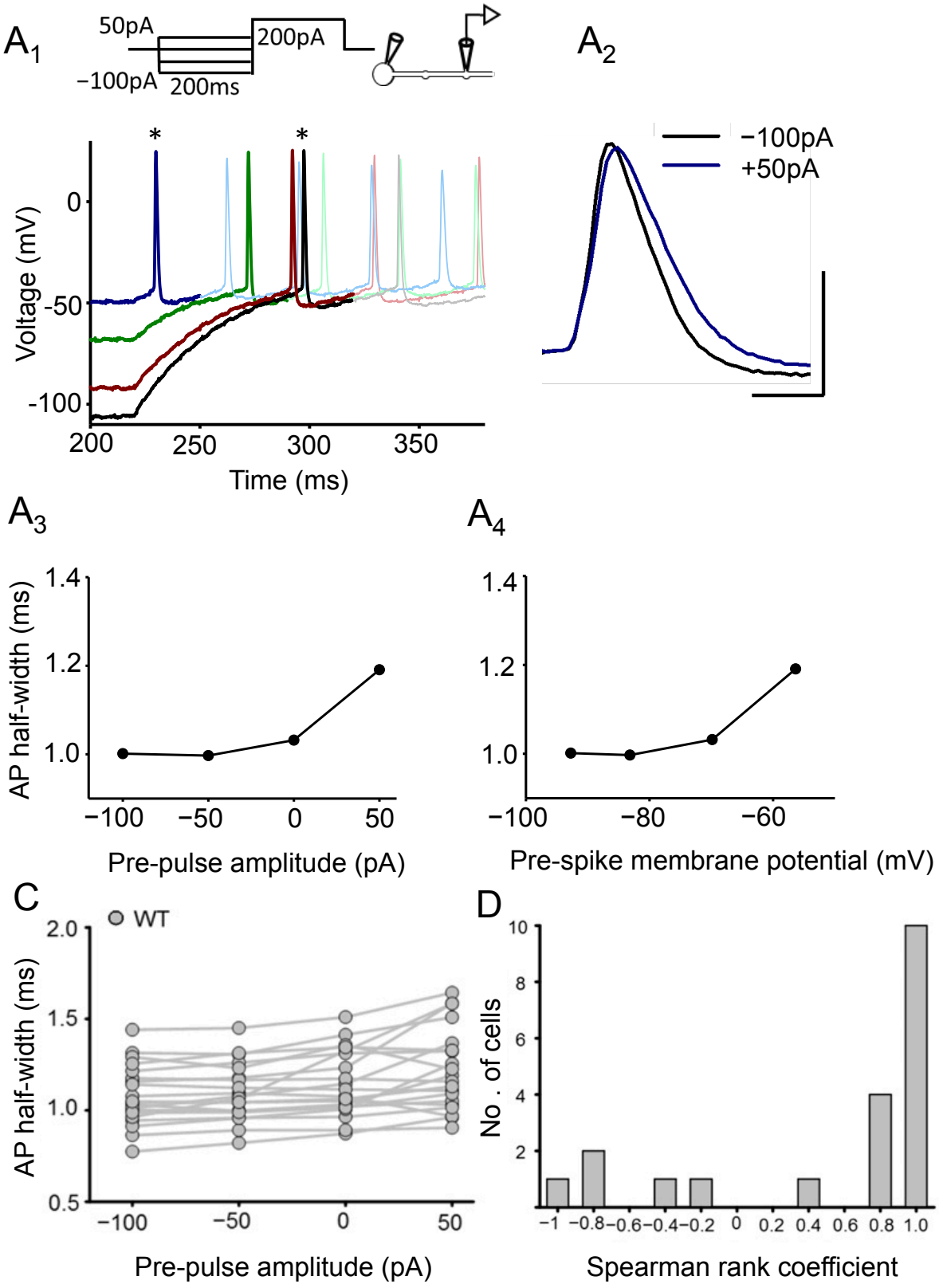

Figure 7.0.3 **Analogue modulation of presynaptic spike width in WT neurons.** **(A)** Traces from one wild type cell showing bidirectional changes in presynaptic spike

width by subthreshold somatic current injections prior to evoking action potentials. **(A_1)** Superimposed spikes elicited after prepulses ranging between –100 pA and +50 pA. Each trace is shown in bold until after the first spike. **(A_2)** Zoomed presynaptic spikes obtained following –100 pA and +50 pA pre-pulses (asterisks in (A_1)). **(A_3)** Spike half-width plotted against somatic current injection showing positive dependence (half-width was ranked –50 pA < –100 pA < 0 pA < +50 pA, yielding Spearman rank correlation coefficient ρ = 0.8). **(A_4)** Half-width plotted against membrane potential measured at bouton prior to +200 pA somatic current injection to elicit spike. **(B)** Spike width dependence on somatic pre-pulse current shown for individual WT neurons. **(C)** Corresponding distribution of Spearman rank correlation coefficients (ρ) demonstrating prevalence of cells that show a positive relationship between the spike half-width and the pre-pulse

DTx-K had no significant effect on prepulse-dependent spike broadening (n = 18; dependence on pre-pulse current remained significant at p<0.001, Wilcoxon signed rank test; Figure 7.0.4).

Moreover, when the same protocol was repeated in neurons from *Kcna1*$^{-/-}$ mice, a positive relationship between spike width and prepulse amplitude persisted albeit to a lesser degree (n = 9; Figure 7.0.5). As with previous experiments that did not use the prepulse protocol (**Section 6.2**) the spike width in *Kcna1*$^{-/-}$ neurons was larger than wild type.

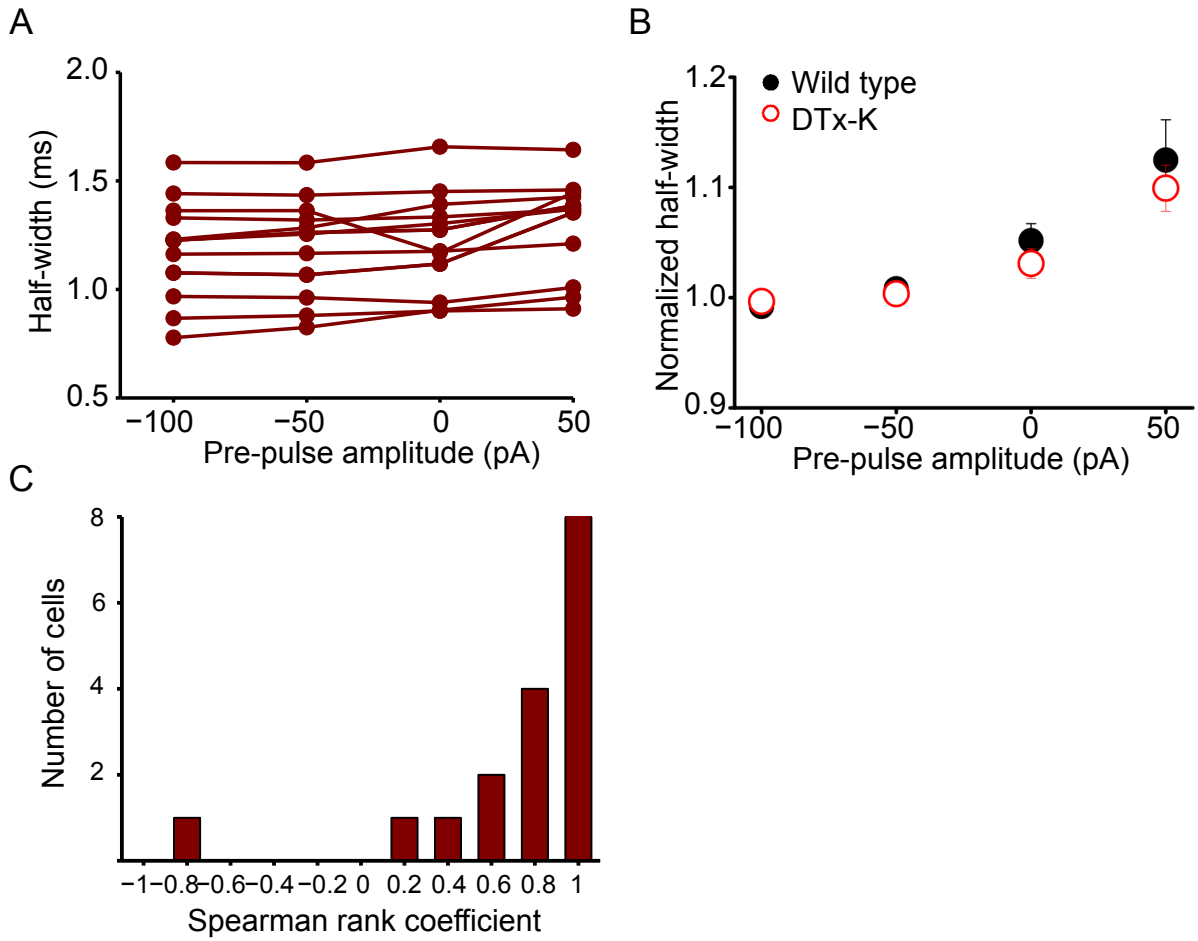

Figure 7.0.4 **Subthreshold modulation of spike width when DTx-K was applied** **(A)** Spike width dependence on somatic pre-pulse current shown for individual WT neurons after DTx-K application. **(B)** Summary data obtained from wild type neurons before (*n* = 20, filled symbols) and after DTx-K (*n* = 18, open symbols), showing persistence of analogue modulation of spike width. **(C)** Corresponding distribution of Spearman rank correlation coefficients (ρ) demonstrating prevalence of cells that show a positive relationship between the spike half-width and the pre-pulse

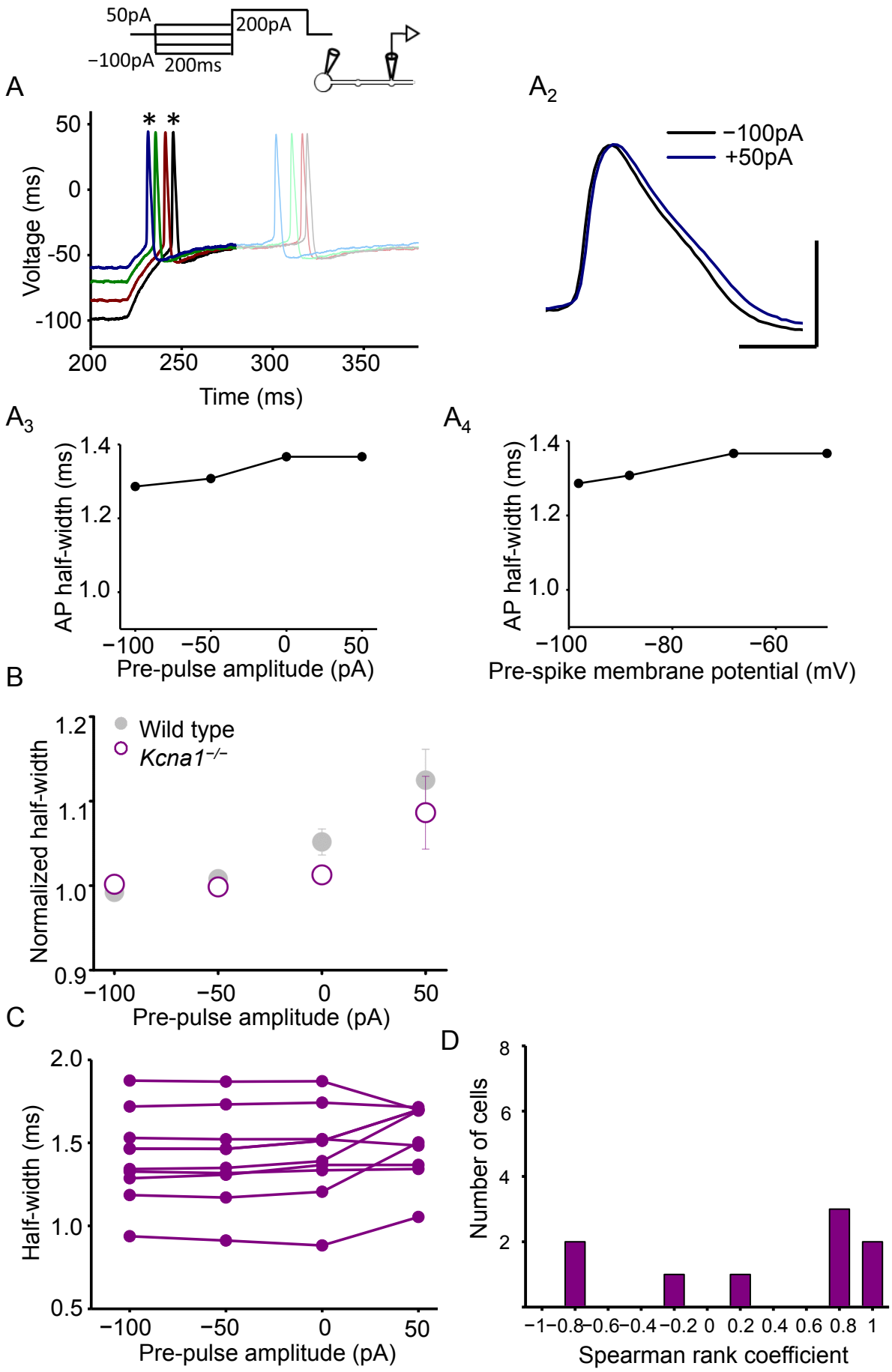
A
50pA
200pA
−100pA
200ms
Voltage (ms)
Time (ms)
A2
−100pA
+50pA
A3
AP half-width (ms)
Pre-pulse amplitude (pA)
A4
AP half-width (ms)
Pre-spike membrane potential (mV)
B
Wild type
Kcna1−/−
Normalized half-width
Pre-pulse amplitude (pA)
C
Half-width (ms)
Pre-pulse amplitude (pA)
D
Number of cells
Spearman rank coefficient

Figure 7.0.5 **Subthreshold modulation of spike width in a *Kcna1*$^{-/-}$ neuron. (A)** Sample traces showing spikes evoked by somatic +200 pA current injection following subthreshold somatic prepulses. Each trace is shown in bold until after the first spike. The spikes evoked following –100 pA and +50 pA prepulses (asterisks) are expanded at right. Scale bar: 40 mV / 1 ms. **(A_3)** Spike half-width plotted against somatic current injection showing positive dependence. **(A_4)** Half-width plotted against the membrane potential measured at the bouton prior to the +200 pA somatic current injection used to elicit spike. **(B)** Genetic deletion of Kv1.1 also failed to abolish pre-pulse evoked spike broadening (*n* = 9; wild type data are replotted from Figure 7.1.4B and shown in gray). Spike half-width was normalized by the mean values for –100 and –50 pA injection. **(C)** Spike width dependence on somatic pre-pulse current shown for individual WT neurons. **(D)** Corresponding distribution of Spearman rank correlation coefficients (ρ) demonstrating prevalence of cells that show a positive relationship between the spike half-width and the pre-pulse

In striking contrast to pharmacological or genetic deletion of $K_V1.1$, prepulses had no effect on spike width in *Kcna1*$^{V408A/+}$ neurons (Figure 7.0.6A, B; *n* = 10; Wilcoxon signed-rank test for ρ versus somatic subthreshold current or bouton voltage: *p* = 0.8; Figure 7.0.6D). The distributions of Spearman rank correlation coefficients in *Kcna1*$^{V408A/+}$ and wild type neurons were significantly different (*p* < 0.03, Mann-Whitney U test). Moreover, the normalized spike widths at 0 or 50 pA were significantly different (*p* = 0.05 and 0.02, respectively, unpaired *t*-tests, Figure 7.0.3B1). The same conclusion held when *Kcna1*$^{V408A/+}$ neurons were compared only to wild type littermates (*n* = 10) recorded on the same days (normalized half-width for 0 and +50 pA prepulses: *p* = 0.02 and 0.01, respectively, Figure 7.0.6B2). Spike

amplitude was not significantly altered with each prepulse (mean 53 ± 0.6mV; p = 0.6 0ne way ANOVA).

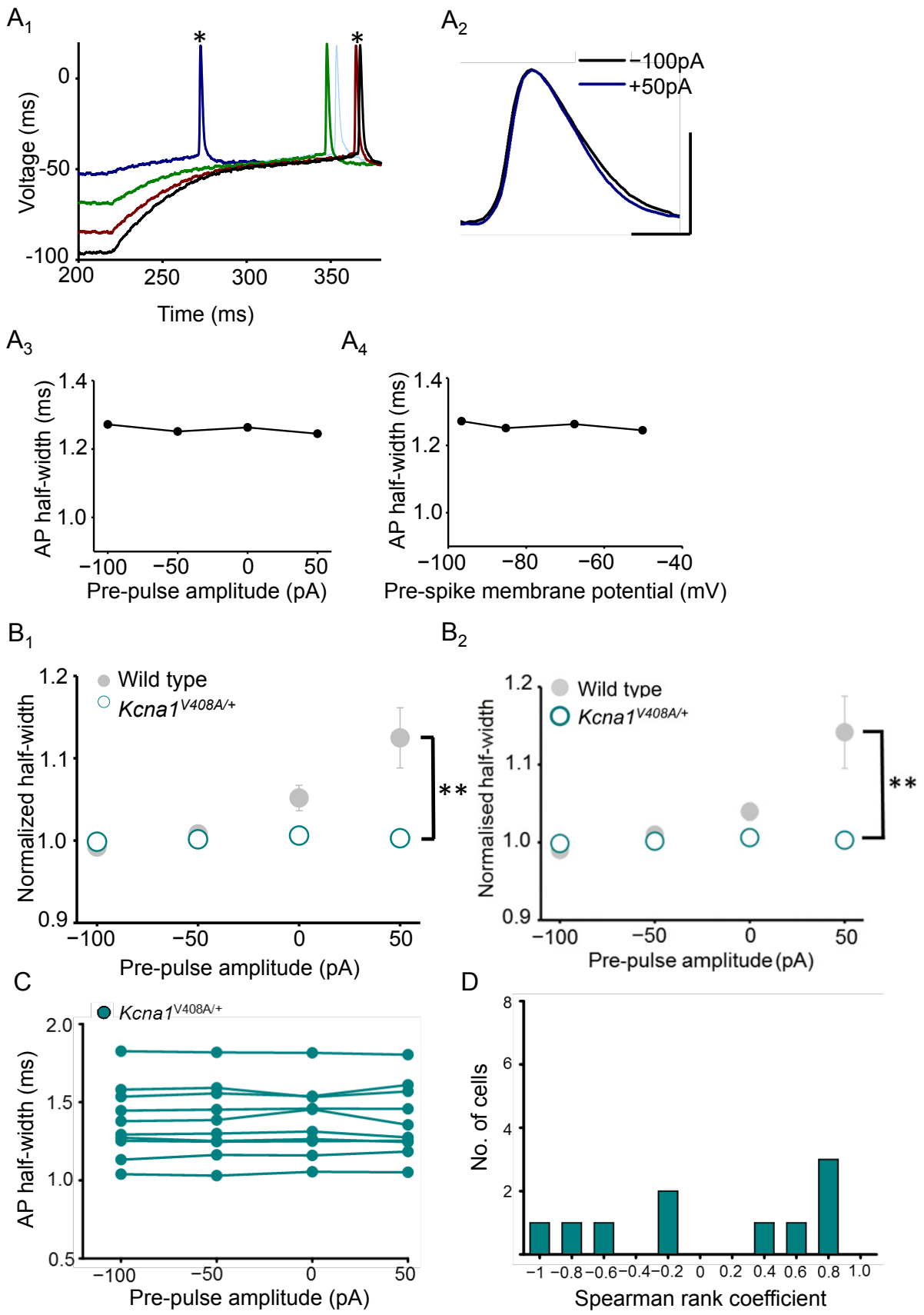
A1
Voltage (ms)
Time (ms)
A2
−100pA
+50pA
A3
AP half-width (ms)
Pre-pulse amplitude (pA)
A4
AP half-width (ms)
Pre-spike membrane potential (mV)
B1
Wild type
Kcna1V408A/+
Normalized half-width
Pre-pulse amplitude (pA)
B2
Wild type
Kcna1V408A/+
Normalised half-width
Pre-pulse amplitude (pA)
C
Kcna1V408A/+
AP half-width (ms)
Pre-pulse amplitude (pA)
D
No. of cells
Spearman rank coefficient

Figure 7.0.6 **A heterozygous Episodic Ataxia mutation abolishes analogue modulation of presynaptic spike width. (A)** Sample traces showing spikes evoked by somatic +200 pA current injection following subthreshold somatic prepulses. Each trace is shown in bold until after the first spike. The spikes evoked following –100 pA and +50 pA prepulses (asterisks) are expanded at right. Scale bar: 40 mV / 1 ms. **(A_3)** Spike half-width plotted against somatic current injection showing absence of spike broadening. **(A_4)** Half-width plotted against the membrane potential measured at the bouton prior to the +200 pA somatic current injection used to elicit spike. **(B_1)** Summary data from *Kcna1*$^{V408A/+}$ neurons (*n* = 10; open symbols) superimposed on wild type data (gray). Error bars are in some cases smaller than the symbols. **, p < 0.01 (*t*-test) **(B_2)** Same data as for B_1 but *Kcna1*$^{V408A/+}$ neurons compared to wild type littermates **(C)** Spike width dependence on somatic pre-pulse current shown for individual *Kcna1*$^{V408A/+}$ neurons. **(D)** Corresponding distribution of Spearman rank correlation coefficients (ρ) showing now systematic relationship between half-width and pre-pulse (n = 10, *p* < 0.8, Wilcoxon signed rank test, *p* < 0.02, Mann-Whitney U test comparing to WT).

Previous studies of analogue-digital modulation have used longer pre-pulses (Kole et al., 2007a). To replicate these conditions, I performed the same prepulse experiment but with prepulses lasting 2s instead of 200ms before delivering the suprathreshold current. This was more technically challenging as longer prepulse stimulation affected cell health. Six wild type and 6 *Kcna1*$^{V408A/+}$ neurons were recorded, and the results were consistent with those obtained with shorter prepulses (Figure 7.0.7). Spike width showed a positive dependence on prepulse amplitude in wild type neurons but not in *Kcna1*$^{V408A/+}$ neurons.

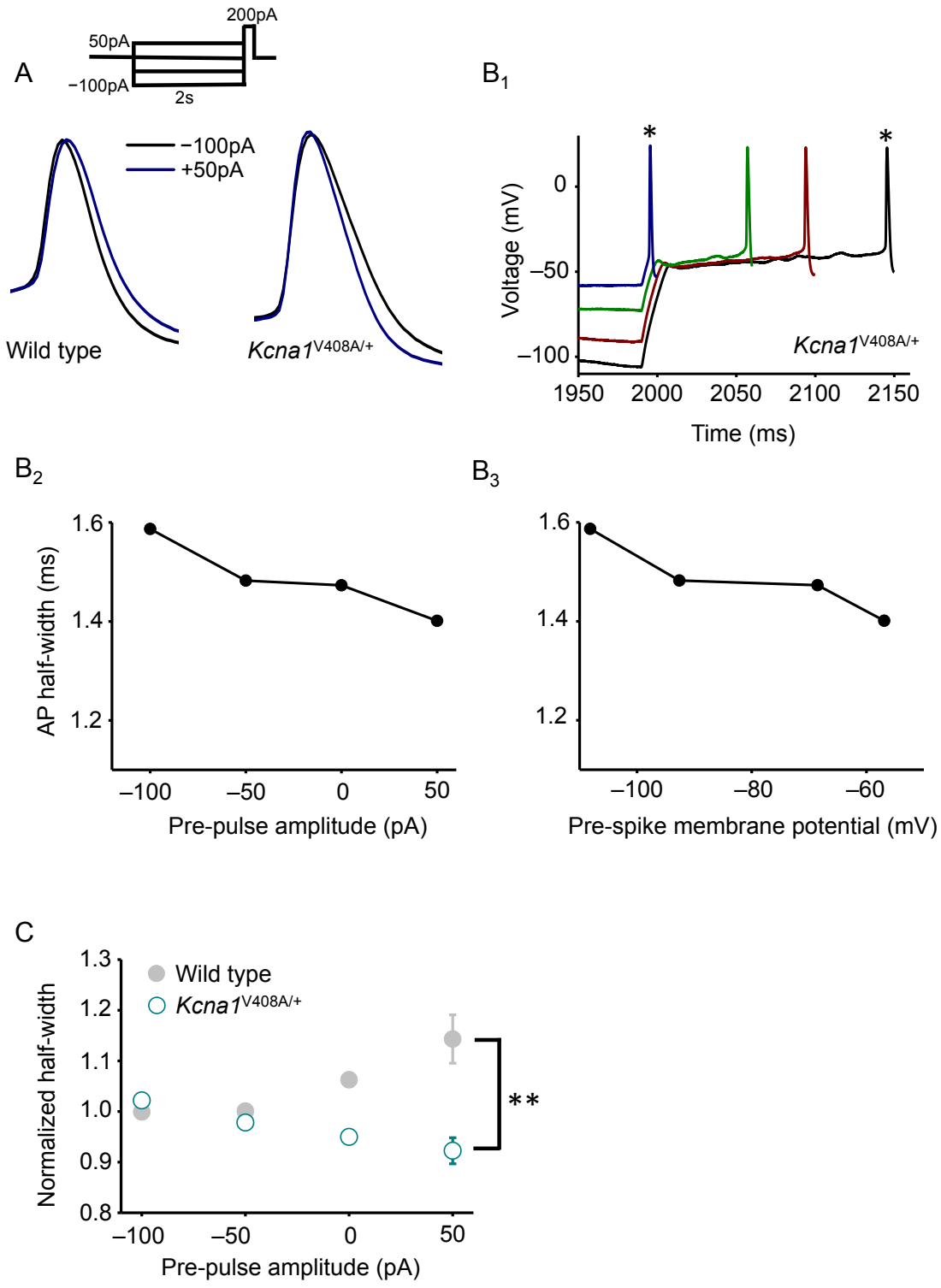

Figure 7.0.7 **Subthreshold modulation of spike width using longer pre-pulses.**

Data plotted as in Figure 7.1.6. Pre-pulses lasted 2 seconds. **, $p < 0.01$ (*t*-test).

In addition, subthreshold depolarisation appeared to have no effect on latency in both wild type and *Kcna1a*$^{V408A/+}$ neurons (Figure 7.0.8 a,b).

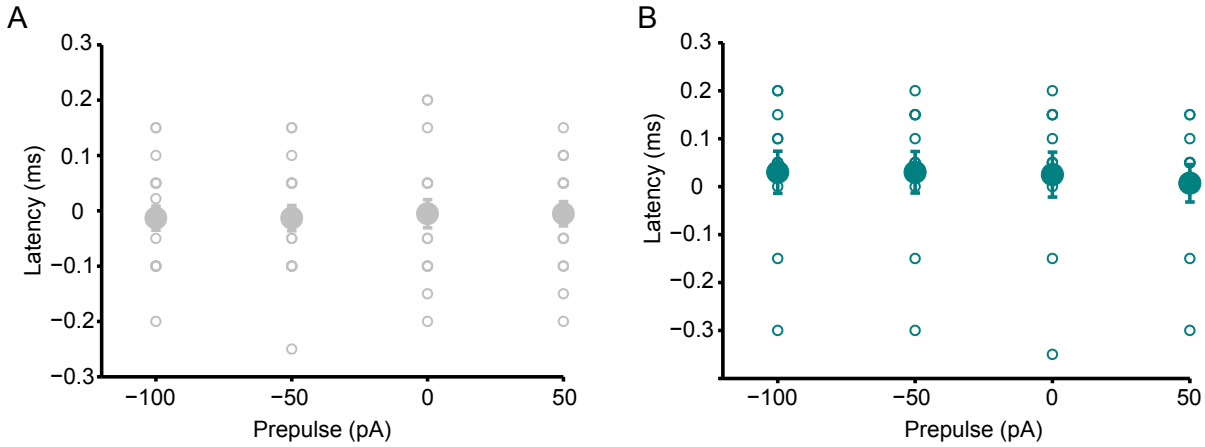

Figure 7.0.8 (A) For wild type neurons spike latency in ms. plotted against prepulse delivered in pA. (B) Same data replotted for *Kcna1a*$^{V408A/+}$

As a separate experiment to assess the involvement of other K_V1 subunits in subthreshold modulation, UK-78282 (Sigma), a compound reported to block Kv1.3 and Kv1.4 channels (Hanson et al., 1999), was used in an identical experiment to DTx-K (Figure 7.0.9). Modulation of spike width by subthreshold pre-pulses was unaffected with UK-78282 (200 nM), arguing against the direct involvement of Kv1.3 and Kv1.4 channels in analogue modulation.

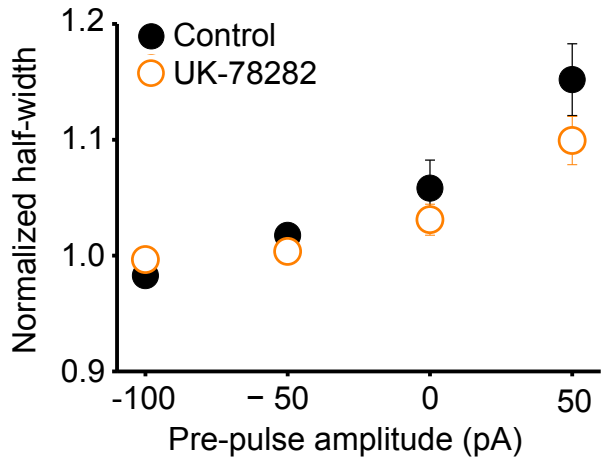

Figure 7.0.9 **Subthreshold modulation of spike width is unaffected by UK-78282.** Data plotted as for Fig. 7.1.4B (n = 5).

7.0.5 Conclusions

By injecting somatic currents ranging between –100 and +50 pA immediately before a supra-threshold somatic depolarizing current, the interplay of analogue-digital signalling could be investigated in the paired somatic-bouton recordings. Prepulses were 200 ms in duration, approximating the time course of subthreshold excitatory postsynaptic potentials (Alle and Geiger, 2006). Long presynaptic depolarization (5-10s) has been shown to mediate analogue-digital facilitation via $K_V1.1$ at rat CA3-CA3 synapses (Bialowas et al., 2015) and we tested this by using longer 2s prepulses. This long depolarization may be relevant to up- and down-states rather than EPSPs. In neurons from wild type mice the presynaptic action potential width showed a positive dependence on the pre-pulse, consistent with voltage-dependent

inactivation of K^+ currents. This suggests that action potential width modulation by subthreshold somatic depolarisations occurs in intact axons.

However there is an unexpected dissociation between the effects of manipulating $K_V1.1$ on the basal presynaptic spike width and on the modulation of spike width by membrane potential changes propagating passively from the soma. Pharmacological blockade or homozygous deletion of $K_V1.1$ broadened the action potential recorded in boutons but did not prevent the effect of subthreshold prepulses. This argues that, despite its relatively negative activation and inactivation kinetics, $K_V1.1$ is not absolutely necessary for spike width modulation by prepulses lasting 200 ms. A heterozygous missense mutation of the $K_V1.1$-encoding gene *Kcna1*, in contrast, completely abolished the effect of prepulses on spike width, even though the basal spike width was no greater than when $K_V1.1$ was deleted.

A possible explanation may be that homozygous deletion of $K_V1.1$ leads to the formation of Kv1 channel stoichiometries that are able to substitute for $K_V1.1$-containing heteromultimers. Such channels most likely have kinetics that are slower or require a larger depolarization to activate, explaining the prolongation of the spike width, and yet undergo a similar slow inactivation upon sustained depolarization, explaining the persistence of analogue modulation of spike width. In contrast, the V408A mutation exerts a dominant negative effect, resulting in functional loss of a wide range of K_V1 channels. This was further investigated using immunoblots for a number of K_V1 channel subunits in cortical synaptosomes made from both wild type$^-$ and *Kcna1*$^{V408A/+}$ (**Section 7.1.5**). More recently it has been demonstrated that K_V3

channels, which govern AP repolarisation and exhibit faster adaptive properties than K_V1, may have a role in increasing spike width and analogue enhancement of AP – evoked release (Rowan and Christie, 2017). We did not focus on the representation of K_V3 in our V408A mutation model and a down regulation of this channel subtype with its effect on analogue-digital facilitation cannot be excluded.

One potential confound is the varying charging time constant seen at the different subthreshold prepulses (e.g. Figure 7.0.6 A1). As discussed in **Section 1.2.2** time constant is a function of the membrane resistance and membrane capacitance. The lower a time constant, the more rapidly a membrane will respond to a current stimulus. Therefore a variable time constant may have its effect especially on fast activation and inactivation kinetics observed in Na^+ channels at central synapses (Engel and Jonas, 2005) and thus AP waveform.

It should be noted that all the above experiments were performed in hippocampal cultures, and what would be of interest for future study is whether analogue-digital modulation is affected in cerebellar inhibitory networks as $K_v1.1$ is found abundantly in basket cells.

7.1 K_V1 subunit expression in the genetic EA1 models

7.1.1 Main aims

1. To investigate the K_V1 subunit composition of *Kcna1*$^{V408A/+}$ in cortical synaptosomes, as we hypothesize that the mutation may lead to a functional loss of more than $K_V1.1$ leading to the abolition of analogue modulation

7.1.2 Methods

The following experiments were performed by our collaborators Oscar Bello and Shyam S Krishnakumar within our department.

Pure synaptosome preparation

Pure synaptosomes were prepared using protocols adapted from refs. (Bai and Witzmann, 2007; Hebb and Whittaker, 1958). Brain cortices from four wild type or four *Kcna1*$^{V408A/+}$ mice (6 – 8 weeks old) were homogenized in 10 volumes of ice-cold HEPES-buffered sucrose (320 mM sucrose, 4 mM HEPES, pH 7.4, protease inhibitor cocktail – Sigma S8830) using a motor driven glass-Teflon homogenizer at ~900 rpm with 15 gentle strokes. The homogenate was centrifuged at 1,000 g for 10

min at 4°C in a Ti 70.1 rotor (Beckman). The pellet (P1) was discarded and the supernatant (S1) was centrifuged at 10,000 g for 15 min in the same rotor. The resulting pellet (P2) was re-suspended in 10 volumes of HEPES-buffered sucrose and then re-spun at 10,000 g for a further 15 min to yield a washed crude synaptosomal fraction. The supernatant was removed and the synaptosome-enriched pellet (P2') was re-suspended in 4 ml of homogenization buffer. The P2' fraction was then layered onto 3 ml of 1.2 M sucrose (supplemented with 4 mM HEPES pH7.4, protease inhibitors), and centrifuged at 230,000 g for 15 min in an SW55 Ti swinging bucket rotor (Beckman). The synaptosomes were recovered at the interface of HEPES-buffered sucrose and 1.2 M sucrose, and diluted to 8 ml with ice-cold HEPES-buffered sucrose. The samples were then layered onto 4 ml of 0.8 M sucrose (supplemented with 4 mM HEPES pH7.4, protease inhibitors) and centrifuged at 230,000 g for 15 min in a Ti 70.1 rotor (Beckman). The resulting pellet containing pure synaptomes was re-suspended in lysis buffer (1% NP40, 50 mM Tris-HCl (pH 8), 150 mM NaCl, and 2 mM EDTA, protease inhibitor) and the protein concentration was then determined with a Bio-Rad protein assay solution with bovine serum albumin (BSA) as a standard.

Western blot analyses

Equal amounts of proteins (30 µg/lane) from pure synaptosomal fraction of wild type or *Kcna1*$^{V408A/+}$ KI mice were separated by SDS-PAGE using Bis-Tris gradient gels (4–12% NuPAGE, Invitrogen) according to the manufacturer's recommendations and electrophoretically transferred onto Immobilon-P transfer membranes (Millipore).

Membranes were immunoblotted with the respective antibodies: rabbit anti-Kv1.1 (APC-161, Alamone Lab, 1:800), anti-Kv1.2 (APC-010, 1:1500), anti-Kv1.3 (APC-101, 1:1000), anti-Kv1.4 (APC-167, 1:500), anti-Kv1.6 (APC-003, 1:2000), and anti-SNAP25 (Abcam ab5666, 1:2000) at 4°C overnight. Blots were then exposed to horseradish peroxidase-conjugated goat anti-rabbit IgG (17210, Bio-Rad Laboratories, 1:5000) for 1 hour at room temperature. Blots were developed using ECL-Prime (GE Healthcare), visualized via a ChemiDoc™ Touch Imaging System, and analysed using Image Lab 5.2 software (Bio-Rab Laboratories). For the quantifications, the signal intensity of each of the Kv1 bands was normalized to the signal intensity of the corresponding SNAP25 bands, and then the *Kcna1*$^{V408A/+}$ synaptosomes were expressed as a percentage of wild type

7.1.3 Results and conclusion

We concentrated on the Kv1.1, Kv1.2, Kv1.3, Kv1.4 and Kv1.6 subunits, as they are known to be expressed in the CNS (**Section 1.4.2**). None of the specific immunoreactive signals, normalized to the corresponding SNAP25 band intensity, differed significantly between wild type and *Kcna1*$^{V408A/+}$ mice, although there were non-significant trends for lower Kv1.3 and higher Kv1.6.

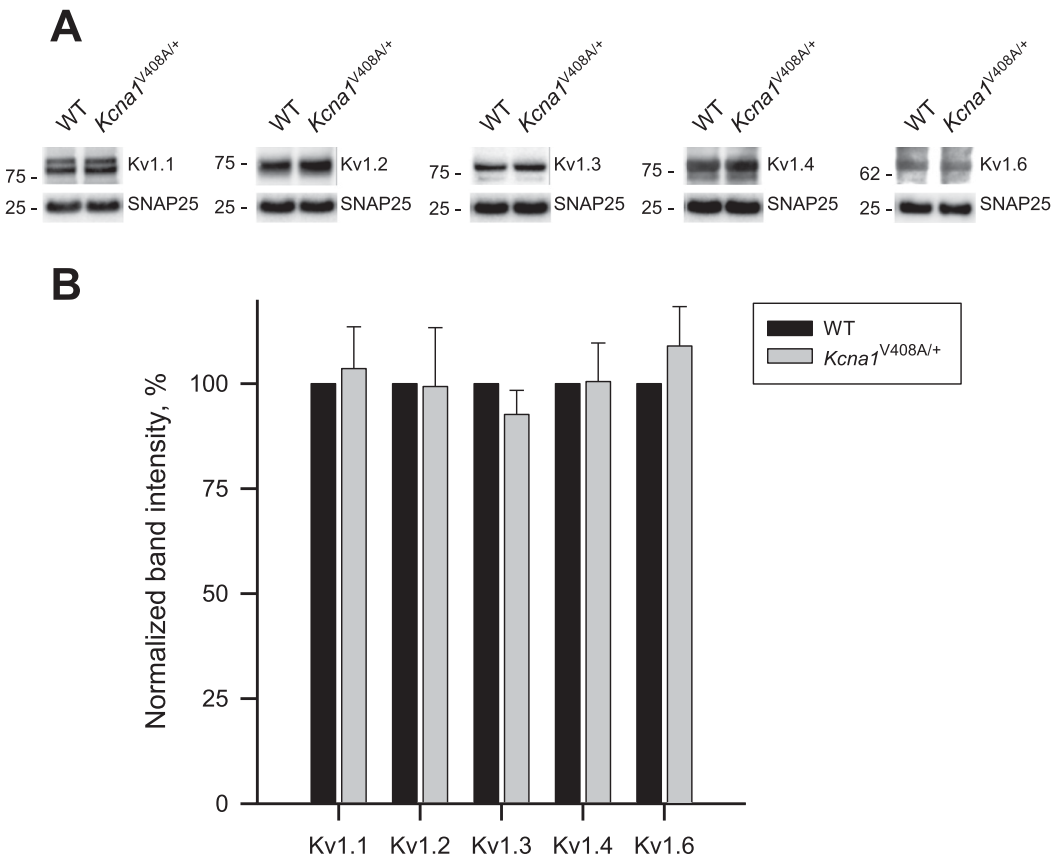

Figure 7.1 **Western blot analysis of Kv1 subunits expression in cortical synaptosomes from control WT and V408A Het KI mice. A)** Representative immunoblot of the Kv1 subunits distribution in synaptosome preparations from wild type mice (WT/WT) and V408A Het KI mice (WT/V408A) respectively. Top panels, immunostaining with subunit specific anti-Kv1 antibodies (Abs); bottom panels, loading control, immunostaining with anti-SNAP25 Ab. Molecular weight protein markers (kDa) are shown on the right of each blot. **B)** Quantification of results. Specific immunoreactive signals for Kv1 subunits in each S(in kDa)WT/V408A lane (integral band intensity) were normalized to the corresponding SNAP25 band intensity and then expressed as a percentage of the corresponding control WT/WT preparation. Data represent mean (±SEM) from n = 3 independent synaptosomal preparations (4 cortex/sample WT/WT or WT/V408A, 3 immunoblots for each samples).

In conclusion quantitative immunoblotting failed to reveal a substantial change in the relative proportion of different members of the Kv1 family in cortical synaptosomes. A potential limitation in relating this negative result to the analogue-digital modulation is that the synaptosomes were obtained at a different developmental stage, and included neocortical as well as hippocampal tissue.

8.0 Final conclusions and considerations

The aims outlined at the start of this thesis were as follows:

1. Optimise the Hopping Probe Ion Conductance method to gain direct electrophysiological recording from small hippocampal synapses
2. Use HPICM to predict the location of voltage gated calcium channels in small synapses
3. Compare presynaptic action potential morphology in models of Episodic Ataxia type 1 and wild type
4. Understand the role of K_V1 channels in axonal analogue-digital signalling

This work describes how hopping probe ion conductance microscopy was integrated with established electrophysiological techniques to provide live topographic images of small CNS synapses (diameter ~1μm), the predominant synapse in the mammalian brain, at sub-micrometre resolution. In addition, by developing a semi-automated approach that allowed precise targeted recordings from small synaptic terminals in cultured hippocampal neurons, we demonstrated for the first time direct electrophysiological data from small synapses in all four configurations of the patch-clamp method (cell-attached, inside-out, whole-cell, and outside-out).

We used this method to demonstrate that no voltage gated calcium channel (VGCC) activity was detected with cell-attached recording on the exposed surface of the presynaptic bouton, whereas VGCC activity was found when whole-bouton configuration was obtained. This strongly suggested that the vast majority of VGCC

in central synapses are located in or very near the active zone and are excluded from the rest of the membrane of the bouton.

The use of HPICM in directly recording presynaptic action potentials of micrometer sized hippocampal boutons in neuronal culture has been a valuable addition to the current methodology in assessing axonal function. Other techniques have included paired recordings from axon terminals of Purkinje cells (1 – 3 μm) and associated postsynaptic cell in cerebellar culture (Kawaguchi and Sakaba, 2015). This was achieved by using enhanced green fluorescent protein (EGFP) to visualise Purkinje cell axons. Optical recordings of membrane voltage using electro-chromic dyes have been used to resolve axonal action potential initiation in cerebellar Purkinje cells (Foust et al., 2010) and layer 5 pyramidal neurons (Popovic et al., 2011). However their use had been limited by factors such as injection technique used to label cells and internalisation of the membrane dye during experiments. Recently genetically encoded optical membrane potential indicators have shown faster response kinetics permitting their use in synaptic boutons (Hoppa et al., 2014). Fluorescent coated patch-clamp pipettes viewed under spinning disc confocal visualisation have provided cell attached recordings of action potentials from axon branches in hippocampal CA3 pyramidal neurons, and demonstrated AP waveform modulation in response to local glutamate release (Sasaki et al., 2011, 2012). The enlarged axonal bleb formed at the cut end of an axon during cell slicing for patch-clamp can also be a target for patching (Hu et al., 2009; Shu et al., 2007b). Finally two−photon targeted patching, using two photon imaging to guide whole-cell recordings in genetically manipulated neurons, has enabled both in vitro and in vivo assessment of axonal function (Komai et al., 2006; Margrie et al., 2003).

It is likely that the AP within an axon may be more heterogeneous than the binary pulse previously thought, influenced by the types and sublocalisation of ion channels at any particular region. In hippocampal mossy fibre cells and fast-spiking hippocampal interneurons, Na^+ channel density increases with distance from the soma to ensure fast and reliable AP propagation in an extensively branching arbor (Engel and Jonas, 2005; Hu and Jonas, 2014). Potassium channels and in particular K_V1 has been shown to be key in determining axon spike morphology at the axon initial segment of layer 5 pyramidal cells and cerebellar stellate cells (Kole et al., 2007a; Rowan et al., 2014). Indeed K_V1 mediated control of AP repolarisation occurs throughout the axonal arbor in layer 5 pyramidal cells, and in neocortical fast-spiking interneurons this role thought to be performed by K_V3 (Goldberg et al., 2005). However at the bouton in stellate cells, the calyx of Held and hippocampal mossy fibre boutons it is K_V3 that mediates AP repolarisation, thus providing tight control over neurotransmitter release (Alle et al., 2011; Ishikawa et al., 2003; Rowan et al., 2014, 2016). A potential mechanism for regulation of neurotransmitter release in small CNS nerve terminals is modulation of AP amplitude which controls Ca^{2+} entry, thus providing adaptive plasticity in synaptic function (Hoppa et al., 2014). This phenomenon was not seen in our experiments (Figure 6.2.4). In addition, computational analysis of mossy fibre boutons has suggested Na^+ channels preferentially amplify the presynaptic action potential and enhance Ca^{2+} inflow (Engel and Jonas, 2005).

Although a role of $K_V1.1$ in determining action potential width has been proposed in previous studies, it had never been previously directly shown in submicrometer sized synapses. Nor has it been studied with genetic (as opposed to pharmacological) manipulation of $K_V1.1$ channels. My work has demonstrated that the presynaptic action potential half-width (t/2) is increased in both the $K_v1.1$ knockout mouse and in a knock-in model of Episodic Ataxia type 1; both by eliciting APs directly at the bouton via the HPICM pipette and by using the adapted dual patch method where APs were elicited in the soma and actively propagated to the presynaptic bouton. The double patch method also confirmed that the difference in t/2 is a solely presynaptic or axonal phenomenon, as t/2 was not significantly increased in either *Kcna1a*$^{-/-}$ or *Kcna1a*$^{V408A/+}$ somatic recordings compared with wild type.

We demonstrate that manipulating $K_V1.1$ by progressively depolarising the presynaptic element via subthreshold prepulses causes a concomitant increase in bouton t/2 in wild type neurons, and that a similar effect is obtained with pharmacological blockade of Kv1.1 using DTX-K and after homozygous deletion of $K_V1.1$. This argues that, despite its relatively negative activation and inactivation kinetics, Kv1.1 is not absolutely necessary for spike width modulation by prepulses lasting 200 ms. However a heterozygous missense mutation of the $K_V1.1$-encoding gene *Kcna1*, in contrast, completely abolished the effect of prepulses on spike width. A possible explanation for this result is that the dominant negative effect of the V408A mutation may result in a change in the stoichiometry of K_V1 channels. Such channels would be impaired both in their ability to repolarize boutons following action potentials (explaining the increase in t/2), and become insensitive to subthreshold depolarizing pre-pulses lasting 200ms or 2s. Analogue-digital facilitation has also

been demonstrated in cerebellar stellate interneurons and thought to be mediated by K_V3 (Rowan and Christie, 2017). Interestingly this feature diminishes in the maturing cerebellum, and whether thus is true for the hippocampus is course for further work.

We saw no obvious change in expression of different Kv1 subunits in forebrain synaptosomes. Nevertheless, given the very large number of possible permutations of subunits in heterotetramers, failure to detect a change in subunit abundance does not rule out subtle rearrangements in channel composition. Among other possible explanations for the dissociation between pharmacological and genetic ablation of Kv1.1 on one hand, and the *Kcna1*$^{V408A/+}$ model on the other hand, is a change in the subcellular location of channels. This could be explored with NEURON modelling (see Appendix).

There are a number of future considerations both in terms of developing the HPICM method and furthering our work concerning K_V1 channels. HPICM to date has only been trialled in dissociated neuronal cultures. Although a very useful model to examine specific channel function within a simple neuronal circuit (with application of drugs etc.), working in more complex models such as cell slices and even in vivo would add further information as circuits that have retained their natural synaptic connections. The semi-automated smart patch function of HPICM relies on the nanopipette being held vertically at all times, meaning the X and Y co-ordinates of the pipette do not alter, and the pipette can be navigated exactly to the targeted bouton. Thus a flat surface like neuronal culture lends itself to this form of

microscopy; for angled surfaces such as slices and moving surfaces such as in vivo recordings, the method would need to be advanced.

When considering the work of axonal signalling in EA1 one important point to make is that all experiments were performed in hippocampal cultures, where 90% of synapses are excitatory. We know that the symptoms described in EA1, namely paroxysms of cerebellar incoordination and myokymia are most likely attributable to abnormal GABA release from cerebellar basket cells (Herson et al., 2003) and to motor axon hyperexcitability respectively (Brunetti et al., 2012), both sites where Kv1.1 is especially abundantly expressed . What would be of interest for future study is whether analogue-digital modulation is similarly affected in cerebellar inhibitory networks, or whether it is a solely excitatory phenomenon. Finally future experiments could examine how intra-bouton calcium in stimulated synapses is affected by knocking out $K_V1.1$ and knock-in of the V408A mutation in hippocampal cells. It is expected that both these EA1 models would show greater calcium increase upon stimulation in keeping with increased neurotransmitter release, but it would be interesting to see whether the amount of calcium increase is quantitatively related to the increased presynaptic action potential width already shown in this work. The differential presynaptic transmission of information in excitatory and inhibitory circuits may in part explain the pathogenesis of EA1, and temptingly may point to a target for future therapies.

References

Adelman, J.P., Bond, C.T., Pessia, M., and Maylie, J. (1995). Episodic ataxia results from voltage-dependent potassium channels with altered functions. Neuron *15*, 1449–1454.

Ahnert-Hilger, G., Höltje, M., Pahner, I., Winter, S., and Brunk, I. (2003). Regulation of vesicular neurotransmitter transporters. Rev. Physiol. Biochem. Pharmacol. *150*, 140–160.

Alle, H., and Geiger, J.R.P. (2006). Combined analog and action potential coding in hippocampal mossy fibers. Science *311*, 1290–1293.

Alle, H., Kubota, H., and Geiger, J.R.P. (2011). Sparse but highly efficient Kv3 outpace BKCa channels in action potential repolarization at hippocampal mossy fiber boutons. J. Neurosci. Off. J. Soc. Neurosci. *31*, 8001–8012.

An, W.F., Bowlby, M.R., Betty, M., Cao, J., Ling, H.P., Mendoza, G., Hinson, J.W., Mattsson, K.I., Strassle, B.W., Trimmer, J.S., et al. (2000). Modulation of A-type potassium channels by a family of calcium sensors. Nature *403*, 553–556.

Andersen, P., Soleng, A.F., and Raastad, M. (2000). The hippocampal lamella hypothesis revisited. Brain Res. *886*, 165–171.

Anderson, P., Storm, J., and Wheal, H.V. (1987). Thresholds of action potentials evoked by synapses on the dendrites of pyramidal cells in the rat hippocampus in vitro. J. Physiol. *383*, 509–526.

Awatramani, G.B., Price, G.D., and Trussell, L.O. (2005a). Modulation of transmitter release by presynaptic resting potential and background calcium levels. Neuron *48*, 109–121.

Awatramani, G.B., Price, G.D., and Trussell, L.O. (2005b). Modulation of transmitter release by presynaptic resting potential and background calcium levels. Neuron *48*, 109–121.

Bai, F., and Witzmann, F.A. (2007). Synaptosome proteomics. Subcell. Biochem. *43*, 77–98.

Banker, G., and Goslin, K. (1988). Developments in neuronal cell culture. Nature *336*, 185–186.

Bean, B.P. (1989). Multiple types of calcium channels in heart muscle and neurons. Modulation by drugs and neurotransmitters. Ann. N. Y. Acad. Sci. *560*, 334–345.

Begum, R., Bakiri, Y., Volynski, K.E., and Kullmann, D.M. (2016). Action potential broadening in a presynaptic channelopathy. Nat. Commun. *7*, 12102.

Benishin, C.G., Sorensen, R.G., Brown, W.E., Krueger, B.K., and Blaustein, M.P. (1988). Four polypeptide components of green mamba venom selectively block

certain potassium channels in rat brain synaptosomes. Mol. Pharmacol. *34*, 152–159.

Bennett, M.V.L., and Zukin, R.S. (2004). Electrical coupling and neuronal synchronization in the Mammalian brain. Neuron *41*, 495–511.

Benson, D.L., Watkins, F.H., Steward, O., and Banker, G. (1994). Characterization of GABAergic neurons in hippocampal cell cultures. J. Neurocytol. *23*, 279–295.

Bernèche, S., and Roux, B. (2001). Energetics of ion conduction through the K+ channel. Nature *414*, 73–77.

Bezanilla, F., and Armstrong, C.M. (1972). Negative conductance caused by entry of sodium and cesium ions into the potassium channels of squid axons. J. Gen. Physiol. *60*, 588–608.

Bialowas, A., Rama, S., Zbili, M., Marra, V., Fronzaroli-Molinieres, L., Ankri, N., Carlier, E., and Debanne, D. (2015). Analog modulation of spike-evoked transmission in CA3 circuits is determined by axonal Kv1.1 channels in a time-dependent manner. Eur. J. Neurosci. *41*, 293–304.

Bischofberger, J., Engel, D., Li, L., Geiger, J.R.P., and Jonas, P. (2006). Patch-clamp recording from mossy fiber terminals in hippocampal slices. Nat. Protoc. *1*, 2075–2081.

Böhle, T., and Benndorf, K. (1994). Facilitated giga-seal formation with a just originated glass surface. Pflugers Arch. *427*, 487–491.

Boiko, T., Rasband, M.N., Levinson, S.R., Caldwell, J.H., Mandel, G., Trimmer, J.S., and Matthews, G. (2001). Compact myelin dictates the differential targeting of two sodium channel isoforms in the same axon. Neuron *30*, 91–104.

Boiko, T., Wart, A.V., Caldwell, J.H., Levinson, S.R., Trimmer, J.S., and Matthews, G. (2003). Functional Specialization of the Axon Initial Segment by Isoform-Specific Sodium Channel Targeting. J. Neurosci. *23*, 2306–2313.

Boland, L.M., Price, D.L., and Jackson, K.A. (1999). Episodic ataxia/myokymia mutations functionally expressed in the Shaker potassium channel. Neuroscience *91*, 1557–1564.

Boudkkazi, S., Fronzaroli-Molinieres, L., and Debanne, D. (2011). Presynaptic action potential waveform determines cortical synaptic latency. J. Physiol. *589*, 1117–1131.

Bouhours, B., Trigo, F.F., and Marty, A. (2011). Somatic depolarization enhances GABA release in cerebellar interneurons via a calcium/protein kinase C pathway. J. Neurosci. Off. J. Soc. Neurosci. *31*, 5804–5815.

Bourinet, E., Soong, T.W., Sutton, K., Slaymaker, S., Mathews, E., Monteil, A., Zamponi, G.W., Nargeot, J., and Snutch, T.P. (1999). Splicing of alpha 1A subunit gene generates phenotypic variants of P- and Q-type calcium channels. Nat. Neurosci. *2*, 407–415.

Brain, K.L., and Bennett, M.R. (1995). Calcium in the nerve terminals of chick ciliary ganglia during facilitation, augmentation and potentiation. J. Physiol. *489 (Pt 3)*, 637–648.

von Brederlow, B., Hahn, A.F., Koopman, W.J., Ebers, G.C., and Bulman, D.E. (1995). Mapping the gene for acetazolamide responsive hereditary paryoxysmal cerebellar ataxia to chromosome 19p. Hum. Mol. Genet. *4*, 279–284.

Bretschneider, F., Wrisch, A., Lehmann-Horn, F., and Grissmer, S. (1999). Expression in mammalian cells and electrophysiological characterization of two mutant Kv1.1 channels causing episodic ataxia type 1 (EA-1). Eur. J. Neurosci. *11*, 2403–2412.

Browne, D.L., Gancher, S.T., Nutt, J.G., Brunt, E.R., Smith, E.A., Kramer, P., and Litt, M. (1994). Episodic ataxia/myokymia syndrome is associated with point mutations in the human potassium channel gene, KCNA1. Nat. Genet. *8*, 136–140.

Brunetti, O., Imbrici, P., Botti, F.M., Pettorossi, V.E., D'Adamo, M.C., Valentino, M., Zammit, C., Mora, M., Gibertini, S., Di Giovanni, G., et al. (2012). Kv1.1 knock-in ataxic mice exhibit spontaneous myokymic activity exacerbated by fatigue, ischemia and low temperature. Neurobiol. Dis. *47*, 310–321.

Buchhalter, J.R., and Dichter, M.A. (1991). Electrophysiological comparison of pyramidal and stellate nonpyramidal neurons in dissociated cell culture of rat hippocampus. Brain Res. Bull. *26*, 333–338.

Catterall, W.A. (2000). Structure and regulation of voltage-gated Ca2+ channels. Annu. Rev. Cell Dev. Biol. *16*, 521–555.

Catterall, W.A., Goldin, A.L., and Waxman, S.G. (2005). International Union of Pharmacology. XLVII. Nomenclature and structure-function relationships of voltage-gated sodium channels. Pharmacol. Rev. *57*, 397–409.

Ceccarelli, B., Hurlbut, W.P., and Mauro, A. (1973). Turnover of transmitter and synaptic vesicles at the frog neuromuscular junction. J. Cell Biol. *57*, 499–524.

Cha, A., Snyder, G.E., Selvin, P.R., and Bezanilla, F. (1999). Atomic scale movement of the voltage-sensing region in a potassium channel measured via spectroscopy. Nature *402*, 809–813.

Chang, S.Y., Zagha, E., Kwon, E.S., Ozaita, A., Bobik, M., Martone, M.E., Ellisman, M.H., Heintz, N., and Rudy, B. (2007). Distribution of Kv3.3 potassium channel subunits in distinct neuronal populations of mouse brain. J. Comp. Neurol. *502*, 953–972.

Chernomordik, L.V., and Kozlov, M.M. (2008). Mechanics of membrane fusion. Nat. Struct. Mol. Biol. *15*, 675–683.

Choe, S. (2002). Potassium channel structures. Nat. Rev. Neurosci. *3*, 115–121.

Chow, A., Erisir, A., Farb, C., Nadal, M.S., Ozaita, A., Lau, D., Welker, E., and Rudy, B. (1999). K(+) channel expression distinguishes subpopulations of parvalbumin-

and somatostatin-containing neocortical interneurons. J. Neurosci. Off. J. Soc. Neurosci. *19*, 9332–9345.

Christie, J.M., Chiu, D.N., and Jahr, C.E. (2011). Ca(2+)-dependent enhancement of release by subthreshold somatic depolarization. Nat. Neurosci. *14*, 62–68.

Coetzee, W.A., Amarillo, Y., Chiu, J., Chow, A., Lau, D., McCormack, T., Moreno, H., Nadal, M.S., Ozaita, A., Pountney, D., et al. (1999). Molecular diversity of K+ channels. Ann. N. Y. Acad. Sci. *868*, 233–285.

Cox, C.L., Denk, W., Tank, D.W., and Svoboda, K. (2000). Action potentials reliably invade axonal arbors of rat neocortical neurons. Proc. Natl. Acad. Sci. U. S. A. *97*, 9724–9728.

D'Adamo, M.C., Liu, Z., Adelman, J.P., Maylie, J., and Pessia, M. (1998). Episodic ataxia type-1 mutations in the hKv1.1 cytoplasmic pore region alter the gating properties of the channel. EMBO J. *17*, 1200–1207.

D'Adamo, M.C., Hasan, S., Guglielmi, L., Servettini, I., Cenciarini, M., Catacuzzeno, L., and Franciolini, F. (2015). New insights into the pathogenesis and therapeutics of episodic ataxia type 1. Front. Cell. Neurosci. *9*, 317.

Dai, H., Shen, N., Araç, D., and Rizo, J. (2007). A quaternary SNARE-synaptotagmin-Ca2+-phospholipid complex in neurotransmitter release. J. Mol. Biol. *367*, 848–863.

Debanne, D. (2004). Information processing in the axon. Nat. Rev. Neurosci. *5*, 304–316.

Debanne, D., Guérineau, N.C., Gähwiler, B.H., and Thompson, S.M. (1997). Action-potential propagation gated by an axonal I(A)-like K+ conductance in hippocampus. Nature *389*, 286–289.

Debanne, D., Campanac, E., Bialowas, A., Carlier, E., and Alcaraz, G. (2011). Axon physiology. Physiol. Rev. *91*, 555–602.

Debanne, D., Bialowas, A., and Rama, S. (2013). What are the mechanisms for analogue and digital signalling in the brain? Nat. Rev. Neurosci. *14*, 63–69.

Delaney, K.R., and Tank, D.W. (1994). A quantitative measurement of the dependence of short-term synaptic enhancement on presynaptic residual calcium. J. Neurosci. Off. J. Soc. Neurosci. *14*, 5885–5902.

Demos, M.K., Macri, V., Farrell, K., Nelson, T.N., Chapman, K., Accili, E., and Armstrong, L. (2009). A novel KCNA1 mutation associated with global delay and persistent cerebellar dysfunction. Mov. Disord. Off. J. Mov. Disord. Soc. *24*, 778–782.

Denier, C., Ducros, A., Durr, A., Eymard, B., Chassande, B., and Tournier-Lasserve, E. (2001). Missense CACNA1A mutation causing episodic ataxia type 2. Arch. Neurol. *58*, 292–295.

Devaux, J., Alcaraz, G., Grinspan, J., Bennett, V., Joho, R., Crest, M., and Scherer, S.S. (2003). Kv3.1b is a novel component of CNS nodes. J. Neurosci. Off. J. Soc. Neurosci. *23*, 4509–4518.

Devaux, J.J., Kleopa, K.A., Cooper, E.C., and Scherer, S.S. (2004). KCNQ2 is a nodal K+ channel. J. Neurosci. Off. J. Soc. Neurosci. *24*, 1236–1244.

Dodson, P.D., and Forsythe, I.D. (2004). Presynaptic K+ channels: electrifying regulators of synaptic terminal excitability. Trends Neurosci. *27*, 210–217.

Dodson, P.D., Barker, M.C., and Forsythe, I.D. (2002). Two heteromeric Kv1 potassium channels differentially regulate action potential firing. J. Neurosci. Off. J. Soc. Neurosci. *22*, 6953–6961.

Dolphin, A.C. (2006). A short history of voltage-gated calcium channels. Br. J. Pharmacol. *147 Suppl 1*, S56-62.

Doyle, D.A., Morais Cabral, J., Pfuetzner, R.A., Kuo, A., Gulbis, J.M., Cohen, S.L., Chait, B.T., and MacKinnon, R. (1998). The structure of the potassium channel: molecular basis of K+ conduction and selectivity. Science *280*, 69–77.

Dreyer, F., and Penner, R. (1987). The actions of presynaptic snake toxins on membrane currents of mouse motor nerve terminals. J. Physiol. *386*, 455–463.

Dufrêne, Y.F. (2008). Towards nanomicrobiology using atomic force microscopy. Nat. Rev. Microbiol. *6*, 674–680.

Dulla, C.G., and Huguenard, J.R. (2009). Who let the spikes out? Nat. Neurosci. *12*, 959–960.

Eggermann, E., Bucurenciu, I., Goswami, S.P., and Jonas, P. (2012). Nanodomain coupling between Ca^{2+} channels and sensors of exocytosis at fast mammalian synapses. Nat. Rev. Neurosci. *13*, 7–21.

Eijkelkamp, N., Linley, J.E., Baker, M.D., Minett, M.S., Cregg, R., Werdehausen, R., Rugiero, F., and Wood, J.N. (2012). Neurological perspectives on voltage-gated sodium channels. Brain J. Neurol. *135*, 2585–2612.

Elezgarai, I., Díez, J., Puente, N., Azkue, J.J., Benítez, R., Bilbao, A., Knöpfel, T., Doñate-Oliver, F., and Grandes, P. (2003). Subcellular localization of the voltage-dependent potassium channel Kv3.1b in postnatal and adult rat medial nucleus of the trapezoid body. Neuroscience *118*, 889–898.

Engel, D., and Jonas, P. (2005). Presynaptic action potential amplification by voltage-gated Na+ channels in hippocampal mossy fiber boutons. Neuron *45*, 405–417.

Ermolyuk, Y.S., Alder, F.G., Henneberger, C., Rusakov, D.A., Kullmann, D.M., and Volynski, K.E. (2012). Independent regulation of basal neurotransmitter release efficacy by variable Ca^2+ influx and bouton size at small central synapses. PLoS Biol. *10*, e1001396.

Eunson, L.H., Rea, R., Zuberi, S.M., Youroukos, S., Panayiotopoulos, C.P., Liguori, R., Avoni, P., McWilliam, R.C., Stephenson, J.B., Hanna, M.G., et al. (2000). Clinical, genetic, and expression studies of mutations in the potassium channel gene KCNA1 reveal new phenotypic variability. Ann. Neurol. *48*, 647–656.

Fernandes, E.S., Fernandes, M.A., and Keeble, J.E. (2012). The functions of TRPA1 and TRPV1: moving away from sensory nerves. Br. J. Pharmacol. *166*, 510–521.

Fleidervish, I.A., Lasser-Ross, N., Gutnick, M.J., and Ross, W.N. (2010). Na+ imaging reveals little difference in action potential-evoked Na+ influx between axon and soma. Nat. Neurosci. *13*, 852–860.

Foust, A., Popovic, M., Zecevic, D., and McCormick, D.A. (2010). Action potentials initiate in the axon initial segment and propagate through axon collaterals reliably in cerebellar Purkinje neurons. J. Neurosci. Off. J. Soc. Neurosci. *30*, 6891–6902.

Friedman, H.V., Bresler, T., Garner, C.C., and Ziv, N.E. (2000). Assembly of new individual excitatory synapses: time course and temporal order of synaptic molecule recruitment. Neuron *27*, 57–69.

Frotscher, M., Drakew, A., and Heimrich, B. (2000). Role of afferent innervation and neuronal activity in dendritic development and spine maturation of fascia dentata granule cells. Cereb. Cortex N. Y. N 1991 *10*, 946–951.

Garrido, J.J., Giraud, P., Carlier, E., Fernandes, F., Moussif, A., Fache, M.-P., Debanne, D., and Dargent, B. (2003). A targeting motif involved in sodium channel clustering at the axonal initial segment. Science *300*, 2091–2094.

Gasser, U.E., and Hatten, M.E. (1990). Neuron-glia interactions of rat hippocampal cells in vitro: glial-guided neuronal migration and neuronal regulation of glial differentiation. J. Neurosci. Off. J. Soc. Neurosci. *10*, 1276–1285.

Geiger, J.R., and Jonas, P. (2000). Dynamic control of presynaptic Ca(2+) inflow by fast-inactivating K(+) channels in hippocampal mossy fiber boutons. Neuron *28*, 927–939.

Glauner, K.S., Mannuzzu, L.M., Gandhi, C.S., and Isacoff, E.Y. (1999). Spectroscopic mapping of voltage sensor movement in the Shaker potassium channel. Nature *402*, 813–817.

Goldberg, E.M., Watanabe, S., Chang, S.Y., Joho, R.H., Huang, Z.J., Leonard, C.S., and Rudy, B. (2005). Specific functions of synaptically localized potassium channels in synaptic transmission at the neocortical GABAergic fast-spiking cell synapse. J. Neurosci. Off. J. Soc. Neurosci. *25*, 5230–5235.

Goldberg, E.M., Clark, B.D., Zagha, E., Nahmani, M., Erisir, A., and Rudy, B. (2008). K+ channels at the axon initial segment dampen near-threshold excitability of neocortical fast-spiking GABAergic interneurons. Neuron *58*, 387–400.

Goldin, A.L. (2003). Mechanisms of sodium channel inactivation. Curr. Opin. Neurobiol. *13*, 284–290.

Goldstein, S.A.N., Bayliss, D.A., Kim, D., Lesage, F., Plant, L.D., and Rajan, S. (2005). International Union of Pharmacology. LV. Nomenclature and molecular relationships of two-P potassium channels. Pharmacol. Rev. *57*, 527–540.

Gonzalez, C., Lopez-Rodriguez, A., Srikumar, D., Rosenthal, J.J.C., and Holmgren, M. (2011). Editing of human K(V)1.1 channel mRNAs disrupts binding of the N-terminus tip at the intracellular cavity. Nat. Commun. *2*, 436.

Graves, T.D., Cha, Y.-H., Hahn, A.F., Barohn, R., Salajegheh, M.K., Griggs, R.C., Bundy, B.N., Jen, J.C., Baloh, R.W., Hanna, M.G., et al. (2014). Episodic ataxia type 1: clinical characterization, quality of life and genotype-phenotype correlation. Brain J. Neurol. *137*, 1009–1018.

Griggs, R.C., and Nutt, J.G. (1995). Episodic ataxias as channelopathies. Ann. Neurol. *37*, 285–287.

Grosse, G., Tapp, R., Wartenberg, M., Sauer, H., Fox, P.A., Grosse, J., Gratzl, M., and Bergmann, M. (1998). Prenatal hippocampal granule cells in primary cell culture form mossy fiber boutons at pyramidal cell dendrites. J. Neurosci. Res. *51*, 602–611.

Gu, N., Vervaeke, K., Hu, H., and Storm, J.F. (2005). Kv7/KCNQ/M and HCN/h, but not KCa2/SK channels, contribute to the somatic medium after-hyperpolarization and excitability control in CA1 hippocampal pyramidal cells. J. Physiol. *566*, 689–715.

Guida, S., Trettel, F., Pagnutti, S., Mantuano, E., Tottene, A., Veneziano, L., Fellin, T., Spadaro, M., Stauderman, K., Williams, M., et al. (2001). Complete loss of P/Q calcium channel activity caused by a CACNA1A missense mutation carried by patients with episodic ataxia type 2. Am. J. Hum. Genet. *68*, 759–764.

Hama, H., Hara, C., Yamaguchi, K., and Miyawaki, A. (2004). PKC signaling mediates global enhancement of excitatory synaptogenesis in neurons triggered by local contact with astrocytes. Neuron *41*, 405–415.

Han, C., Vasylyev, D., Macala, L.J., Gerrits, M.M., Hoeijmakers, J.G.J., Bekelaar, K.J., Dib-Hajj, S.D., Faber, C.G., Merkies, I.S.J., and Waxman, S.G. (2014). The G1662S NaV1.8 mutation in small fibre neuropathy: impaired inactivation underlying DRG neuron hyperexcitability. J. Neurol. Neurosurg. Psychiatry *85*, 499–505.

Hansma, P.K., Drake, B., Marti, O., Gould, S.A., and Prater, C.B. (1989). The scanning ion-conductance microscope. Science *243*, 641–643.

Hanson, D.C., Nguyen, A., Mather, R.J., Rauer, H., Koch, K., Burgess, L.E., Rizzi, J.P., Donovan, C.B., Bruns, M.J., Canniff, P.C., et al. (1999). UK-78,282, a novel piperidine compound that potently blocks the Kv1.3 voltage-gated potassium channel and inhibits human T cell activation. Br. J. Pharmacol. *126*, 1707–1716.

Harata, N.C., Aravanis, A.M., and Tsien, R.W. (2006). Kiss-and-run and full-collapse fusion as modes of exo-endocytosis in neurosecretion. J. Neurochem. *97*, 1546–1570.

Harrison, R.G. (1910). The outgrowth of the nerve fiber as a mode of protoplasmic movement. J Exp Zool 787-U727.

Harvey, A.L. (2001). Twenty years of dendrotoxins. Toxicon Off. J. Int. Soc. Toxinology *39*, 15–26.

He, Y., Zorumski, C.F., and Mennerick, S. (2002). Contribution of presynaptic Na(+) channel inactivation to paired-pulse synaptic depression in cultured hippocampal neurons. J. Neurophysiol. *87*, 925–936.

Hebb, C.O., and Whittaker, V.P. (1958). Intracellular distributions of acetylcholine and choline acetylase. J. Physiol. *142*, 187–196.

Heeroma, J.H., Henneberger, C., Rajakulendran, S., Hanna, M.G., Schorge, S., and Kullmann, D.M. (2009). Episodic ataxia type 1 mutations differentially affect neuronal excitability and transmitter release. Dis. Model. Mech. *2*, 612–619.

Herson, P.S., Virk, M., Rustay, N.R., Bond, C.T., Crabbe, J.C., Adelman, J.P., and Maylie, J. (2003). A mouse model of episodic ataxia type-1. Nat. Neurosci. *6*, 378–383.

Hess, P. (1990). Calcium channels in vertebrate cells. Annu. Rev. Neurosci. *13*, 337–356.

Hille, B. (2001). Ion channels of excitable membranes (Sunderland).

Hodgkin, A.L. (1939). The relation between conduction velocity and the electrical resistance outside a nerve fibre. J. Physiol. *94*, 560–570.

Hodgkin, A.L., and Huxley, A.F. (1952). Propagation of electrical signals along giant nerve fibers. Proc. R. Soc. Lond. B Biol. Sci. *140*, 177–183.

Hofmann, F., Biel, M., and Flockerzi, V. (1994). Molecular basis for Ca2+ channel diversity. Annu. Rev. Neurosci. *17*, 399–418.

Holderith, N., Lorincz, A., Katona, G., Rózsa, B., Kulik, A., Watanabe, M., and Nusser, Z. (2012). Release probability of hippocampal glutamatergic terminals scales with the size of the active zone. Nat. Neurosci. *15*, 988–997.

Hoppa, M.B., Gouzer, G., Armbruster, M., and Ryan, T.A. (2014). Control and plasticity of the presynaptic action potential waveform at small CNS nerve terminals. Neuron *84*, 778–789.

H.S. Carslaw, and J.C. Jaeger (1959). Conduction of Heat in Solids (Oxford University Press).

Hu, H., and Jonas, P. (2014). A supercritical density of Na(+) channels ensures fast signaling in GABAergic interneuron axons. Nat. Neurosci. *17*, 686–693.

Hu, W., Tian, C., Li, T., Yang, M., Hou, H., and Shu, Y. (2009). Distinct contributions of Na(v)1.6 and Na(v)1.2 in action potential initiation and backpropagation. Nat. Neurosci. *12*, 996–1002.

Hursh, J.B. (1939). Conduction velocity and diameter of nerve fibers. Am.J.Physiol *127*, 131–139.

Imbrici, P., D'Adamo, M.C., Kullmann, D.M., and Pessia, M. (2006). Episodic ataxia type 1 mutations in the KCNA1 gene impair the fast inactivation properties of the human potassium channels Kv1.4-1.1/Kvbeta1.1 and Kv1.4-1.1/Kvbeta1.2. Eur. J. Neurosci. *24*, 3073–3083.

Inchauspe, C.G., Urbano, F.J., Di Guilmi, M.N., Ferrari, M.D., van den Maagdenberg, A.M.J.M., Forsythe, I.D., and Uchitel, O.D. (2012). Presynaptic CaV2.1 calcium channels carrying familial hemiplegic migraine mutation R192Q allow faster recovery from synaptic depression in mouse calyx of Held. J. Neurophysiol. *108*, 2967–2976.

Inda, M.C., DeFelipe, J., and Muñoz, A. (2006). Voltage-gated ion channels in the axon initial segment of human cortical pyramidal cells and their relationship with chandelier cells. Proc. Natl. Acad. Sci. U. S. A. *103*, 2920–2925.

Ishikawa, T., Nakamura, Y., Saitoh, N., Li, W.-B., Iwasaki, S., and Takahashi, T. (2003). Distinct Roles of Kv1 and Kv3 Potassium Channels at the Calyx of Held Presynaptic Terminal. J. Neurosci. *23*, 10445–10453.

Isomoto, S., Kondo, C., and Kurachi, Y. (1997). Inwardly rectifying potassium channels: their molecular heterogeneity and function. Jpn. J. Physiol. *47*, 11–39.

Jackman, S.L., Turecek, J., Belinsky, J.E., and Regehr, W.G. (2016). The calcium sensor synaptotagmin 7 is required for synaptic facilitation. Nature *529*, 88–91.

Jackson, M.B. (1993). Passive current flow and morphology in the terminal arborizations of the posterior pituitary. J. Neurophysiol. *69*, 692–702.

Johnston, J., Griffin, S.J., Baker, C., Skrzypiec, A., Chernova, T., and Forsythe, I.D. (2008). Initial segment Kv2.2 channels mediate a slow delayed rectifier and maintain high frequency action potential firing in medial nucleus of the trapezoid body neurons. J. Physiol. *586*, 3493–3509.

Kaech, S., and Banker, G. (2006). Culturing hippocampal neurons. Nat. Protoc. *1*, 2406–2415.

Kamb, A., Iverson, L.E., and Tanouye, M.A. (1987). Molecular characterization of Shaker, a Drosophila gene that encodes a potassium channel. Cell *50*, 405–413.

Katz, B., and Miledi, R. (1967). A study of synaptic transmission in the absence of nerve impulses. J. Physiol. *192*, 407–436.

Kawaguchi, S., and Sakaba, T. (2015). Control of inhibitory synaptic outputs by low excitability of axon terminals revealed by direct recording. Neuron *85*, 1273–1288.

van Kempen, G.T.H., vanderLeest, H.T., van den Berg, R.J., Eilers, P., and Westerink, R.H.S. (2011). Three distinct modes of exocytosis revealed by amperometry in neuroendocrine cells. Biophys. J. *100*, 968–977.

Ketchum, K.A., Joiner, W.J., Sellers, A.J., Kaczmarek, L.K., and Goldstein, S.A. (1995). A new family of outwardly rectifying potassium channel proteins with two pore domains in tandem. Nature *376*, 690–695.

Kim, S. (2014). Action Potential Modulation in CA1 Pyramidal Neuron Axons Facilitates OLM Interneuron Activation in Recurrent Inhibitory Microcircuits of Rat Hippocampus. PLOS ONE *9*, e113124.

Kinali, M., Jungbluth, H., Eunson, L.H., Sewry, C.A., Manzur, A.Y., Mercuri, E., Hanna, M.G., and Muntoni, F. (2004). Expanding the phenotype of potassium channelopathy: severe neuromyotonia and skeletal deformities without prominent Episodic Ataxia. Neuromuscul. Disord. NMD *14*, 689–693.

Kita, H., and Van der Kloot, W. (1974). Calcium ionophore X-537A increases spontaneous and phasic quantal release of acetylcholine at frog neuromuscular junction. Nature *250*, 658–660.

Klingauf, J., Kavalali, E.T., and Tsien, R.W. (1998). Kinetics and regulation of fast endocytosis at hippocampal synapses. Nature *394*, 581–585.

Knaus, H.G., Schwarzer, C., Koch, R.O., Eberhart, A., Kaczorowski, G.J., Glossmann, H., Wunder, F., Pongs, O., Garcia, M.L., and Sperk, G. (1996). Distribution of high-conductance Ca(2+)-activated K+ channels in rat brain: targeting to axons and nerve terminals. J. Neurosci. Off. J. Soc. Neurosci. *16*, 955–963.

Kole, M.H.P., Letzkus, J.J., and Stuart, G.J. (2007a). Axon initial segment Kv1 channels control axonal action potential waveform and synaptic efficacy. Neuron *55*, 633–647.

Kole, M.H.P., Letzkus, J.J., and Stuart, G.J. (2007b). Axon initial segment Kv1 channels control axonal action potential waveform and synaptic efficacy. Neuron *55*, 633–647.

Kole, M.H.P., Ilschner, S.U., Kampa, B.M., Williams, S.R., Ruben, P.C., and Stuart, G.J. (2008). Action potential generation requires a high sodium channel density in the axon initial segment. Nat. Neurosci. *11*, 178–186.

Komai, S., Denk, W., Osten, P., Brecht, M., and Margrie, T.W. (2006). Two-photon targeted patching (TPTP) in vivo. Nat. Protoc. *1*, 647–652.

Kress, G.J., Dowling, M.J., Meeks, J.P., and Mennerick, S. (2008). High threshold, proximal initiation, and slow conduction velocity of action potentials in dentate granule neuron mossy fibers. J. Neurophysiol. *100*, 281–291.

Kues, W.A., and Wunder, F. (1992). Heterogeneous Expression Patterns of Mammalian Potassium Channel Genes in Developing and Adult Rat Brain. Eur. J. Neurosci. *4*, 1296–1308.

Kullmann, D.M. (2010). Neurological channelopathies. Annu. Rev. Neurosci. *33*, 151–172.

Kümmel, D., Krishnakumar, S.S., Radoff, D.T., Li, F., Giraudo, C.G., Pincet, F., Rothman, J.E., and Reinisch, K.M. (2011). Complexin cross-links prefusion SNAREs into a zigzag array. Nat. Struct. Mol. Biol. *18*, 927–933.

Ladera, C., del Carmen Godino, M., José Cabañero, M., Torres, M., Watanabe, M., Luján, R., and Sánchez-Prieto, J. (2008). Pre-synaptic GABA receptors inhibit glutamate release through GIRK channels in rat cerebral cortex. J. Neurochem. *107*, 1506–1517.

Lai, H.C., and Jan, L.Y. (2006). The distribution and targeting of neuronal voltage-gated ion channels. Nat. Rev. Neurosci. *7*, 548–562.

Lasek, R.J., Gainer, H., and Barker, J.L. (1977). Cell-to-cell transfer of glial proteins to the squid giant axon. The glia-neuron protein trnasfer hypothesis. J. Cell Biol. *74*, 501–523.

Lehmann-Horn, F., and Jurkat-Rott, K. (1999). Voltage-gated ion channels and hereditary disease. Physiol. Rev. *79*, 1317–1372.

Lenkey, N., Kirizs, T., Holderith, N., Máté, Z., Szabó, G., Vizi, E.S., Hájos, N., and Nusser, Z. (2015). Tonic endocannabinoid-mediated modulation of GABA release is independent of the CB1 content of axon terminals. Nat. Commun. *6*, 6557.

Li, F., Kümmel, D., Coleman, J., Reinisch, K.M., Rothman, J.E., and Pincet, F. (2014). A half-zippered SNARE complex represents a functional intermediate in membrane fusion. J. Am. Chem. Soc. *136*, 3456–3464.

Lindgren, C.A., and Moore, J.W. (1989). Identification of ionic currents at presynaptic nerve endings of the lizard. J. Physiol. *414*, 201–222.

Llinás, R., Sugimori, M., Hillman, D.E., and Cherksey, B. (1992). Distribution and functional significance of the P-type, voltage-dependent Ca2+ channels in the mammalian central nervous system. Trends Neurosci. *15*, 351–355.

Lorincz, A., and Nusser, Z. (2008a). Cell-type-dependent molecular composition of the axon initial segment. J. Neurosci. Off. J. Soc. Neurosci. *28*, 14329–14340.

Lorincz, A., and Nusser, Z. (2008b). Cell-type-dependent molecular composition of the axon initial segment. J. Neurosci. Off. J. Soc. Neurosci. *28*, 14329–14340.

Luján, R., Albasanz, J.L., Shigemoto, R., and Juiz, J.M. (2005). Preferential localization of the hyperpolarization-activated cyclic nucleotide-gated cation channel subunit HCN1 in basket cell terminals of the rat cerebellum. Eur. J. Neurosci. *21*, 2073–2082.

Lussier, J.J., and Rushton, W. a. H. (1951). Excitability of the nodes of Ranvier in a nerve trunk. J. Physiol. *115*, 53 P.

Maletic-Savatic, M., Lenn, N.J., and Trimmer, J.S. (1995). Differential spatiotemporal expression of K+ channel polypeptides in rat hippocampal neurons developing in situ and in vitro. J. Neurosci. Off. J. Soc. Neurosci. *15*, 3840–3851.

Manganas, L.N., Akhtar, S., Antonucci, D.E., Campomanes, C.R., Dolly, J.O., and Trimmer, J.S. (2001). Episodic ataxia type-1 mutations in the Kv1.1 potassium channel display distinct folding and intracellular trafficking properties. J. Biol. Chem. *276*, 49427–49434.

Margrie, T.W., Meyer, A.H., Caputi, A., Monyer, H., Hasan, M.T., Schaefer, A.T., Denk, W., and Brecht, M. (2003). Targeted whole-cell recordings in the mammalian brain in vivo. Neuron *39*, 911–918.

Maximov, A., and Bezprozvanny, I. (2002). Synaptic targeting of N-type calcium channels in hippocampal neurons. J. Neurosci. Off. J. Soc. Neurosci. *22*, 6939–6952.

Maylie, B., Bissonnette, E., Virk, M., Adelman, J.P., and Maylie, J.G. (2002). Episodic ataxia type 1 mutations in the human Kv1.1 potassium channel alter hKvbeta 1-induced N-type inactivation. J. Neurosci. Off. J. Soc. Neurosci. *22*, 4786–4793.

Meeks, J.P., and Mennerick, S. (2007). Action potential initiation and propagation in CA3 pyramidal axons. J. Neurophysiol. *97*, 3460–3472.

Miyawaki, H., and Hirano, T. (2011). Different correlations among physiological and morphological properties at single glutamatergic synapses in the rat hippocampus and the cerebellum. Synap. N. Y. N *65*, 412–423.

Mochida, S., Westenbroek, R.E., Yokoyama, C.T., Zhong, H., Myers, S.J., Scheuer, T., Itoh, K., and Catterall, W.A. (2003). Requirement for the synaptic protein interaction site for reconstitution of synaptic transmission by P/Q-type calcium channels. Proc. Natl. Acad. Sci. U. S. A. *100*, 2819–2824.

Mohrmann, R., de Wit, H., Verhage, M., Neher, E., and Sørensen, J.B. (2010). Fast vesicle fusion in living cells requires at least three SNARE complexes. Science *330*, 502–505.

Nadal, M.S., Ozaita, A., Amarillo, Y., Vega-Saenz de Miera, E., Ma, Y., Mo, W., Goldberg, E.M., Misumi, Y., Ikehara, Y., Neubert, T.A., et al. (2003). The CD26-related dipeptidyl aminopeptidase-like protein DPPX is a critical component of neuronal A-type K+ channels. Neuron *37*, 449–461.

Nadkarni, S., Bartol, T.M., Stevens, C.F., Sejnowski, T.J., and Levine, H. (2012). Short-term plasticity constrains spatial organization of a hippocampal presynaptic terminal. Proc. Natl. Acad. Sci. U. S. A. *109*, 14657–14662.

Nakamura, Y., Harada, H., Kamasawa, N., Matsui, K., Rothman, J.S., Shigemoto, R., Silver, R.A., DiGregorio, D.A., and Takahashi, T. (2015). Nanoscale distribution of presynaptic Ca(2+) channels and its impact on vesicular release during development. Neuron *85*, 145–158.

Neher, E., and Sakaba, T. (2008). Multiple roles of calcium ions in the regulation of neurotransmitter release. Neuron *59*, 861–872.

Neusch, C., Weishaupt, J.H., and Bähr, M. (2003). Kir channels in the CNS: emerging new roles and implications for neurological diseases. Cell Tissue Res. *311*, 131–138.

Nicholls, J., and Wallace, B.G. (1978). Modulation of transmission at an inhibitory synapse in the central nervous system of the leech. J. Physiol. *281*, 157–170.

Notomi, T., and Shigemoto, R. (2004). Immunohistochemical localization of Ih channel subunits, HCN1-4, in the rat brain. J. Comp. Neurol. *471*, 241–276.

Novak, P., Li, C., Shevchuk, A.I., Stepanyan, R., Caldwell, M., Hughes, S., Smart, T.G., Gorelik, J., Ostanin, V.P., Lab, M.J., et al. (2009). Nanoscale live-cell imaging using hopping probe ion conductance microscopy. Nat. Methods *6*, 279–281.

Novak, P., Gorelik, J., Vivekananda, U., Shevchuk, A.I., Ermolyuk, Y.S., Bailey, R.J., Bushby, A.J., Moss, G.W.J., Rusakov, D.A., Klenerman, D., et al. (2013). Nanoscale-targeted patch-clamp recordings of functional presynaptic ion channels. Neuron *79*, 1067–1077.

O'Brien, J.E., and Meisler, M.H. (2013). Sodium channel SCN8A (Nav1.6): properties and de novo mutations in epileptic encephalopathy and intellectual disability. Front. Genet. *4*.

Ogawa, Y., Horresh, I., Trimmer, J.S., Bredt, D.S., Peles, E., and Rasband, M.N. (2008). Postsynaptic density-93 clusters Kv1 channels at axon initial segments independently of Caspr2. J. Neurosci. Off. J. Soc. Neurosci. *28*, 5731–5739.

Ogden, D. (1994). Microelectrode Techniques - The PlymouthWorkshop Handbook.

Ogiwara, I., Miyamoto, H., Morita, N., Atapour, N., Mazaki, E., Inoue, I., Takeuchi, T., Itohara, S., Yanagawa, Y., Obata, K., et al. (2007). Nav1.1 localizes to axons of parvalbumin-positive inhibitory interneurons: a circuit basis for epileptic seizures in mice carrying an Scn1a gene mutation. J. Neurosci. Off. J. Soc. Neurosci. *27*, 5903–5914.

Ohana, O., and Sakmann, B. (1998). Transmitter release modulation in nerve terminals of rat neocortical pyramidal cells by intracellular calcium buffers. J. Physiol. *513 (Pt 1)*, 135–148.

Ophoff, R.A., Terwindt, G.M., Vergouwe, M.N., van Eijk, R., Oefner, P.J., Hoffman, S.M., Lamerdin, J.E., Mohrenweiser, H.W., Bulman, D.E., Ferrari, M., et al. (1996). Familial hemiplegic migraine and episodic ataxia type-2 are caused by mutations in the Ca2+ channel gene CACNL1A4. Cell *87*, 543–552.

Overbeek, J.T. (1956). The Donnan equilibrium. Prog. Biophys. Biophys. Chem. *6*, 57–84.

Palani, D., Baginskas, A., and Raastad, M. (2010). Bursts and hyperexcitability in non-myelinated axons of the rat hippocampus. Neuroscience *167*, 1004–1013.

Palmer, L.M., and Stuart, G.J. (2006). Site of action potential initiation in layer 5 pyramidal neurons. J. Neurosci. Off. J. Soc. Neurosci. *26*, 1854–1863.

Pan, Z., Kao, T., Horvath, Z., Lemos, J., Sul, J.-Y., Cranstoun, S.D., Bennett, V., Scherer, S.S., and Cooper, E.C. (2006). A common ankyrin-G-based mechanism retains KCNQ and NaV channels at electrically active domains of the axon. J. Neurosci. Off. J. Soc. Neurosci. *26*, 2599–2613.

Papazian, D.M., Schwarz, T.L., Tempel, B.L., Jan, Y.N., and Jan, L.Y. (1987). Cloning of genomic and complementary DNA from Shaker, a putative potassium channel gene from Drosophila. Science *237*, 749–753.

Patel, A.J., Lazdunski, M., and Honoré, E. (1997). Kv2.1/Kv9.3, a novel ATP-dependent delayed-rectifier K+ channel in oxygen-sensitive pulmonary artery myocytes. EMBO J. *16*, 6615–6625.

Pfrieger, F.W., and Barres, B.A. (1997). Synaptic efficacy enhanced by glial cells in vitro. Science *277*, 1684–1687.

Piontek, J., Régnier-Vigouroux, A., and Brandt, R. (2002). Contact with astroglial membranes induces axonal and dendritic growth of human CNS model neurons and affects the distribution of the growth-associated proteins MAP1B and GAP43. J. Neurosci. Res. *67*, 471–483.

Popovic, M.A., Foust, A.J., McCormick, D.A., and Zecevic, D. (2011). The spatio-temporal characteristics of action potential initiation in layer 5 pyramidal neurons: a voltage imaging study. J. Physiol. *589*, 4167–4187.

Prüss, H., Grosse, G., Brunk, I., Veh, R.W., and Ahnert-Hilger, G. (2010). Age-dependent axonal expression of potassium channel proteins during development in mouse hippocampus. Histochem. Cell Biol. *133*, 301–312.

Rajakulendran, S., Schorge, S., Kullmann, D.M., and Hanna, M.G. (2007). Episodic ataxia type 1: a neuronal potassium channelopathy. Neurother. J. Am. Soc. Exp. Neurother. *4*, 258–266.

Rajakulendran, S., Schorge, S., Kullmann, D.M., and Hanna, M.G. (2010). Dysfunction of the Ca(V)2.1 calcium channel in cerebellar ataxias. F1000 Biol. Rep. *2*.

Rall, W. (1959). Branching dendritic trees and motoneuron membrane resistivity. Exp. Neurol. *1*, 491–527.

Rea, R., Spauschus, A., Eunson, L.H., Hanna, M.G., and Kullmann, D.M. (2002). Variable K(+) channel subunit dysfunction in inherited mutations of KCNA1. J. Physiol. *538*, 5–23.

Regehr, W.G., Delaney, K.R., and Tank, D.W. (1994). The role of presynaptic calcium in short-term enhancement at the hippocampal mossy fiber synapse. J. Neurosci. Off. J. Soc. Neurosci. *14*, 523–537.

Rettig, J., Heinemann, S.H., Wunder, F., Lorra, C., Parcej, D.N., Dolly, J.O., and Pongs, O. (1994). Inactivation properties of voltage-gated K+ channels altered by presence of beta-subunit. Nature *369*, 289–294.

Reuter, H. (1967). The dependence of slow inward current in Purkinje fibres on the extracellular calcium-concentration. J. Physiol. *192*, 479–492.

Richards, D.A., Bai, J., and Chapman, E.R. (2005). Two modes of exocytosis at hippocampal synapses revealed by rate of FM1-43 efflux from individual vesicles. J. Cell Biol. *168*, 929–939.

Richards, K.S., Swensen, A.M., Lipscombe, D., and Bommert, K. (2007). Novel CaV2.1 clone replicates many properties of Purkinje cell CaV2.1 current. Eur. J. Neurosci. *26*, 2950–2961.

Ringer, S., and Buxton, D.W. (1887). Concerning the Action of Calcium, Potassium, and Sodium Salts upon the Eel's Heart and upon the Skeletal Muscles of the Frog. J. Physiol. *8*, 15–19.

Rizo, J., and Xu, J. (2015). The Synaptic Vesicle Release Machinery. Annu. Rev. Biophys. *44*, 339–367.

Rothman, J.S., Kocsis, L., Herzog, E., Nusser, Z., and Silver, R.A. (2016). Physical determinants of vesicle mobility and supply at a central synapse. eLife *5*.

Rowan, M.J.M., and Christie, J.M. (2017). Rapid state-dependent alteration in Kv3 channel availability drives flexible synaptic signaling dependent on somatic subthreshold depolarization. Cell Rep. *18*, 2018–2029.

Rowan, M.J.M., Tranquil, E., and Christie, J.M. (2014). Distinct Kv Channel Subtypes Contribute to Differences in Spike Signaling Properties in the Axon Initial Segment and Presynaptic Boutons of Cerebellar Interneurons. J. Neurosci. *34*, 6611–6623.

Rowan, M.J.M., DelCanto, G., Yu, J.J., Kamasawa, N., and Christie, J.M. (2016). Synapse-Level Determination of Action Potential Duration by K+ Channel Clustering in Axons. Neuron *91*, 370–383.

Ruiz, A., Campanac, E., Scott, R.S., Rusakov, D.A., and Kullmann, D.M. (2010). Presynaptic GABAA receptors enhance transmission and LTP induction at hippocampal mossy fiber synapses. Nat. Neurosci. *13*, 431–438.

Sánchez, D., Johnson, N., Li, C., Novak, P., Rheinlaender, J., Zhang, Y., Anand, U., Anand, P., Gorelik, J., Frolenkov, G.I., et al. (2008). Noncontact measurement of the local mechanical properties of living cells using pressure applied via a pipette. Biophys. J. *95*, 3017–3027.

Sasaki, T., Matsuki, N., and Ikegaya, Y. (2011). Action-potential modulation during axonal conduction. Science *331*, 599–601.

Sasaki, T., Matsuki, N., and Ikegaya, Y. (2012). Targeted axon-attached recording with fluorescent patch-clamp pipettes in brain slices. Nat. Protoc. *7*, 1228–1234.

Saviane, C., Mohajerani, M.H., and Cherubini, E. (2003). An ID-like current that is downregulated by Ca2+ modulates information coding at CA3-CA3 synapses in the rat hippocampus. J. Physiol. *552*, 513–524.

Savio-Galimberti, E., Gollob, M.H., and Darbar, D. (2012). Voltage-gated sodium channels: biophysics, pharmacology, and related channelopathies. Front. Pharmacol. *3*, 124.

Schikorski, T., and Stevens, C.F. (2001). Morphological correlates of functionally defined synaptic vesicle populations. Nat. Neurosci. *4*, 391–395.

Schneggenburger, R., and Neher, E. (2005). Presynaptic calcium and control of vesicle fusion. Curr. Opin. Neurobiol. *15*, 266–274.

Schweitz, H., Bidard, J.N., and Lazdunski, M. (1990). Purification and pharmacological characterization of peptide toxins from the black mamba (Dendroaspis polylepis) venom. Toxicon Off. J. Int. Soc. Toxinology *28*, 847–856.

Scott, R., Ruiz, A., Henneberger, C., Kullmann, D.M., and Rusakov, D.A. (2008). Analog modulation of mossy fiber transmission is uncoupled from changes in presynaptic Ca2+. J. Neurosci. Off. J. Soc. Neurosci. *28*, 7765–7773.

Scott, R.S., Henneberger, C., Padmashri, R., Anders, S., Jensen, T.P., and Rusakov, D.A. (2014). Neuronal adaptation involves rapid expansion of the action potential initiation site. Nat. Commun. *5*, 3817.

Shah, M.M., Mistry, M., Marsh, S.J., Brown, D.A., and Delmas, P. (2002). Molecular correlates of the M-current in cultured rat hippocampal neurons. J. Physiol. *544*, 29–37.

Shah, M.M., Migliore, M., Valencia, I., Cooper, E.C., and Brown, D.A. (2008). Functional significance of axonal Kv7 channels in hippocampal pyramidal neurons. Proc. Natl. Acad. Sci. U. S. A. *105*, 7869–7874.

Sheng, J., He, L., Zheng, H., Xue, L., Luo, F., Shin, W., Sun, T., Kuner, T., Yue, D.T., and Wu, L.-G. (2012). Calcium-channel number critically influences synaptic strength and plasticity at the active zone. Nat. Neurosci. *15*, 998–1006.

Shepherd, G.M., and Koch, C. (1998). The synaptic organisation of the brain: Introduction to synpatic cicuits (Oxford University Press).

Shimahara, T., and Peretz, B. (1980). Quantal transmitter release in an identified inhibitory cholinergic synapse of Aplysia. Proc. R. Soc. Lond. B Biol. Sci. *206*, 403–409.

Shu, Y., Hasenstaub, A., Duque, A., Yu, Y., and McCormick, D.A. (2006). Modulation of intracortical synaptic potentials by presynaptic somatic membrane potential. Nature *441*, 761–765.

Shu, Y., Yu, Y., Yang, J., and McCormick, D.A. (2007a). Selective control of cortical axonal spikes by a slowly inactivating K+ current. Proc. Natl. Acad. Sci. U. S. A. *104*, 11453–11458.

Shu, Y., Duque, A., Yu, Y., Haider, B., and McCormick, D.A. (2007b). Properties of action-potential initiation in neocortical pyramidal cells: evidence from whole cell axon recordings. J. Neurophysiol. *97*, 746–760.

Smart, S.L., Lopantsev, V., Zhang, C.L., Robbins, C.A., Wang, H., Chiu, S.Y., Schwartzkroin, P.A., Messing, A., and Tempel, B.L. (1998). Deletion of the K(V)1.1 potassium channel causes epilepsy in mice. Neuron *20*, 809–819.

Squire, L.R., Bloom, F.E., McConnell, S.K., Roberts, J.L., Spitzer, N.C., and Zigmond, M.J. (2003). Fundamental neuroscience (Academic Press).

Steinert, J.R., Robinson, S.W., Tong, H., Haustein, M.D., Kopp-Scheinpflug, C., and Forsythe, I.D. (2011). Nitric oxide is an activity-dependent regulator of target neuron intrinsic excitability. Neuron *71*, 291–305.

Südhof, T.C. (1995). The synaptic vesicle cycle: a cascade of protein-protein interactions. Nature *375*, 645–653.

Sudhof, T.C. (2004). The synaptic vesicle cycle. Annu. Rev. Neurosci. *27*, 509–547.

Südhof, T.C. (2013). Neurotransmitter release: the last millisecond in the life of a synaptic vesicle. Neuron *80*, 675–690.

Südhof, T.C., and Rothman, J.E. (2009). Membrane fusion: grappling with SNARE and SM proteins. Science *323*, 474–477.

Sun, P., Laforge, F.O., Abeyweera, T.P., Rotenberg, S.A., Carpino, J., and Mirkin, M.V. (2008). Nanoelectrochemistry of mammalian cells. Proc. Natl. Acad. Sci. U. S. A. *105*, 443–448.

Tang, J., Maximov, A., Shin, O.-H., Dai, H., Rizo, J., and Südhof, T.C. (2006). A complexin/synaptotagmin 1 switch controls fast synaptic vesicle exocytosis. Cell *126*, 1175–1187.

Tomlinson, S.E., Tan, S.V., Kullmann, D.M., Griggs, R.C., Burke, D., Hanna, M.G., and Bostock, H. (2010). Nerve excitability studies characterize Kv1.1 fast potassium channel dysfunction in patients with episodic ataxia type 1. Brain J. Neurol. *133*, 3530–3540.

Tottene, A., Fellin, T., Pagnutti, S., Luvisetto, S., Striessnig, J., Fletcher, C., and Pietrobon, D. (2002). Familial hemiplegic migraine mutations increase Ca(2+) influx through single human CaV2.1 channels and decrease maximal CaV2.1 current density in neurons. Proc. Natl. Acad. Sci. U. S. A. *99*, 13284–13289.

Trimmer, J.S., and Rhodes, K.J. (2004). Localization of voltage-gated ion channels in mammalian brain. Annu. Rev. Physiol. *66*, 477–519.

Tsien, R.W., Lipscombe, D., Madison, D.V., Bley, K.R., and Fox, A.P. (1988). Multiple types of neuronal calcium channels and their selective modulation. Trends Neurosci. *11*, 431–438.

Turecek, R., and Trussell, L.O. (2001). Presynaptic glycine receptors enhance transmitter release at a mammalian central synapse. Nature *411*, 587–590.

Turrigiano, G.G., and Nelson, S.B. (2004). Homeostatic plasticity in the developing nervous system. Nat. Rev. Neurosci. *5*, 97–107.

Vacher, H., Mohapatra, D.P., and Trimmer, J.S. (2008). Localization and targeting of voltage-dependent ion channels in mammalian central neurons. Physiol. Rev. *88*, 1407–1447.

Van Wart, A., Trimmer, J.S., and Matthews, G. (2007). Polarized distribution of ion channels within microdomains of the axon initial segment. J. Comp. Neurol. *500*, 339–352.

VanDyke, D.H., Griggs, R.C., Murphy, M.J., and Goldstein, M.N. (1975). Hereditary myokymia and periodic ataxia. J. Neurol. Sci. *25*, 109–118.

Veh, R.W., Lichtinghagen, R., Sewing, S., Wunder, F., Grumbach, I.M., and Pongs, O. (1995). Immunohistochemical localization of five members of the Kv1 channel subunits: contrasting subcellular locations and neuron-specific co-localizations in rat brain. Eur. J. Neurosci. *7*, 2189–2205.

Verkerk, A.O., Remme, C.A., Schumacher, C.A., Scicluna, B.P., Wolswinkel, R., de Jonge, B., Bezzina, C.R., and Veldkamp, M.W. (2012). Functional Nav1.8 channels in intracardiac neurons: the link between SCN10A and cardiac electrophysiology. Circ. Res. *111*, 333–343.

Vicario-Abejón, C. (2004). Long-term culture of hippocampal neurons. Curr. Protoc. Neurosci. Editor. Board Jacqueline N Crawley Al *Chapter 3*, Unit 3.2.

Viesselmann, C., Ballweg, J., Lumbard, D., and Dent, E.W. (2011). Nucleofection and primary culture of embryonic mouse hippocampal and cortical neurons. J. Vis. Exp. JoVE.

Vincent, A., Lang, B., and Kleopa, K.A. (2006). Autoimmune channelopathies and related neurological disorders. Neuron *52*, 123–138.

W. Rall (1958). Dendritic cement distribution and whole neuron properties. Nav.Med.Res.Inst.Res.Rep. 479–525.

Wang, H., Kunkel, D.D., Martin, T.M., Schwartzkroin, P.A., and Tempel, B.L. (1993). Heteromultimeric K+ channels in terminal and juxtaparanodal regions of neurons. Nature *365*, 75–79.

Wang, H., Kunkel, D.D., Schwartzkroin, P.A., and Tempel, B.L. (1994). Localization of Kv1.1 and Kv1.2, two K channel proteins, to synaptic terminals, somata, and dendrites in the mouse brain. J. Neurosci. Off. J. Soc. Neurosci. *14*, 4588–4599.

Waxman, S.G. (2001). Transcriptional channelopathies: an emerging class of disorders. Nat. Rev. Neurosci. *2*, 652–659.

Wei, A.D., Gutman, G.A., Aldrich, R., Chandy, K.G., Grissmer, S., and Wulff, H. (2005). International Union of Pharmacology. LII. Nomenclature and molecular relationships of calcium-activated potassium channels. Pharmacol. Rev. *57*, 463–472.

Westenbroek, R.E., Merrick, D.K., and Catterall, W.A. (1989). Differential subcellular localization of the RI and RII Na+ channel subtypes in central neurons. Neuron *3*, 695–704.

Williams, S.R., and Stuart, G.J. (1999). Mechanisms and consequences of action potential burst firing in rat neocortical pyramidal neurons. J. Physiol. *521*, 467–482.

Wollner, D.A., and Catterall, W.A. (1986). Localization of sodium channels in axon hillocks and initial segments of retinal ganglion cells. Proc. Natl. Acad. Sci. U. S. A. *83*, 8424–8428.

Wu, R.L., and Barish, M.E. (1992). Two pharmacologically and kinetically distinct transient potassium currents in cultured embryonic mouse hippocampal neurons. J. Neurosci. Off. J. Soc. Neurosci. *12*, 2235–2246.

Xu-Friedman, M.A., Harris, K.M., and Regehr, W.G. (2001). Three-dimensional comparison of ultrastructural characteristics at depressing and facilitating synapses onto cerebellar Purkinje cells. J. Neurosci. Off. J. Soc. Neurosci. *21*, 6666–6672.

Yu, Y., Maureira, C., Liu, X., and McCormick, D. (2010). P/Q and N channels control baseline and spike-triggered calcium levels in neocortical axons and synaptic boutons. J. Neurosci. Off. J. Soc. Neurosci. *30*, 11858–11869.

Yue, C., and Yaari, Y. (2006). Axo-somatic and apical dendritic Kv7/M channels differentially regulate the intrinsic excitability of adult rat CA1 pyramidal cells. J. Neurophysiol. *95*, 3480–3495.

Zerr, P., Adelman, J.P., and Maylie, J. (1998). Episodic ataxia mutations in Kv1.1 alter potassium channel function by dominant negative effects or haploinsufficiency. J. Neurosci. Off. J. Soc. Neurosci. *18*, 2842–2848.

Zhou, L., Messing, A., and Chiu, S.Y. (1999). Determinants of excitability at transition zones in Kv1.1-deficient myelinated nerves. J. Neurosci. Off. J. Soc. Neurosci. *19*, 5768–5781.

Zuberi, S.M., Eunson, L.H., Spauschus, A., De Silva, R., Tolmie, J., Wood, N.W., McWilliam, R.C., Stephenson, J.B., Stephenson, J.P., Kullmann, D.M., et al. (1999). A novel mutation in the human voltage-gated potassium channel gene (Kv1.1) associates with episodic ataxia type 1 and sometimes with partial epilepsy. Brain J. Neurol. *122 (Pt 5)*, 817–825.

Zucker, R.S., and Regehr, W.G. (2002). Short-term synaptic plasticity. Annu. Rev. Physiol. *64*, 355–405.

Appendix I Exploratory: Modelling presynaptic action potentials of the EA1 mutation using *NEURON*

As a preliminary attempt to model the finding reported in **Section 6.3**, i.e. that presynaptic action potential width is greater in the EA1 mutations than wild-type, I created a computer model based on one created by Alle and Geiger for mossy fibre boutons (Alle and Geiger, 2006). The membrane excitability was described by Hodgkin – Huxley kinetics. The modelled neuron had a cell body and five boutons, each 150 μm away from each other. The other parameters are in Table 7.2. As found in our experiments the resting membrane potential of the bouton was more depolarised than the soma. Ideally the model would have been based on accurate potassium channel data for opening and closing states in wild type and mutant derived from experiment. However to provide a preliminary model I solely altered the potassium conductance between wild type and mutation. Action potentials were elicited with a 200 ms pulse delivered at the soma (as in our experiments) and recording was performed over 2 s.

Chosen parameters for neuronal circuit	'Wild type'	'EA1 mutation'
Axon: Axial resistance (Ω-cm)	100	100
Membrane capacitance (μF/cm^2)	1	1
Resting voltage (mV)	−70	−70

Diameter (μm)	0.4	0.4
Length (μm)	150	150
Bouton: Axial resistance (Ω-cm)	100	100
Membrane capacitance (μF/cm^2)	1	1
Resting voltage (mV)	−75	−75
Diameter (μm)	1	1
Length (μm)	1	1
Sodium: Threshold voltage (mV)	−57	−57
Reversal potential (mV)	+55	+55
Conductance (S/cm^2)	0.004	0.004
Calcium: Threshold voltage (mV)	−57	−57
Reversal potential (mV)	+75	+75
Conductance (S/cm^2)	0.003	0.003
Potassium: Threshold voltage (mV)	−57	−57
Reversal potential (mV)	−100	−100
Conductance (S/cm^2)	0.008	**0.004**

Table APP1 Chosen parameters for ‘wild type’ and ‘mutant’ computer model

As Figure 7.2 shows with change in potassium conductance, action potential width is greater in the 'mutant' model (7.2D) than in the 'wild type' model (7.2B). This is unaltered up to 600 μm away from the soma. In addition, the action potentials in the 'mutant' model occur earlier in the stimulating pulse than in the 'wild type' model, suggesting a more excitable state.

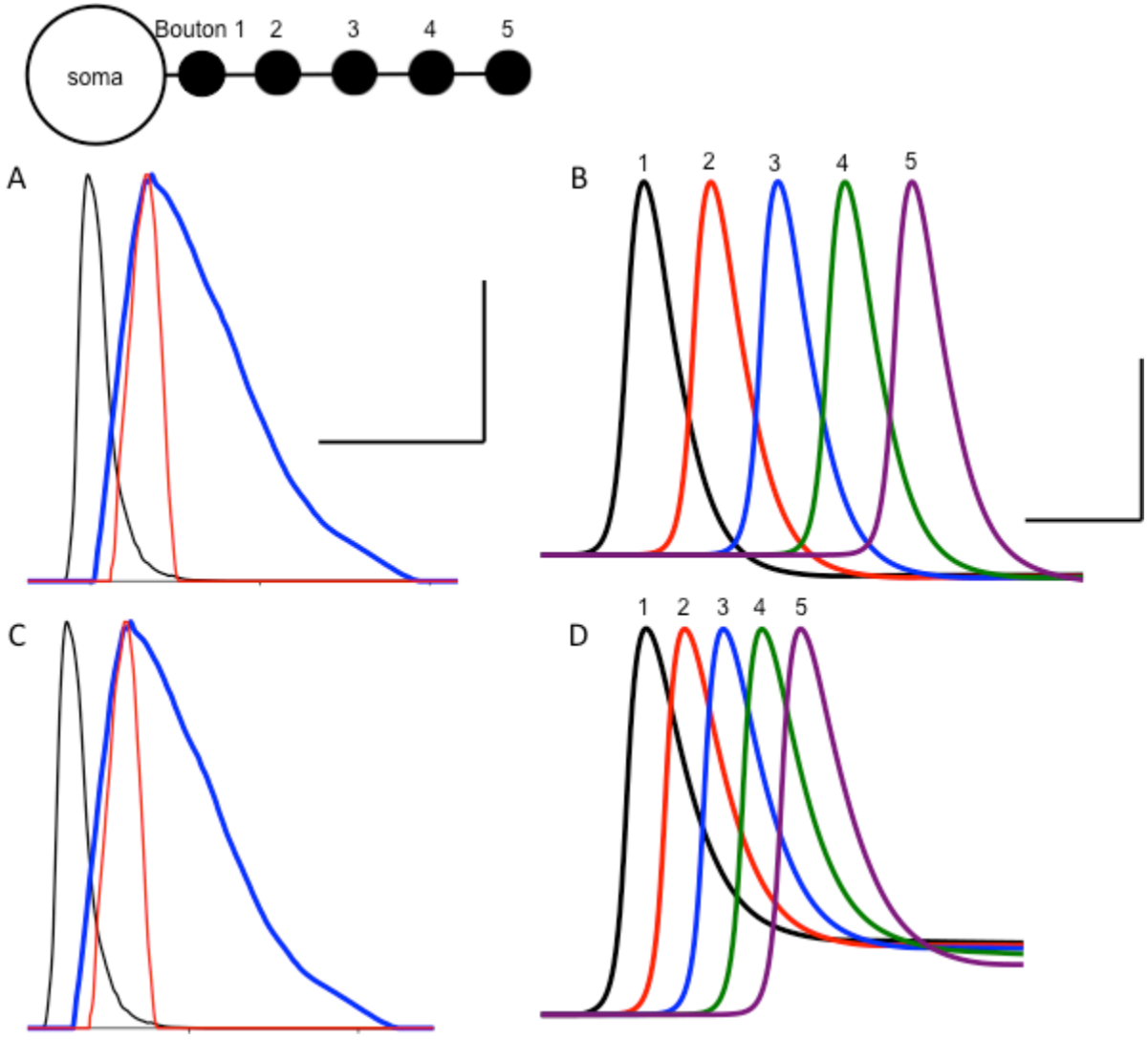

Figure APP1. ***NEURON*** **model of five bouton circuit in 'wild type' and 'mutant'.** (A) 'Wild type' conductances for sodium (black), calcium (red) and potassium (blue)

(B) Wild type action potential morphology at each of the five boutons (C) Same as (A) for 'mutant' (D) Same as (B) for 'mutant'.

Appendix II Exploratory: **Intra-bouton calcium response to somatic excitation**

This section describes some preliminary work performed to integrate quantitative fluorescence imaging to the SICM/electrophysiology setup. We hypothesized that the broader action potentials seen in submicrometer presynaptic boutons in the *Kcna1*$^{-/-}$ and EA1 model would be associated with increased calcium influx and neurotransmitter release as has been demonstrated in mossy fibre boutons (Geiger and Jonas, 2000). Although neurotransmitter release and calcium influx in small central synapses has been investigated separately within the lab (Ermolyuk et al., 2012), relating that to direct electrophysiological recording would be powerful. In addition the components already used for fluorescence imaging in confirming axonal morphology (**Section 6.1**) such as LED illumination and EM-CCD for acquisition, could also be used for detecting responses from specific calcium promoters. We transfected hippocampal neurons with a synaptophysin-GCaMP3 plasmid. Initially only wild type neurons were used in order to optimize the transfection protocol.

Aims

1. Establish a robust transfection protocol for rat hippocampal cultures

2. Establish a method for quantifying intra-bouton calcium changes with repetitive stimulation of the cell.

Method and Results

P0-P1 rat hippocampal neurons were cultured on rat astrocyte feeder layer-coated glass coverslips in 12 well plates for one day and transfected using Optimem containing 1000 ng of plasmidic DNA synaptophysin-GCaMP3 (SyGCaMP3) in combination with a reporter DNA, B-actin promoter monomeric red fluorescent protein (mRFP), and 1.5ul Lipofectamine 3000 and 2.0 ul P3000 (Invitrogen) per well. After 3 hours, transfection medium was replaced with culture medium and neurons were cultured for 14 days (**Section 4.1**) before experimenting.

Experiments were performed as before between day 14 and 18. Manipulation of the somatic pipette was the same as outlined in **Section 6.2**. To identify an RFP transfected cell, the coverslip was viewed at 10x objective under green LED (via a red longpass dichroic mirror with 560nm cut-off wavelength) illumination. On average 10% of cells were transfected per coverslip. The cell chosen for patch clamp was then viewed under higher magnification (60x). The cell body and associated axons could then be viewed as the RFP was stimulated (Figure 7.3a). The axons were then viewed under blue LED illumination (via a green longpass dichroic mirror with 505nm cut-off wavelength) to stimulate the GFP and obtain a basal calcium response (Figure 7.3b). The cell body was then patched by a large pipette (resistance 3 –

5MΩ) and action potentials elicited with a 200pA pulse lasting 1 second (**Section 6.2**). During this period epifluorescence images were acquired under blue LED light to observe increase in intensity of boutons (Figure 7.3c). The relative change in fluorescence could then be used to examine intra-bouton Ca^{2+} concentration.

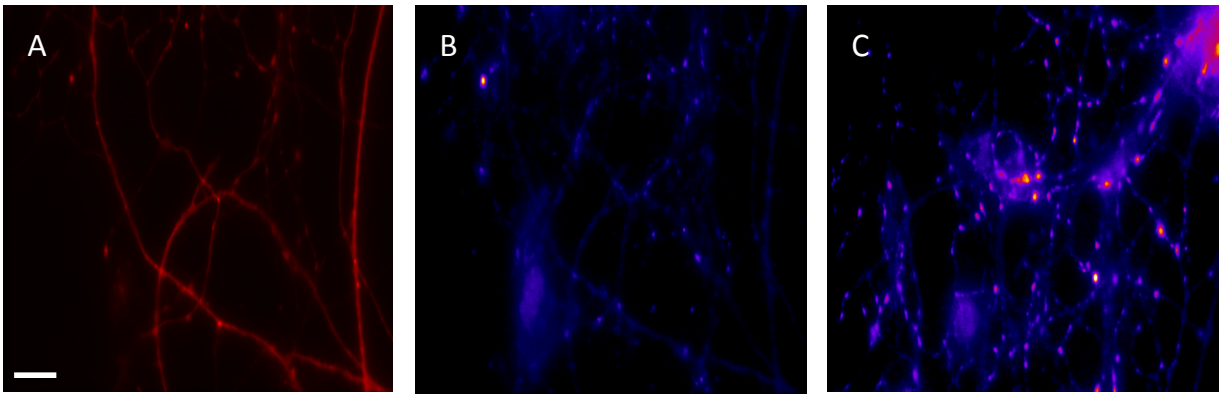

Figure APP2. **Rat hippocampal calcium experiments** (A) Cell and associated axons viewed under green LED illumination; scale bar 10 microns. (B) Same cell viewed under blue LED illumination prior to cell stimulation. (C) After stimulation many more boutons fluoresce indicating calcium response to cell stimulation

Conclusions

The transfection process did yield a low percentage of transfected cells; however our experience was that any larger amount of DNA used for transfection produced sick cells, which were not usable for electrophysiology. Once the protocol was established in rat hippocampal cultures, this could then be translated to mouse cultures with wild type and *Kcna1a*$^{V408A/+}$ neurons. A future experiment would be to stimulate wild type and *Kcna1a*$^{V408A/+}$ cells by eliciting action potentials, and

separately observe changes in intra-bouton calcium. Then a high resolution topographic image of a bouton that demonstrates calcium increase could be acquired. The same bouton would then be patched and action potentials elicited as described in **Section 6.2**. We would then be able to compare presynaptic action potential and intra-bouton calcium change between wild type and *Kcna1a*$^{V408A/+}$ neurons, and confirm whether calcium change is greater in *Kcna1a*$^{V408A/+}$ excitatory synapses to reflect increased neurotransmitter release as previous studies have indicated would be the case (Begum et al., 2016; Heeroma et al., 2009).